Version 3.10

Dissertation Submitted to
Graduate School of Science of Osaka University
for the Degree of Master of Physics

Baryon resonances in the chiral unitary model

Tetsuo Hyodo

~ 2003 ~

Research Center for Nuclear Physics (RCNP), Osaka University
Mihogaoka 10-1, Ibaraki, Osaka 567-0047, Japan

Acknowledgement

First of all, I would like to sincerely express my gratitude to Dr. D. Jido for his continuous discussions and helpful suggestions. I owe most of the study in this thesis to him. I am very grateful to my supervisor, Professor A. Hosaka for fruitful discussions and giving me an interesting subject of the chiral unitary model. I would like to acknowledge Mr. S. I. Nam and his Professor H. -Ch. Kim (Pusan National Univ.), for their stimulating discussions and friendships. Without their affectionate support, I could not finish my master work. I would like to thank them again for their fruitful collaborations.

I would like to acknowledge Dr. M. Koma (Max-Planck Inst.) for introducing a useful computer environment. I am grateful to Professor E. Oset (Valencia Univ.) for giving me interesting comments and checking the calculations of magnetic moments in detail. I thank to Dr. A. Sugita (YITP) for organizing a study hour of the textbook [1] at RCNP. I wish to thank Professors W. Weise (ECT*), M. Dillig (Erlangen Univ.) and Y. Nambu (Chicago Univ.) for their valuable suggestions, discussions, and encouragement.

I am grateful to all the members of theory group of Research Center for Nuclear Physics for their kind helps. Finally, I wish to acknowledge Professor H. Toki for his continuous encouragement and providing a comfortable environment, collaborators and colleagues.

Abstract

We study s wave meson-baryon scatterings using the chiral unitary model and investigate properties of excited baryons which appear as resonances. In the chiral unitary model, we sum up non-perturbatively the interactions of the chiral perturbation theory, which is one of the effective theories of QCD respecting chiral symmetry, so that the model provides a good description of hadron physics in low and intermediate energy region. Due to the non-perturbative resummation, in s wave scatterings, $1/2^-$ baryon resonances are generated dynamically, and they are regarded as quasibound states of the low lying mesons (π, K, η) and baryons $(N, \Lambda, \Sigma, \Xi)$.

In this thesis, we first review the foundations of the model, chiral perturbation theory and the method of unitarization. According to the previous works, the chiral unitary model has two features. On one hand, the chiral unitary model needs several parameters whose origin is not clear. On the other hand, with the use of proper parameters, the model is in excellent agreement with experimental data. Therefore, we study theoretical aspects of the model and apply it to the investigation of the resonance structure. We study flavor $SU(3)$ breaking effects and compute the magnetic moments of the baryon resonances.

In previous works of the chiral unitary model, the subtraction constants in loop integrals largely depended on channels, where it was necessary to fit these constants to reproduce the data. In order to extend this model to all channels with fewer parameters, we introduce flavor $SU(3)$ breaking interactions in the framework of chiral perturbation theory. It is found, however, that the observed $SU(3)$ breaking in meson-baryon scatterings cannot be explained by the present $SU(3)$ breaking interactions. The essential physics of the resonances seems to lie in the subtraction constants.

As an application of the chiral unitary model, we calculate the magnetic moments of the $N(1535)$ resonance. So far, the magnetic moments of excited baryons have not been measured, because they are unstable and decay quickly. However, with the recent developments of the experimental technique, it is planned to extract the magnetic moments of $N(1535)$ from the reaction $\gamma p \to \gamma \eta p$ at LNS (Tohoku) and MAMI (Mainz). In the chiral unitary model, we calculate the diagrams in which a photon couples to $N(1535)$, and extract the magnetic moments without using explicit resonance fields. The results are $\mu_{p^*} \sim +1.1\mu_N$ and $\mu_{n^*} \sim -0.25\mu_N$, where μ_N is the nuclear magneton. Physical origin of these numbers is briefly discussed.

Contents

List of Figures

List of Tables

Chapter 1

Introduction

Today we understand that the strong interaction is governed by quantum chromodynamics (QCD), which is the color $SU(3)$ gauge theory with quarks as fundamental fields and gluons as gauge fields. Because QCD has non-Abelian symmetry, the gluons interact with themselves, so that the running coupling constant of QCD behaves asymptotically free, according to the renormalization group equations. Inversely, the coupling constant becomes large at low energy region, where the perturbative calculation breaks down. In this non-perturbative region, the fundamental degrees of freedom become mesons and baryons due to the color confinement. We call these mesons and baryons together as hadrons, and the investigation of the hadron dynamics at low energy region is of our interest. In order to study the behavior of hadrons, we adopt effective field theories using the principle of symmetry.

Chiral symmetry of QCD plays an important role in low energy hadron physics [1]. Several low energy theorems are derived from chiral symmetry and its spontaneous breaking. Originally, before the establishment of QCD, the notion of the chiral symmetry has been developed in current algebra [2]. Being started with the Goldberger-Treiman relation [3], an idea of partially conserved axial current (PCAC) were introduced. PCAC was later understood by the spontaneous breaking of chiral symmetry, where pions appear as the Nambu-Goldstone (NG) bosons of the broken generators. Consideration of the process with more than one pion, such as πN scatterings, determines the commutation relations of the broken generators, so that the broken symmetry group is specified as $SU(2) \times SU(2)$. One of the reasons that QCD is accepted is that $SU(2) \times SU(2)$ can be interpreted as the results of small masses of u and d quarks.

The chiral perturbation theory (ChPT) [4, 5, 6, 7, 8] is one of the low energy effective theory of QCD respecting chiral symmetry, where mesons and baryons are the fundamental degrees of freedom. It is based on the nonlinear realization of chiral symmetry, and the spontaneous breakdown of the symmetry is assumed from the beginning. Advantages of this

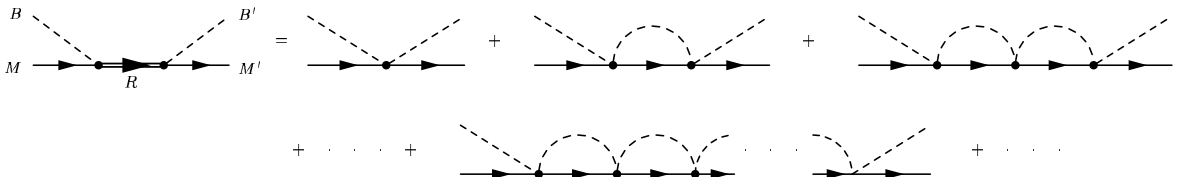

Figure 1.1: Diagrammatic interpretation of dynamical generation of resonances. Solid, dashed and double lines represent baryons mesons, and baryon resonance, respectively. Summing the loops up to infinite order, we can generate a resonance dynamically.

theory are as follows. First, we can establish a power counting rule in terms of momenta of the NG bosons. With this chiral counting rule, we can perform perturbative calculation, which works well at low energy region. Second, the results of current algebra relations and several mass formulae, such as Gell-Mann-Okubo mass relation, are easily derived from the effective Lagrangian. Therefore, in order to study the low energy hadron dynamics, we adopt the ChPT as the foundation.

1.1 Chiral unitary model

The study of meson-baryon scatterings in a unified way is important to understand hadron dynamics at low and intermediate energy regions from the viewpoint of QCD. Especially the properties of baryonic excited states observed in the meson-baryon scatterings as resonances are investigated with great interest both theoretically and experimentally. So far, there are several established approaches to describe the properties of the baryon resonances. A recent development in this field has been made by the success of the chiral unitary model [9, 9, 11, 12, 13, 14], where $1/2^-$ baryon resonances are dynamically generated in s wave meson-baryon scatterings (Fig. 1.1). In this formulation, we regard the resonances as quasibound states of mesons and baryons, and one of the advantage of the chiral unitary model is the dynamical generation, with which the information of the resonances such as masses, widths and the couplings to meson-baryon channels is produced only from mesons and baryons. This point differs from the explicit resonance approach [15, 16], where the resonance fields are introduced in ChPT and the information of the resonances are inputted by hand. The meson-baryon picture of resonances is also superior than the conventional quark model approach, where the baryon resonances are described as three-quark states with an excitation of one of the quarks [17, 18]. Experimentally, it is known that the excited baryons strongly couple to the meson-baryon channels, which cannot be described by simple quark model. This important feature implies the meson-baryon picture of resonances.

The chiral unitary model is based on the ChPT. Imposing the unitarity condition, the ChPT can be extended to higher energy regions than in the original perturbative calculation.

In this way, we can study properties of resonances generated by non-perturbative resummations. In the implementation of the unitarity condition, regularization of loop integrals brings parameters into this model, such as the three-momentum cut-off and the "subtraction constants" in the dimensional regularization.

In Refs. [9, 13], the s wave scatterings of the meson and baryon systems with the strangeness $S = -1$ were investigated by solving the Lippman-Schwinger equation in the coupled channels, where the $\Lambda(1405)$ resonance was dynamically generated by the meson-baryon scatterings. In the regularization procedure, parameters were introduced for the finite ranges in the kernel potential [9], and for the three-momentum cut-off in the loop integral [13]. In Refs. [19, 20, 21], they extended the chiral unitary approach to other strangeness channels and obtained the baryonic resonances, $\Lambda(1405), N(1535), \Lambda(1670), \Sigma(1620)$ and $\Xi(1620)$, as dynamically generated objects. They used the dimensional regularization scheme with channel dependent subtraction constants (a_i). In particular, the subtraction constants in $S = 0$ depended significantly on channels, while as reported in Ref. [22], a common subtraction constant was found in the $S = -1$ channel to reproduce the total cross sections of the $K^- p$ scattering as well as $\Lambda(1405)$ properties.

Here, we would like to make two remarks on the chiral unitary model. On one hand, the chiral unitary model needs channel dependent subtraction constants. However, their microscopic origin is not clear. On the other hand, with the use of proper subtraction constants, the chiral unitary model is very powerful to describe not only meson-baryon scatterings but resonances. Based on these two remarks, we study the following two original works in this thesis.

- Study of theoretical aspects : flavor $SU(3)$ breaking effects
- Investigation of the resonance structure : magnetic moments of the baryon resonances

In sections 1.2 and 1.3, we present motivations and backgrounds of these studies in detail.

1.2 Flavor $SU(3)$ breaking effects

In this work, we raise a question whether the channel dependence of the subtraction constants could be dictated by the flavor $SU(3)$ breaking effects of an underlying theory, or not. The $SU(3)$ breaking should have significant effects on observed quantities. This is expected from, for instance, the large dependence of the threshold energies on the meson-baryon channels as shown in Fig. 1.2. This is particularly the case for $S = 0$, where the lowest threshold energy of the πN channel deviates considerably from the mean value.

In order to study the above questions, we consider the following two cases;

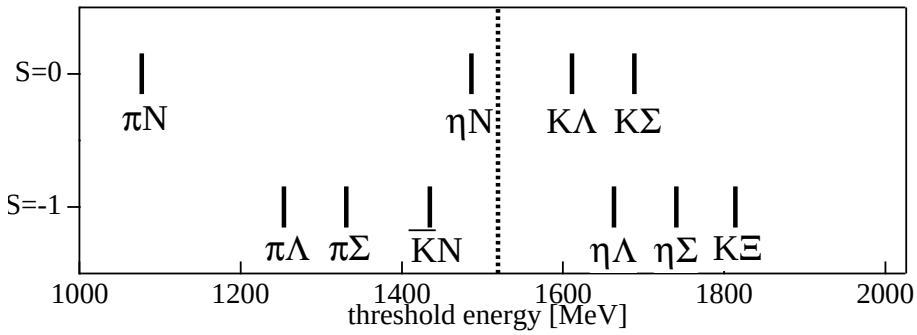

Figure 1.2: Threshold energies of the meson-baryon scatterings in the $S = -1$ and $S = 0$ channels. The dotted line in the middle represents the averaged energy of all meson-baryon thresholds.

- We use a common subtraction constant for all scattering channels and see whether this simplified calculation works or not (chapter 4).
- When this method does not work, we introduce the flavor $SU(3)$ breaking effects in the interaction kernel (chapter 5).

In this way, we expect that the free parameters in the previous works could be controlled with suitable physics ground, which allows us to extend this model to other channels with predictive power. In this work, we concentrate on the s wave scatterings, since the p wave contribution to the total cross sections is shown to be small in the $S = -1$ channel in Ref. [23].

1.3 Magnetic moments of the baryon resonances

As an application of the chiral unitary model to investigation of the structure of resonances, we calculate the magnetic moments of the $N(1535)$ resonance. In general, it is not easy to measure the magnetic moments of excited baryons experimentally, because they have too short lifetimes for the spin precession measurements. However, with the recent developments of the experimental technique, several experiments are performed and planned. Indeed, through the reaction $\pi^+ p \to \gamma\pi^+ p$, the measurements for the magnetic moments of $\Delta^{++}(1232)$ have already been done in Refs. [24] and [25], although the result is not so precise, $\mu_{\Delta^{++}} = 3.7 \sim 7.5\mu_N$, due to ambiguities of the reaction mechanism. In recent experiment [26] the magnetic moments of $\Delta^+(1232)$ are measured from $\gamma p \to \gamma\pi^0 p$, and further experiments are planned at MAMI (Mainz). For $N(1535)$, it is also planned to extract the magnetic moments of the resonance from the reaction $\gamma p \to \gamma\eta p$ at LNS (Tohoku) and MAMI.

From theoretical point of view, calculation of the magnetic moments of $N(1535)$ are done in Ref. [27], where the constituent quark model is adopted. In the chiral unitary model, the

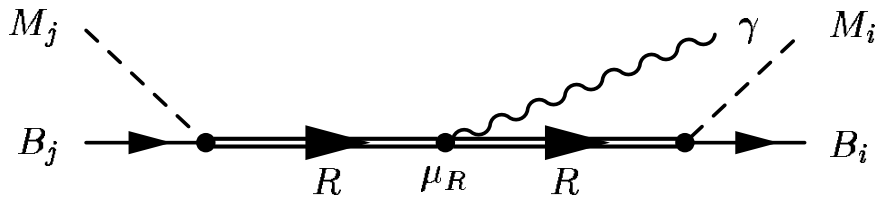

Figure 1.3: Feynman diagram from which we extract the magnetic moments of the resonance. Solid, dashed, wavy and double lines represent baryons, mesons, photon and baryon resonances, respectively. We consider the limit where the photon has zero momentum. Note that this diagram contains not only the magnetic moments but also electric parts.

magnetic moments of the Λ resonances are calculated in the $S = -1$ channel [28]. They compute the diagrams in which a photon couples to resonance field (Fig. 1.3), and the magnetic moments of the resonance are extracted. Here we follow the same procedure. The differences from Ref. [28] are as follows.

- The $N(1535)$ resonance is an isospin doublet, so that there are two components which correspond to proton and neutron resonances.
- Because the $N(1535)$ resonance carries isospin $1/2$, the effect of the ground state $\Sigma^0\Lambda$ transition becomes important, while this effect is almost negligible for the Λ resonances.
- We present a simple estimation of the magnetic moments based on meson-baryon picture of resonances.

We study these points in detail, and compute the magnetic moments of $N(1535)$ resonance in the chiral unitary model. Compared with the results of the quark model [27] and the simple estimation , we discuss the present results.

1.4 Organization of this thesis

Here we present the organization of this thesis. This thesis consists of two main parts, review part (chapters 2 and 3) and research part (chapters 4, 5 and 6). In the review part, we show the foundations of the model, chiral perturbation theory and the method of unitarization, while original works and numerical results are presented in the research part.

In chapter 2, we present the formulation of the ChPT. We construct an effective Lagrangian, based on the spontaneous chiral symmetry breakdown. All the terms of chiral Lagrangian, which will be used in later chapters are introduced. We then present the unitarization method in chapter 3. The analytic structure of the scattering amplitude are studied and the unitarity condition of S-matrix is formulated in the N/D method. Performing ana-

lytic continuation to the complex energy plane, we discuss the branches and Riemann sheets of the scattering amplitudes.

In chapter 4, combining the interaction of the ChPT in chapter 2 and the unitarity condition in chapter 3, we formulate the chiral unitary model. The numerical calculation with a common subtraction constant and comparison with the previous works are shown. We also discuss how to extract the information of resonances from the scattering amplitude. In chapter 5 we introduce the flavor $SU(3)$ breaking terms of chiral Lagrangian. After deriving the meson and baryon masses which satisfy the mass formulae, we formulate the chiral unitary model with the $SU(3)$ breaking effects. The contents of the chapters 4 and 5 are summarized in Ref. [29]. Chapter 6 is devoted to the calculation of the magnetic moments of the $N(1535)$ resonance. We present an estimation of the magnetic moments, and the numerical results are compared with the results obtained in Refs. [27] and [28].

In chapter 7 we discuss and summarize the results obtained in the chapters of research part. The conclusion of this study and future plans are also presented. In Appendices, we show various formulae in detail, which are useful in practical calculations.

Chapter 2

Chiral perturbation theory

In this chapter we construct the Lagrangian of the chiral perturbation theory (ChPT) for meson and baryon systems. ChPT [4, 5, 6, 7] is a low energy effective field theory based on the nonlinear realization of chiral symmetry of QCD. There are many excellent review papers which deal with the ChPT [30, 31, 32, 33], where various examples of applications of ChPT, not only to the processes of the strong interactions but also to weak and electromagnetic processes are presented. The main purpose of this chapter is to show the effective Lagrangian that we will use in the calculations of the chiral unitary model in later chapters. Therefore, we concentrate on the construction of the chiral Lagrangian and do not discuss the applications in detail.

In the following, we first discuss the chiral symmetry of the QCD Lagrangian and its spontaneous breakdown. When a continuous symmetry is spontaneously broken, there appears the Nambu-Goldstone (NG) bosons, whose number corresponds to the broken generators of the symmetry. Then we present a guiding principle to construct effective Lagrangians. In section 2.3, from general point of view, we show a method to construct nonlinear Lagrangians for the system which has a global symmetry and its spontaneous breakdown. The standard transformation low, which is unique up to the redefinition of the NG boson fields, are constructed explicitly. In section 2.4 we deal with the case of the flavor $SU(3)$ QCD, where $SU(3)_L \times SU(3)_R$ breaks into $SU(3)_V$. We construct an effective chiral Lagrangian for octet mesons, which are the NG bosons of this case. Here we establish a counting rule, with which we perform perturbative calculations. This is called chiral perturbation theory. We also introduce the external fields into the effective Lagrangian, in the way consistent with the underlying QCD. These external fields are used for later applications of the chiral unitary model, namely, when introducing explicit $SU(3)$ breaking effects and photon fields. Finally we introduce the octet baryons into the chiral Lagrangian. Because of the large baryon masses, we should reform the counting rule to include momenta of baryons.

2.1 Chiral symmetry

In this section we review the chiral symmetry of N_f flavor QCD and its spontaneous breakdown. Here we discuss the case of QCD with massless quarks, where the Lagrangian is invariant under a global symmetry, which is called chiral symmetry. In real world, due to the non-perturbative vacuum, chiral symmetry is spontaneously broken, which is accompanied by the appearance of the NG bosons, such as pions. Furthermore, chiral symmetry holds only approximately, because quarks have small but nonzero masses. Nevertheless, it is important to discuss the low energy hadron physics respecting chiral symmetry, because the explicit breaking effects are small, and we can neglect and treat them as perturbative collections. Success of the low energy theorems and the current algebra also show the importance of the chiral symmetry in low energy hadron physics [34].

2.1.1 Chiral symmetry of QCD Lagrangian

The N_f flavor QCD Lagrangian without quark masses is given by

$$\begin{aligned} \mathcal{L}^0_{QCD} &= -\frac{1}{2}G_{\mu\nu}G^{\mu\nu} + \bar{q}i\gamma^\mu D_\mu q, \\ G_{\mu\nu} &= \partial_\mu A_\mu - \partial_\nu A_\mu + ig[A_\mu, A_\nu], \quad D_\mu = \partial_\mu + igA_\mu, \quad A_\mu = \sum_a T^a A^a_\mu, \end{aligned} \tag{2.1.1}$$

where q is the quark field which is represented as a N_f component column vector, and $A^a_\mu, (a = 1 \sim 8)$ the gluon fields, which are associated with the color $SU(3)$ gauge symmetry of QCD. In Eq. (2.1.1), T^a are the generators of the color $SU(3)$ and g is the coupling constant of QCD. We define the left-handed and right-handed quarks as

$$\begin{aligned} q_L &= P_L q \ , \quad P_L = \frac{1}{2}(1-\gamma_5) \ , \\ q_R &= P_R q \ , \quad P_R = \frac{1}{2}(1+\gamma_5) \ , \end{aligned} \tag{2.1.2}$$

where the projection operators $P_{L,R}$ have the properties

$$P^2_{L,R} = P_{L,R} \ , \quad P_L P_R = 0 \ , \quad P_L + P_R = 1 \ . \tag{2.1.3}$$

With q_L and q_R, the Lagrangian (2.1.1) is written as

$$\mathcal{L}^0_{QCD} = -\frac{1}{2}G_{\mu\nu}G^{\mu\nu} + \bar{q}_L i\gamma^\mu D_\mu q_L + \bar{q}_R i\gamma^\mu D_\mu q_R \tag{2.1.4}$$

In the Lagrangian (2.1.4), q_L and q_R do not interact with each other, which means that the Lagrangian has a global symmetry $U(N_f)_L \times U(N_f)_R$. However, $U(1)_A$ is broken by axial anomaly at loop level, while $U(1)_V$ holds trivially as the quark number conservation. Except

for these $U(1)$ parts, we refer to the global $SU(N_f)_L \times SU(N_f)_R$ as chiral symmetry of QCD. Under chiral transformations, the quark fields transform as

$$\begin{aligned} &q_L \to Lq_L, \quad L = e^{i\theta_L^a t^a} \in SU(N_f)_L \\ &q_R \to Rq_R, \quad R = e^{i\theta_R^a t^a} \in SU(N_f)_R \end{aligned} \quad (a = 1 \sim N_f^2 - 1) \ , \tag{2.1.5}$$

where $\theta_{L,R}^a$ are arbitrary real parameters and t^a are the generators of $SU(N_f)$. When we consider the group $G = SU(N_f)_L \times SU(N_f)_R$, it is convenient to write an element of G in two component form as

$$\begin{aligned} g &= (R, L) \ , \\ g_R &= (R, 1) \ , \quad g_L = (1, L) \ , \end{aligned} \tag{2.1.6}$$

where we follow the notation in Ref. [1]. Note that R is an element of $SU(N_f)_R$, while g_R is an element of $SU(N_f)_L \times SU(N_f)_R$. Then we define generators as

$$t_R^a = (t^a, 0) \ , \quad t_L^a = (0, t^a) \ , \tag{2.1.7}$$

where t^a are the generators of $SU(N_f)$. Then the commutation relations among t_L^a and t_R^a are given by

$$\begin{aligned} [t_L^a, t_L^b] &= if^{ab}{}_c t_L^c \ , \\ [t_R^a, t_R^b] &= if^{ab}{}_c t_R^c \ , \\ [t_L^a, t_R^b] &= 0 \ , \end{aligned} \tag{2.1.8}$$

where $f^{ab}{}_c$ are the structure constants of $SU(N_f)$.

2.1.2 Spontaneous chiral symmetry breaking

In the previous subsection, the chiral symmetry is manifested among the field operators in the Lagrangian (2.1.1). If an operator has a finite vacuum expectation value, which is not invariant under chiral transformations, then the symmetry is spontaneously broken. If quark condensate $\bar{q}q = \bar{q}_R q_L + \bar{q}_L q_R$ has a finite vacuum expectation value v

$$\langle 0 | \bar{q}_R q_L + \bar{q}_L q_R | 0 \rangle = v \ , \tag{2.1.9}$$

then under $g = (R, L) \in SU(3)_L \times SU(3)_R$, the expectation value transforms

$$\langle 0 | \bar{q}_R q_L + \bar{q}_L q_R | 0 \rangle \xrightarrow{g} \langle 0 | \bar{q}_R R^\dagger L q_L + \bar{q}_L L^\dagger R q_R | 0 \rangle \ , \tag{2.1.10}$$

which is not invariant, because the parameters $\theta_{L,R}^a$ in L and R are arbitrary. In order to consider the transformation which makes the expectation value invariant, we define the generators t_V^a and t_A^a as

$$\begin{aligned} t_V^a &\equiv t_R^a + t_L^a = (t^a, t^a) \ , \\ t_A^a &\equiv t_R^a - t_L^a = (t^a, -t^a) \ . \end{aligned} \tag{2.1.11}$$

Then it turns out that the group $SU(N_f)_V$, which is a subgroup of G generated by t^a_V,

$$\begin{aligned} SU(3)_V \ni h &= e^{i\theta^a_V t^a_V} \\ &= (e^{i\theta^a_V t^a}, e^{i\theta^a_V t^a}) \end{aligned}$$

preserves the symmetry, as we see

$$\langle 0|\bar{q}_R q_L + \bar{q}_L q_R|0\rangle \xrightarrow{h} \langle 0|\bar{q}_R e^{-i\theta^a_V t^a} e^{i\theta^a_V t^a} q_L + \bar{q}_L e^{-i\theta^a_V t^a} e^{i\theta^a_V t^a} q_R|0\rangle = v \ . \tag{2.1.12}$$

In this way we see that the $SU(N_f)_L \times SU(N_f)_R$ symmetry is broken to the subgroup $SU(N_f)_V$. This is called spontaneous breaking of chiral symmetry, where the vacuum expectation value breaks the symmetry of the Lagrangian. From Eq. (2.1.11), it is clear that the commutation relations among t^a_V and t^a_A are given by

$$\begin{aligned} [t^a_V, t^b_V] &= i f^{ab}{}_c t^c_V \ , \\ [t^a_V, t^b_A] &= i f^{ab}{}_c t^c_A \ , \\ [t^a_A, t^b_A] &= i f^{ab}{}_c t^c_V \ . \end{aligned} \tag{2.1.13}$$

This relation is important for later sections.

When the symmetry is spontaneously broken, there is a theorem that the spectrum of physical particles must contain one particle of zero mass and spin for each broken symmetry [35]. These bosons are called the Nambu-Goldstone (NG) bosons. In the case of QCD with two flavors (u and d), the NG bosons are three pions, while in the case of QCD with three flavors (u, d and s), pions, kaons and eta are regarded as the NG bosons.

2.2 Effective field theory

An effective field theory well describes the low energy dynamics, using a phenomenological Lagrangian determined by symmetry restrictions. The asymptotic fields in the effective Lagrangian can be different from those of the fundamental theory, when we integrate out the original degrees of freedom using the path integral formulation. The effects from the original fields in the underlying theory are assumed to be included in the low energy constants of the effective Lagrangian. In order to construct the effective Lagrangian, there is a guiding principle [4, 36, 30];

> For a given set of asymptotic states, perturbation theory with the most general Lagrangian containing all terms allowed by the assumed symmetries will yield the most general S-matrix elements consistent with analyticity, perturbative unitarity, cluster decomposition and the assumed symmetries.

In order to construct the chiral Lagrangian, we adopt this principle in the following.

2.3 Nonlinear realization of chiral symmetry

In this section, from general point of view, we construct an effective Lagrangian in terms of the nonlinearly transforming NG bosons using the principle of symmetry. It is called nonlinear realization of symmetry [2, 37, 38]. We consider a general system, where a global symmetry G is broken spontaneously into a subgroup $H \subset G$. It is important that spontaneous symmetry breaking of the system is already assumed from the beginning. We also assume that G and H are compact, connected and semi-simple Lie groups.

Since we express a symmetry of certain system by a Lie group, in order to specify a representation, we should define representation matrices for group elements $D(g)$ and elements of the representation space ψ, which are transformed by $D(g)$. The meaning of the word "linear" or "nonlinear" is related to the transformation low of the representation ψ. When a field ψ transforms

$$\psi_a \xrightarrow{g} \psi'_a = \sum_b D(g)_{ab}\psi_b \ , \tag{2.3.1}$$

a component of ψ' is written by linear combination of the components of the original ψ. Hence, this is a linear representation of G. The QCD Lagrangian (2.1.1) is one of the examples, where the quark fields linearly transform under $SU(N_f) \times SU(N_f)$.

Historically, the nonlinear representation (of chiral symmetry) is derived from the linear representation through the nonlinear transformation. However, in order to construct the nonlinear Lagrangians it is not necessary to start with linear Lagrangian, such as the linear sigma model [2]. In the following, we discuss the nonlinear representations without using linear representations, parametrizing the transformation low (2.3.1) using the NG boson fields, which make it nonlinear.

2.3.1 Commutation relations of generators

First we briefly summarize several words of the group theory. Let us consider a Lie group G. In some neighborhood of the identity, any element of G is generated by a set of generators, which satisfy commutation relations characterized by the structure constants of the group. The space which spanned by the generators is called the Lie algebra. We can choose any set of generators, as long as they span the Lie algebra. Once we specify the Lie group, associated Lie algebra is determined uniquely. On the other hand, the Lie algebra only determines the structure of the group in some neighborhood of the identity, and the global structure of the group can not be determined by the Lie algebra. For instance, although $O(N)$ and $SO(N)$ have the same generators, their global structures are different each other. In the following, we denote the Lie group and its Lie algebra by G and $\mathcal{G}$, respectively.

Now we consider the symmetry G, which spontaneously breaks into the subgroup H. We separate the generators of the group G into 'unbroken generators' $S^\alpha \in \mathcal{H}$ and 'broken generators' $X^a \in \mathcal{G} - \mathcal{H}$;

$$\{T^A \in \mathcal{G}\} = \{S^\alpha \in \mathcal{H}, X^a \in \mathcal{G} - \mathcal{H}\} \ ,$$

where $A = 1 \cdots, \mathrm{dim}G$, $\alpha = 1, \cdots, \mathrm{dim}H$ and $a = \mathrm{dim}H + 1, \cdots, \mathrm{dim}G$. From the definition, H is a group, so that $\mathcal{H}$ form closed algebra.

Orthonormality of generators are given by

$$\mathrm{tr}(T^i T^j) = \frac{1}{2}\delta^{ij} \ , \tag{2.3.2}$$

where $T^i \in \mathcal{G}$. In order to calculate trace, we may specify a representation of the group G in matrix form. However, Eq. (2.3.2) is satisfied for any representations, once we specify the basis of the Lie algebra. In abstract way, Eq. (2.3.2) means that Cartan metric g^{ij} should be $\delta^{ij}/2$. The Cartan metric only depends on the structure constant of the Lie algebra, and therefore, Eq. (2.3.2) does not depend on representations. From Eq. (2.3.2), normalizations of S^α and X^a are

$$\begin{aligned} &\mathrm{tr}(S^\alpha S^\beta) = \frac{1}{2}\delta^{\alpha\beta}, \quad \mathrm{tr}(X^a X^b) = \frac{1}{2}\delta^{ab}, \\ &\mathrm{tr}(S^\alpha X^a) = 0 \ . \end{aligned} \tag{2.3.3}$$

Next we consider commutation relations of S and X. By definition, the subgroup H should be closed in their operations. This means that commutators of generators should be expressed by themselves.

$$[S^\alpha, S^\beta] = i f^{\alpha\beta}{}_\gamma S^\gamma \ , \tag{2.3.4}$$

where $f^{AB}{}_C$ are structure constants of $\mathcal{G}$. From (2.3.4) and (2.3.3), we can derive

$$\begin{aligned} \mathrm{tr}(S^\alpha [S^\beta, X^a]) =& \mathrm{tr}(S^\alpha S^\beta X^a - S^\alpha X^a S^\beta) \\ =& \mathrm{tr}(S^\alpha S^\beta X^a - S^\beta S^\alpha X^a) \\ =& \mathrm{tr}([S^\alpha, S^\beta] X^a) \\ =& i f^{\alpha\beta}{}_\gamma \mathrm{tr}(S^\gamma X^a) \\ =& 0 \ . \end{aligned}$$

Since $[S^\alpha, X^a]$ is orthogonal to S^α, it is included in $\mathcal{G} - \mathcal{H}$.

$$[\mathcal{H}, \mathcal{G} - \mathcal{H}] \subset \mathcal{G} - \mathcal{H} \tag{2.3.5}$$

Note that this result comes from only the orthonormal condition (2.3.3) and we did not use any other assumptions here.

In general, commutators among X^a are written as a linear combinations of S^α and X^a [2];

$$[X^a, X^b] = if^{ab}{}_\gamma S^\gamma + if^{ab}{}_c X^c. \tag{2.3.6}$$

However, if the algebra is invariant under 'Parity' τ for generators, which is defined by,

$$\begin{aligned} &\tau : \mathcal{G} \to \mathcal{G} \quad \begin{cases} \tau(Y) = +Y & Y \in \mathcal{H} \\ \tau(Y) = -Y & Y \in \mathcal{G} - \mathcal{H} \end{cases}, \\ &\tau^2 = 1 \ , \end{aligned}$$

then commutators among X^a can be written as linear combinations of S^α,

$$[\mathcal{G} - \mathcal{H}, \mathcal{G} - \mathcal{H}] \subset \mathcal{H} \ . \tag{2.3.7}$$

In the case of chiral symmetry of N_f flavor QCD, where $G = SU(N_f)_L \times SU(N_f)_R$, $H = SU(N_f)_V$, $t_A \sim X$ and $t_V \sim S$, Eq. (2.3.7) is valid as shown in Eq. (2.1.13).

Hence the commutation relations among the generators are given as

$$\begin{aligned} [\mathcal{H}, \mathcal{H}] &\subset \mathcal{H} \ , \\ [\mathcal{H}, \mathcal{G} - \mathcal{H}] &\subset \mathcal{G} - \mathcal{H} \ , \\ [\mathcal{G} - \mathcal{H}, \mathcal{G} - \mathcal{H}] &\subset \mathcal{H} \ . \end{aligned} \tag{2.3.8}$$

It is worth noting that elements of G, which are generated by 'the broken generators', do not form a group because the generators are not closed when taking commutators.

2.3.2 Standard transformation

Here we consider to construct a nonlinear representation ψ, which becomes linear when restricted to a given subgroup H. The representation ψ transforms under $g \in G$ and $h \in H$,

$$\begin{aligned} &\psi \xrightarrow{g} D(g)\psi \ , \quad D(g) : \text{nonlinear} \\ &\psi \xrightarrow{h} D(h)\psi \ , \quad D(h) : \text{linear} \end{aligned} \ . \tag{2.3.9}$$

In order to make such a representation, we parametrize the coset space using the NG boson fields ϕ, which also transforms nonlinearly under G. We will obtain a set of transformation

$$\begin{aligned} &\psi \xrightarrow{g} \psi'(g, \phi, \psi) = D(g, \phi)\psi \\ &\phi \xrightarrow{g} \phi'(g, \phi) \end{aligned} \ , \tag{2.3.10}$$

where $\phi'(g, \phi)$ is a nonlinear function of ϕ, so the transformation low of ϕ is nonlinear. Explicit transformation low of ϕ will be given later. In Eq. (2.3.10), although transformed ψ' is written as a linear combination of original ψ, their coefficients include ϕ, so that the transformation low becomes nonlinear. We refer to Eq. (2.3.10) as the standard transformation [37, 38]. It is

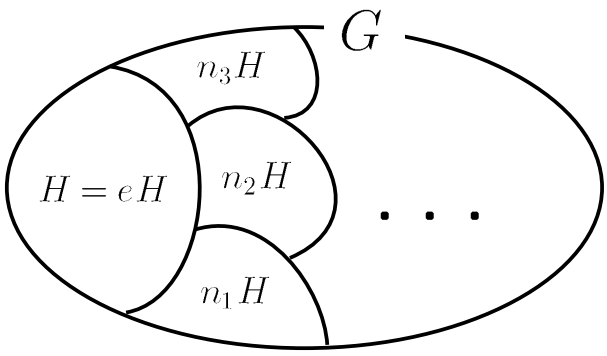

Figure 2.1: A schematic diagram of coset decomposition of G. Here e is a unit element. Since G has an infinite number of elements, the ellipsis denotes an infinite number of cosets, and the number of the representative n_i is also infinite.

shown that all the representations which satisfy the condition (2.3.9) can be made to have the standard form (2.3.10) with suitable redefinition of the NG boson fields, for $SU(2)\times SU(2)$ [39] and for general case [37]. Physically, this means that the redefinition of the NG boson fields does not change the on-shell S-matrix. It is called representation independence, first shown in Ref. [40].

Now we formulate the standard transformation (2.3.10) explicitly. We consider the left coset of the group G. Using the subgroup H, we can decompose the elements of G into left cosets gH. A coset is obtained by multiplying an element of G to all the elements of H from left. Then we pick a representative element n_i from each coset gH. Using n_i, any element of G is written as $g = n_i h$ with $h \in H$. This decomposition is schematically interpreted as in Fig. 2.1. Regarding each coset $H, n_1H, n_2H, \cdots$ as an element, we define the coset space G/H [A)]. If the subgroup H is an invariant subgroup of G, namely,

$$gHg^{-1} = H \quad \text{for} \quad \forall g \in G \ , \tag{2.3.11}$$

then G/H form a group. In the present case, from Eq. (2.3.5) we see that generators in $\mathcal{H}$ do not commute with those in $\mathcal{G} - \mathcal{H}$, which means the $\mathcal{H}$ is not an invariant subalgebra, subsequently, H is not an invariant subgroup. Therefore, G/H does not form a group.

Next we consider the transformation of a representative n under $g_0 \in G$. When we act an element g_0 for n, the image of n belongs to a coset $n'H$, such that (Fig. 2.2)

$$g_0 n = n'(n, g_0)h(n, g_0) \ . \tag{2.3.12}$$

In the present case H is generated by the generators S and G/H by the broken generators

[A)] The coset is a set of elements of the group, so that "an elements of the coset space" is also a set of elements of the group. The representative is an element of the group.

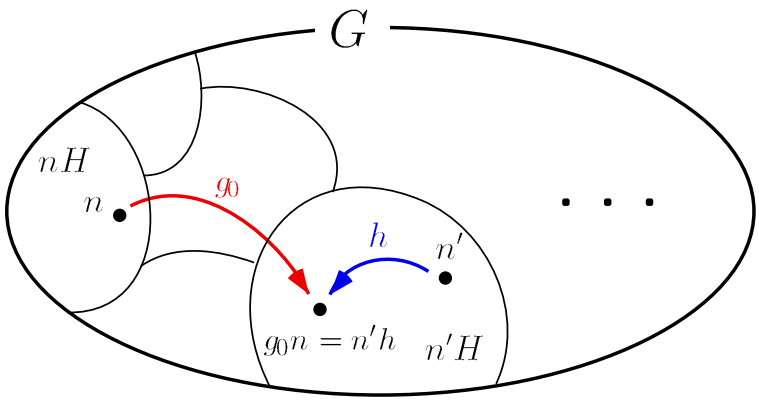

Figure 2.2: Schematic diagram of Eq. (2.3.12). A representative n transforms under g_0.

X;

$$n = e^{i\phi\cdot X} \ , \quad \phi\cdot X = \sum_a \phi_a X_a \ . \tag{2.3.13}$$

$$h = e^{iu\cdot S} \ , \quad u\cdot S = \sum_\alpha u_\alpha S_\alpha \ . \tag{2.3.14}$$

with real parameters ϕ and u. Now we identify the NG boson fields with the variables ϕ_a. Then ϕ becomes a representation of G, so that it transforms under g_0. Eq. (2.3.12) requires

$$g_0 e^{i\phi\cdot X} = e^{i\phi'(\phi,g_0)\cdot X} e^{iu'(\phi,g_0)\cdot S} \ , \tag{2.3.15}$$

and we have a transformation low

$$\phi \overset{G}{\to} \phi'(\phi, g_0) \ , \tag{2.3.16}$$

which satisfy Eq. (2.3.15), and is a nonlinear transformation of ϕ. Simultaneously, we define the transformation low of ψ as

$$\begin{aligned} \psi &\overset{G}{\to} D(e^{iu'(\phi,g_0)\cdot S})\psi \\ &= D(h(\phi, g_0))\psi \ , \end{aligned} \tag{2.3.17}$$

which is also a nonlinear transformation due to the nonlinearity of the ϕ field. Eqs. (2.3.16) and (2.3.17) give the standard form of the nonlinear representation. Both of the transformations depend on the NG boson field ϕ_a through Eq. (2.3.15).

When we consider the transformation low under $h_0 \in H$, $h_0 n$ is written as

$$h_0 n = e^{iu\cdot S} e^{i\phi\cdot X} \ . \tag{2.3.18}$$

Using the formula of Baker-Campbell-Hausdorff

$$e^X e^Y = \exp\left\{X + Y + \frac{1}{2}[X,Y] + \frac{1}{12}([X,[X,Y]] + [Y,[Y,X]]) + \cdots\right\},$$

and Eq. (2.3.8), we obtain

$$h_0 n = e^{iu\cdot S} e^{i\phi\cdot X} = e^{i\phi'\cdot X} e^{iu\cdot S} = e^{i\phi'\cdot X} h_0 \ . \tag{2.3.19}$$

Note that in general ϕ' is different from ϕ. On the other hand, from Eq. (2.3.18) we have

$$h_0 n = h_0 e^{i\phi\cdot X} h_0^{-1} h_0 \ . \tag{2.3.20}$$

Comparing Eqs. (2.3.19) with (2.3.20), we obtain

$$\begin{aligned} e^{i\phi'\cdot X} &= h_0 e^{i\phi\cdot X} h_0^{-1} \\ h_0 e^{i\phi\cdot X} &= e^{i\phi'\cdot X} h_0 \ , \end{aligned} \tag{2.3.21}$$

which is the transformation low of ϕ under h_0, and is a special case of Eq. (2.3.15). We see that $h(n, g_0) = e^{iu'(\phi, g_0)}$ in Eq. (2.3.15) does not depend on ϕ here, therefore, the transformation low of ϕ is linear. The transformation low for ψ becomes

$$\psi \xrightarrow{H} D(h_0)\psi \ , \tag{2.3.22}$$

where h_0 does not depend on ϕ. Since the nonlinearity of the transformation (2.3.17) comes from the dependence of ϕ, Eq. (2.3.22) gives a linear transformation.

2.4 Chiral perturbation theory of mesons

In this section we consider the QCD Lagrangian (2.1.1) with three flavors, where chiral symmetry and its spontaneous breaking is denoted as $SU(3)_L \times SU(3)_R \to SU(3)_V$. We construct an effective Lagrangian of ChPT for pseudo scalar mesons of $SU(3)$ octet, using the standard transformation low for the NG bosons (2.3.15). In this case, the generators S and X are

$$S \sim t_V^a = (t^a, t^a) \ , \quad X \sim t_A^a = (t^a, -t^a) \ , \quad a = 1 \sim 8. \tag{2.4.1}$$

Under $g_0 = (R_0, L_0) \in G = SU(3)_L \times SU(3)_R$, the transformation law of ϕ (2.3.15) is

$$(R_0, L_0)(\exp\{i\phi\cdot t\}, \exp\{-i\phi\cdot t\}) = (\exp\{i\phi'\cdot t\}, \exp\{-i\phi'\cdot t\})(\exp\{iu'\cdot t\}, \exp\{iu'\cdot t\}) \ . \tag{2.4.2}$$

From each component, we obtain

$$\begin{aligned} R_0 \exp\{i\phi\cdot t\} &= \exp\{i\phi'\cdot t\} \exp\{iu'\cdot t\} \\ L_0 \exp\{-i\phi\cdot t\} &= \exp\{-i\phi'\cdot t\} \exp\{iu'\cdot t\} \end{aligned} \ . \tag{2.4.3}$$

We take conjugation of the lower equation,

$$\begin{aligned} R_0 \exp\{i\phi\cdot t\} &= \exp\left\{i\phi'\cdot t\right\}\exp\left\{iu'\cdot t\right\} \\ \exp\{i\phi\cdot t\}\, L_0^\dagger &= \exp\left\{-iu'\cdot t\right\}\exp\left\{i\phi'\cdot t\right\} \end{aligned} . \tag{2.4.4}$$

Multiplying both side of these equations each other, we obtain the transformation law of ϕ as

$$R_0 \exp\{2i\phi\cdot t\}\, L_0^\dagger = \exp\left\{2i\phi'\cdot t\right\}. \tag{2.4.5}$$

The NG bosons which appear due to the spontaneously symmetry breaking are pseudo scalar octet mesons. We assign these mesons for the field ϕ as

$$\phi\cdot t \sim \Phi \equiv \sum_{a=1}^{8}\frac{\lambda^a}{\sqrt{2}}\Phi^a = \begin{pmatrix} \frac{1}{\sqrt{2}}\pi^0+\frac{1}{\sqrt{6}}\eta & \pi^+ & K^+ \\ \pi^- & -\frac{1}{\sqrt{2}}\pi^0+\frac{1}{\sqrt{6}}\eta & K^0 \\ K^- & \bar{K}^0 & -\frac{2}{\sqrt{6}}\eta \end{pmatrix}. \tag{2.4.6}$$

With proper normalization, we define the chiral fields $U(\Phi)$ and $\xi(\Phi)$ as

$$U(\Phi) = \exp\left\{\frac{i\sqrt{2}\Phi}{f}\right\}, \quad \xi(\Phi) = \exp\left\{\frac{i\Phi}{\sqrt{2}f}\right\}, \quad U(\Phi) = \xi^2(\Phi), \tag{2.4.7}$$

where f is a quantity of mass dimension, and will be identified with the meson decay constant. From Eqs. (2.4.4) and (2.4.5), U and ξ satisfy the following transformation laws under $SU(3)_L \times SU(3)_R$;

$$U \xrightarrow{g_0} RUL^\dagger, \quad U^\dagger \xrightarrow{g_0} LUR^\dagger\ , \tag{2.4.8}$$

$$\xi \xrightarrow{g_0} h(\Phi, g_0)^\dagger \xi L = R^\dagger \xi h(\Phi, g_0)\ , \tag{2.4.9}$$

where $h(\Phi, g_0) \in H$ is defined as

$$h(\Phi, g_0) = \exp\left\{iu'(\Phi, g_0)\cdot t\right\}\ . \tag{2.4.10}$$

The $SU(3)$ matrix $h(\Phi, g_0)$ gives a nonlinear transformation under G because of the dependence of Φ field, which transforms nonlinearly.

In order to construct an effective Lagrangian, we organize the most general Lagrangian with $U(\Phi)$ fields, following the principle in section 2.2. First we define a chiral counting rule, which enables us to perform perturbative calculation in clear way. Since we consider the octet mesons as the NG bosons, their masses are zero. This means that if the spatial momentum of a meson $\mathbf{p}$ is small, we can also regard the four-momentum $p_\mu = (|\mathbf{p}|, \mathbf{p})$ as small. This is also valid when we introduce small explicit breakings of chiral symmetry, where mesons do have masses, so that the four momentum of a meson is expressed as

$$p_\mu = (\sqrt{m^2 + |\mathbf{p}|^2}, \mathbf{p}). \tag{2.4.11}$$

As long as the mass m is small, p_μ is also regarded as small. This point will be important when we introduce baryons into ChPT.

In this way the Lagrangian is expanded in powers of momenta, or derivatives of meson fields. At low energy region, where the momentum of each particle is small, lower order terms should be dominant and we can neglect higher order terms. Chiral Lagrangian should be invariant under chiral transformation (2.4.8), Lorentz transformation, charge conjugation, parity and time reversal. Due to the Lorentz invariance, the Lagrangian contains even number of derivatives

$$\mathcal{L}_{\text{eff}}(U) = \sum_n \mathcal{L}_{2n}^M(U) \ , \tag{2.4.12}$$

where $2n$ denotes the number of derivatives. Defining U as a quantity of order $\mathcal{O}(1)$, a term with n derivative is counted as $\mathcal{O}(p^n)$. In Eq. (2.4.12), the terms with $n = 0$ provide unity, because of the unitarity of the field U. Therefore the lowest order Lagrangian consists of two derivatives of U field and is uniquely given as

$$\mathcal{L}_2^M = \frac{f^2}{4}\text{Tr}(\partial_\mu U^\dagger \partial^\mu U) \ , \tag{2.4.13}$$

which is of order $\mathcal{O}(p^2)$. Another candidate

$$\mathcal{L}_2^{M\prime} = C\text{Tr}(U\partial_\mu U^\dagger U \partial^\mu U^\dagger) \ , \tag{2.4.14}$$

seems to be allowed, however, it can be rewritten in the same form as Eq. (2.4.13) with $C = -f^2/4$, using the property of trace and the following formula (2.4.15). Since the chiral field U is a unitary matrix, $U^\dagger U = 1$. Taking derivative of both side,

$$\begin{aligned} \partial_\mu(U^\dagger U) &= 0 \\ \partial_\mu U^\dagger \cdot U + U^\dagger \cdot \partial_\mu U &= 0 \\ \partial_\mu U^\dagger \cdot U &= -U^\dagger \cdot \partial_\mu U \ . \end{aligned} \tag{2.4.15}$$

This formula is important to construct the chiral Lagrangian.

It is easy to show that Lagrangian (2.4.13) is invariant under $SU(3)_L \times SU(3)_R$

$$\begin{aligned} \frac{f^2}{4}\text{Tr}(\partial_\mu U^\dagger \partial^\mu U) &\to \frac{f^2}{4}\text{Tr}(\partial_\mu (LU^\dagger R^\dagger)\partial^\mu (RUL^\dagger)) \\ &= \frac{f^2}{4}\text{Tr}(L(\partial_\mu U^\dagger)\cdot R^\dagger R(\partial^\mu U)L^\dagger) \\ &= \frac{f^2}{4}\text{Tr}(\partial_\mu U^\dagger \partial^\mu U). \end{aligned}$$

We see that the trace in Lagrangian (2.4.13) is essential to be invariant under $SU(3)_L \times SU(3)_R$. The factor $f^2/4$ in Eq. (2.4.13) is fixed to provide the properly normalized kinetic term for the NG bosons

$$\begin{aligned}\frac{f^2}{4}\mathrm{Tr}(\partial_\mu U^\dagger \partial^\mu U) =& \frac{f^2}{4}\mathrm{Tr}\left[\partial_\mu\left(1-\frac{i\sqrt{2}\Phi}{f}+\cdots\right)\partial^\mu\left(1+\frac{i\sqrt{2}\Phi}{f}+\cdots\right)\right]\\ =& \frac{f^2}{4}\mathrm{Tr}\left[\frac{2}{f^2}\partial_\mu\Phi\partial^\mu\Phi+\cdots\right]\\ =& \frac{1}{2}\mathrm{Tr}(\partial_\mu\Phi\partial^\mu\Phi)+\cdots,\end{aligned}$$

where the last line contains terms of even number of meson fields and derivatives. They represent multimeson interactions with one coupling constant f. In the next order $\mathcal{O}(p^4)$, the most general Lagrangian contains three terms [5, 6, 7]

$$\begin{aligned}\mathcal{L}_4^M =& L_1\left[\mathrm{Tr}(\partial_\mu U^\dagger\partial^\mu U)\right]^2 + L_2\mathrm{Tr}(\partial_\mu U^\dagger\partial_\nu U)\mathrm{Tr}(\partial^\mu U^\dagger\partial^\nu U)\\ &+ L_3\mathrm{Tr}(\partial_\mu U^\dagger\partial^\mu U\partial_\nu U^\dagger\partial^\nu U),\end{aligned} \tag{2.4.16}$$

where L_1, L_2 and L_3 are the low energy constants. Here we use Eq. (2.4.15) in order to omit the terms which can be rewritten in the same form. The higher order Lagrangians are also constructed in the same way.

2.5 External fields and local chiral transformation

In chapters 5 and 6, we introduce explicitly $SU(3)$ breaking effects and couplings to the photon field. Therefore we need to contain these effects in the Lagrangian. In order to introduce them in the framework of ChPT, we extend the QCD Lagrangian (2.1.1) with the inclusion of the external fields. The Lagrangian with external fields is given as

$$\mathcal{L}_{QCD}^{\mathrm{ext}} = \mathcal{L}_{QCD}^0 + \bar{q}\gamma^\mu(v_\mu+\gamma^5 a_\mu)q - \bar{q}(s-i\gamma_5 p)q, \tag{2.5.1}$$

where the external fields v_μ, a_μ, s and p are vector current, axial vector current, scalar and pseudo scalar field, respectively. For convenience, we define l_μ and r_μ as

$$l_\mu \equiv v_\mu - a_\mu, \quad r_\mu \equiv v_\mu + a_\mu. \tag{2.5.2}$$

Suppose that under $SU(3)_L \times SU(3)_R$ the external fields l_μ, r_μ, s and p obey the transformation law as

$$\begin{aligned}s+ip &\to R(x)(s+ip)L(x)^\dagger,\\ l_\mu &\to L(x)l_\mu L(x)^\dagger + iL(x)\partial_\mu L(x)^\dagger,\\ r_\mu &\to R(x)r_\mu R(x)^\dagger + iR(x)\partial_\mu R(x)^\dagger.\end{aligned} \tag{2.5.3}$$

Now the Lagrangian (2.5.1) is invariant under $SU(3)_L \times SU(3)_R$. Note that this transformation is local because it contains a derivative. We then incorporate the external fields and their transformation law with the effective chiral Lagrangian (2.4.12). As a consequence of local transformation, derivative of the field $U(\Phi)$ should be replaced by covariant derivative. The covariant derivatives are given by [5, 6, 7]

$$D_\mu U = \partial_\mu U - i r_\mu U + i U l_\mu, \quad D_\mu U^\dagger = \partial_\mu U^\dagger + i U^\dagger r_\mu - i l_\mu U^\dagger. \tag{2.5.4}$$

It is straightforward to check the transformation low of $D_\mu U$;

$$\begin{aligned} D_\mu U = \partial_\mu U - i r_\mu U + i U l_\mu \rightarrow & \partial_\mu (RUL^\dagger) - i(R r_\mu R^\dagger + iR\partial_\mu R^\dagger)(RUL^\dagger) \\ & + i(RUL^\dagger)(L l_\mu L^\dagger + iL\partial_\mu L^\dagger) \\ = & (\partial_\mu R)\cdot UL^\dagger + R\partial_\mu UL^\dagger + RU(\partial_\mu L^\dagger) \\ & - iRr_\mu UL^\dagger + R(-R^\dagger\partial_\mu R)UL^\dagger + iRUl_\mu L^\dagger - RU(\partial_\mu L^\dagger) \\ = & R\partial_\mu UL^\dagger - iRr_\mu UL^\dagger + iRUl_\mu L^\dagger \\ = & R(D_\mu U)L^\dagger. \end{aligned}$$

For convenience, we define χ and field strength tensors as

$$\chi = 2B_0(s+ip)\ , \tag{2.5.5}$$

$$F_L^{\mu\nu} = \partial^\mu l^\nu - \partial^\nu l^\mu - i[l^\mu, l^\nu]\ , \quad F_R^{\mu\nu} = \partial^\mu r^\nu - \partial^\nu r^\mu - i[r^\mu, r^\nu] \tag{2.5.6}$$

with a constant B_0. Their transformation lows are

$$\chi \rightarrow R\chi L^\dagger\ , \tag{2.5.7}$$

$$F_L^{\mu\nu} \rightarrow LF_L^{\mu\nu}L^\dagger\ , \quad F_R^{\mu\nu} \rightarrow RF_R^{\mu\nu}R^\dagger\ . \tag{2.5.8}$$

Up to order $\mathcal{O}(p^2)$, the most general Lagrangian consistent with Lorentz invariance and local chiral symmetry (2.5.3) is given as

$$\mathcal{L}_2^M = \frac{f^2}{4}\mathrm{Tr}(D_\mu U^\dagger D^\mu U + U^\dagger\chi + \chi^\dagger U)\ . \tag{2.5.9}$$

In the next order $\mathcal{O}(p^4)$, there appear seven terms in addition to three terms in the Lagrangian (2.4.16), with changing derivatives into covariant derivative;

$$\begin{aligned} \mathcal{L}_4^M = & L_1\left[\mathrm{Tr}(D_\mu U^\dagger D^\mu U)\right]^2 + L_2\mathrm{Tr}(D_\mu U^\dagger D_\nu U)\mathrm{Tr}(D^\mu U^\dagger D^\nu U) \\ & + L_3\mathrm{Tr}(D_\mu U^\dagger D^\mu U D_\nu U^\dagger D^\nu U) + L_4\mathrm{Tr}(D_\mu U^\dagger D^\mu U)\mathrm{Tr}(U^\dagger\chi + \chi^\dagger U) \\ & + L_5\mathrm{Tr}\left[(D_\mu U^\dagger D^\mu U)(U^\dagger\chi + \chi^\dagger U)\right] + L_6\left[\mathrm{Tr}(U^\dagger\chi + \chi^\dagger U)\right]^2 \\ & + L_7\left[\mathrm{Tr}(U^\dagger\chi - \chi^\dagger U)\right]^2 + L_8\mathrm{Tr}(\chi^\dagger U\chi^\dagger U + U^\dagger\chi U^\dagger\chi) \\ & - iL_9\mathrm{Tr}(F_R^{\mu\nu}D_\mu U D_\nu U^\dagger + F_L^{\mu\nu}D_\mu U^\dagger D_\nu U) + L_{10}\mathrm{Tr}(U^\dagger F_R^{\mu\nu}U F_{L\mu\nu})\ . \end{aligned} \tag{2.5.10}$$

In this way, $\mathcal{O}(p^4)$ Lagrangian contains ten low energy constants $L_1 \sim L_{10}$.

In deriving the above Lagrangians, we use the counting rule for the external fields;

$$U, \xi : \mathcal{O}(1) \ , \quad a_\mu, v_\mu(l_\mu, r_\mu) : \mathcal{O}(p) \ , \quad s, p(\chi) : \mathcal{O}(p^2) \ . \tag{2.5.11}$$

Actually up to this level, there is no reason to include the terms containing χ at the same order as two meson derivatives. For the moment, we just remark that χ is counted of order $\mathcal{O}(p^2)$, or, in other words, chiral expansion is a double expansion in the momentum and in χ, with a fixed ratio χ/p^2. The reason for this is due to the assignment of quark mass matrix $s \sim \mathbf{m}$ and the Gell-Mann-Oakes-Renner(GMOR) relation [41].

Using these external fields, we can introduce $SU(3)$ breaking effects and photon couplings. For example, in order to include the quark mass term, we choose

$$s = \mathbf{m}, \quad \mathbf{m} = \begin{pmatrix} m_u & & \\ & m_d & \\ & & m_s \end{pmatrix} , \tag{2.5.12}$$

or, to consider the couplings to photons, we choose

$$v_\mu = eQA_\mu, \quad Q = \frac{1}{3}\begin{pmatrix} 2 & & \\ & -1 & \\ & & -1 \end{pmatrix} , \tag{2.5.13}$$

where A_μ is the photon field and e is the unit electric charge. It is worth noting that once special directions in flavor space are selected in this way, chiral symmetry is explicitly broken. Indeed, the expression (2.5.12) and (2.5.13) do not satisfy the transformation law (2.5.3). However, the advantage of this method is that we break the chiral symmetry in exactly the same way as the QCD Lagrangian (2.5.1) does.

2.6 Chiral perturbation theory of mesons and baryons

In this section, we introduce $SU(3)$ octet baryon fields in the chiral Lagrangian [42]. For the chiral Lagrangian obtained in previous sections, we can introduce any kinds of fields using the transformation low (2.3.17). To do this, we need following procedures.

- We specify the representation of the additional field and make a transformation low (2.3.17).
- We construct the most general Lagrangian with respect to the symmetry constraints, using the NG boson fields and the additional field.

In this way we can construct chiral Lagrangian not only with baryon octet fields but also, for example, with vector meson fields or baryon decouplet fields.

As an example, in the $SU(2)$ ChPT, we introduce the $SU(2)$ baryon field, namely nucleon field. Since the nucleon is classified as a doublet of $SU(2)$ symmetry, we assign a fundamental representation of $SU(2)$ for the nucleon field N;

$$N \equiv \begin{pmatrix} p \\ n \end{pmatrix}, \quad \bar{N} = N^\dagger \gamma^0 = (\bar{p}, \bar{n}) \ , \tag{2.6.1}$$

and they transform as

$$N \xrightarrow{G} hN \ , \quad \bar{N} \xrightarrow{G} \bar{N} h^\dagger \ , \tag{2.6.2}$$

where $h = h(\phi, g_0) \in SU(2)_V$. In the case of $SU(3)$, we introduce the octet baryon field, therefore we assign an adjoint representation of $SU(3)$ for baryon field B;

$$B \equiv \sum_{a=1}^{8} \lambda^a B^a = \begin{pmatrix} \frac{1}{\sqrt{2}}\Sigma^0 + \frac{1}{\sqrt{6}}\Lambda & \Sigma^+ & p \\ \Sigma^- & -\frac{1}{\sqrt{2}}\Sigma^0 + \frac{1}{\sqrt{6}}\Lambda & n \\ \Xi^- & \Xi^0 & -\frac{2}{\sqrt{6}}\Lambda \end{pmatrix}, \quad \bar{B} = B^\dagger \gamma^0 \ .$$

Because B and $\bar{B}$ are adjoint representations, they transform under $SU(3)_L \times SU(3)_R$ as

$$\begin{aligned} &B \xrightarrow{G} hBh^\dagger \ , \\ &\bar{B} \xrightarrow{G} (hBh^\dagger)^\dagger \gamma^0 = h\bar{B}h^\dagger \ , \end{aligned} \tag{2.6.3}$$

where $h = h(\Phi, g_0) \in SU(3)_V$ defined in (2.4.10).

2.6.1 Difficulties of treating baryons in chiral perturbation theory

When we introduce the baryon fields into ChPT, a problem concerning the chiral counting appears. As a consequence of the transformation law (2.6.3), a chiral invariant mass term $M_0 \mathrm{Tr}(\bar{B}B)$ can exist

$$\begin{aligned} M_0 \mathrm{Tr}(\bar{B}B) \rightarrow & M_0 \mathrm{Tr}(h\bar{B}h^\dagger hBh^\dagger) \\ = & M_0 \mathrm{Tr}(\bar{B}B) \ . \end{aligned}$$

The presence of the mass term in baryon sector can be understood by the spontaneous breaking of chiral symmetry, but this is an important difference from the meson case. In the meson sector, we define chiral counting rule using the fact that the meson mass is zero or very small. However, we see that in the baryon sector a large mass can exist. This means that m in the expression (2.4.11) might be large, so that the energy of baryon $p_0 = \sqrt{m^2 + |\mathbf{p}|^2}$ is not small when $|\mathbf{p}|$ is small. We cannot treat the four-momentum of the baryons as a small quantity any more.

This fact also causes the complicated counting for loops. In the meson sector, contributions from n-loop diagrams are suppressed of order $(p^2)^n$, so that there is a one-to-one

correspondence between the loop and small momentum expansions of Lagrangian. However, in the baryon sector, the baryon propagator gives a contribution of the baryon mass instead of typical low momenta, since the baryon mass is not small.

Actually there is a method which allows us to perform power counting in a consistent way [42]. In that case the counting rule becomes more complicated and many terms appear even in the next-to-leading order. Another way to avoid this difficulty is to adopt the heavy baryon chiral perturbation theory (HBchPT), where we take the limit $p/M_0 \ll 1$. With this approximation, the number of terms are suppressed and counting rule becomes much simpler. We will discuss briefly this formulation later.

2.6.2 Chiral counting rule for baryons

Here we discuss the counting rule for baryons. First we write down the quantities, with which the chiral Lagrangian is constructed. Then we assign power counting of order $\mathcal{O}(p^n)$ for these quantities.

In order to construct a meson-baryon couplings, it is convenient to introduce the quantities, which transforms

$$O \to hOh^\dagger \ , \tag{2.6.4}$$

because of the transformation low of B and $\bar{B}$ (2.6.3). First we only use the meson fields to construct O, which has physical meanings. Such quantities are the vector current V_μ and axial vector current A_μ defined by

$$\begin{aligned} V_\mu &= -\frac{i}{2}(\xi^\dagger\partial_\mu\xi + \xi\partial_\mu\xi^\dagger) \ , \\ A_\mu &= -\frac{i}{2}(\xi^\dagger\partial_\mu\xi - \xi\partial_\mu\xi^\dagger) \ . \end{aligned} \tag{2.6.5}$$

Next we introduce the external fields. Using χ defined in Eq. (2.5.5), we construct scalar (σ) and pseudo scalar (ρ) quantities

$$\begin{aligned} \sigma &\equiv \xi\chi^\dagger\xi + \xi^\dagger\chi\xi^\dagger \ , \\ \rho &\equiv \xi\chi^\dagger\xi - \xi^\dagger\chi\xi^\dagger \ . \end{aligned} \tag{2.6.6}$$

With the currents l_μ and r_μ in Eq. (2.5.2) we extend Eq. (2.6.5) as

$$\begin{aligned} V_\mu &= -\frac{i}{2}(\xi^\dagger\partial_\mu\xi + \xi\partial_\mu\xi^\dagger) + \frac{1}{2}(\xi^\dagger r_\mu\xi + \xi l_\mu\xi^\dagger) \ , \\ A_\mu &= -\frac{i}{2}(\xi^\dagger\partial_\mu\xi - \xi\partial_\mu\xi^\dagger) + \frac{1}{2}(\xi^\dagger r_\mu\xi - \xi l_\mu\xi^\dagger) \ . \end{aligned} \tag{2.6.7}$$

Using the field strength tensors (2.5.6), we define

$$\tilde{F}_R^{\mu\nu} = \xi^\dagger F_R^{\mu\nu}\xi \ , \quad \tilde{F}_L^{\mu\nu} = \xi F_L^{\mu\nu}\xi^\dagger \ . \tag{2.6.8}$$

From the transformation lows (2.4.9), (2.5.7) and (2.5.8), it is straightforward to show that V_μ, A_μ, σ, ρ, $\tilde{F}_R^{\mu\nu}$ and $\tilde{F}_L^{\mu\nu}$ satisfy the transformation (2.6.4).

According to the detailed discussion of chiral power counting for the baryons in Ref. [42], the quantities we defined above are counted as

$$\sigma, \rho : \mathcal{O}(p^2) \ , \quad A_\mu, V_\mu : \mathcal{O}(p) \ , \quad \tilde{F}_R^{\mu\nu}, \tilde{F}_L^{\mu\nu} : \mathcal{O}(p^2) \ , \tag{2.6.9}$$

and baryon fields are

$$B, \bar{B} : \mathcal{O}(1) \ , \quad [D_\mu, B] : \mathcal{O}(1) \ , \quad i\gamma^\mu [D_\mu, B] - M_0 B : \mathcal{O}(p) \ . \tag{2.6.10}$$

With the rules (2.6.9) and (2.6.10), we construct the effective Lagrangian with mesons and baryons.

2.6.3 Chiral Lagrangian of mesons and baryons

In baryon case, an effective Lagrangian can contain the terms of order odd number of momentum,

$$\mathcal{L}_{\text{eff}}(B, \Phi) = \sum_n \mathcal{L}_n^{MB}(B, \Phi) \ . \tag{2.6.11}$$

Considering the Lorentz structure of the currents, the most general Lagrangian with baryons in the lowest order of the chiral expansion is given by

$$\mathcal{L}_1^{MB} = \mathrm{Tr}\Big(\bar{B}(i\not{\mathcal{D}} - M_0)B - D(\bar{B}\gamma^\mu\gamma_5\{A_\mu, B\}) - F(\bar{B}\gamma^\mu\gamma_5[A_\mu, B]) \Big) \ , \tag{2.6.12}$$

$$\mathcal{D}_\mu B = \partial_\mu B + i[V_\mu, B] \ , \tag{2.6.13}$$

where D and F are coupling constants and M_0 denotes a common mass of the octet baryons. Here we follow the notation in Ref. [43].

In next-to-leading order $\mathcal{O}(p^2)$, we have twenty one terms in the most general effective Lagrangian [42]. Among them, here we show the terms that we will use in later chapters, the $SU(3)$ breaking terms, which are given by

$$\mathcal{L}_{SB}^{MB} = b_0 \mathrm{Tr}(\bar{B}B)\mathrm{Tr}(\sigma) + b_1 \mathrm{Tr}\big(\bar{B}\{\sigma, B\}\big) + b_2 \mathrm{Tr}\big(\bar{B}[\sigma, B]\big) \ , \tag{2.6.14}$$

and photon coupling terms

$$\mathcal{L}_{(\gamma)}^{MB} = b_6^d \mathrm{Tr}\big(\bar{B}\sigma^{\mu\nu}\{F_{\mu\nu}^+, B\}\big) + b_6^f \mathrm{Tr}\big(\bar{B}\sigma^{\mu\nu}[F_{\mu\nu}^+, B]\big) \ , \tag{2.6.15}$$

where

$$F_+^{\mu\nu} = F_L^{\mu\nu} + F_R^{\mu\nu} \ , \quad \sigma^{\mu\nu} = \frac{i}{2}[\gamma^\mu, \gamma^\nu] \ . \tag{2.6.16}$$

2.6.4 Heavy baryon chiral perturbation theory

The heavy baryon ChPT [44, 45] has been developed by introducing the techniques of heavy quark effective theory [46, 47]. We consider heavy static baryons whose velocities are almost unchanged during interactions with mesons. The momentum of a baryon p^μ is written as

$$p^\mu = M_B v^\mu + k^\mu, \tag{2.6.17}$$

where M_B is the mass of the baryon, k^μ is off-shell part of momentum and v^μ is the four-velocity of the baryon, which satisfies $v_\mu v^\mu = 1$. Because we consider the heavy baryon, M_B is large and k^μ is small. We then define the velocity dependent fields [48]

$$B_v(x) \equiv e^{iM_B v_\mu x^\mu} P_v^+ B(x), \quad P_v^+ = \frac{1+\not{v}}{2} \ , \tag{2.6.18}$$

in Lorentz covariant way. In the baryon rest frame, the operator P_v^+ projects a relativistic baryon to the non-relativistic one of the Dirac spinor. The advantage of the use of this field is that this field B_v obeys a massless Dirac equation;

$$\begin{aligned}
i\not{\partial} B_v =& i\not{\partial}\left(e^{iM_B v_\mu x^\mu}\frac{1+\not{v}}{2}B(x)\right) \\
=& \frac{1}{2}\left[i\gamma_\nu \partial^\nu e^{iM_B v_\mu x^\mu} B(x) + i\gamma_\nu \partial^\nu \gamma_\lambda v^\lambda e^{iM_B v_\mu x^\mu} B(x)\right] \\
=& \frac{1}{2}\left[i\gamma_\nu i M_B v^\nu e^{iM_B v_\mu x^\mu} B(x) + i e^{iM_B v_\mu x^\mu}\gamma_\nu \partial^\nu B(x)\right. \\
& \left. + i\gamma_\nu\gamma_\lambda v^\lambda i M_B v^\nu e^{iM_B v_\mu x^\mu} B(x) + i\gamma_\nu\gamma_\lambda v^\lambda e^{iM_B v_\mu x^\mu}\partial^\nu B(x)\right] \\
=& \frac{1}{2}\Big[-M_B \not{v} e^{iM_B v_\mu x^\mu} B(x) + e^{iM_B v_\mu x^\mu} i\not{\partial} B(x) \\
& - \not{v}\not{v} M_B e^{iM_B v_\mu x^\mu} B(x) + i\not{\partial} B(x)\not{v} e^{iM_B v_\mu x^\mu}\Big] \\
=& \frac{1}{2}\Big[-M_B \not{v} e^{iM_B v_\mu x^\mu} B(x) + e^{iM_B v_\mu x^\mu} M_B B(x) \\
& - M_B e^{iM_B v_\mu x^\mu} B(x) + M_B B(x)\not{v} e^{iM_B v_\mu x^\mu}\Big] \\
=& 0 \ ,
\end{aligned} \tag{2.6.19}$$

which means that we can avoid the appearance of the baryon mass term in the Lagrangian. Using the B_v field, we can construct the lowest order Lagrangian which corresponds to $\mathcal{L}_1^{MB} + \mathcal{L}_{SB}^{MB}$

$$\begin{aligned}
\mathcal{L}_v =& \mathrm{Tr}\Big(\bar{B}_v(iv^\mu \mathcal{D}_\mu)B_v - D(\bar{B}_v S_v^\mu \{\xi_\mu, B_v\}) - F(\bar{B}_v S_v^\mu [\xi_\mu, B_v])\Big) \\
& - \mathrm{Tr}(\tilde{b}_1 \bar{B}_v \sigma B_v + \tilde{b}_2 \bar{B}_v B_v \sigma) - \tilde{b}_0 \mathrm{Tr}(\sigma)\mathrm{Tr}(\bar{B}_v B_v)
\end{aligned} \ , \tag{2.6.20}$$

where spin operators S_v^μ are defined as

$$\begin{aligned}
& v\cdot S_v = 0 \ , \quad S_v^2 B_v = -\frac{3}{4} B_v \ , \\
& \{S_v^\lambda, S_v^\sigma\} = \frac{1}{2}(v^\lambda v^\sigma - g^{\lambda\sigma}) \ , \quad [S_v^\lambda, S_v^\sigma] = i\epsilon^{\lambda\alpha\beta} v_\alpha (S_v)_\beta \ .
\end{aligned} \tag{2.6.21}$$

Chapter 3

Unitarization and the analytic structure of the T-matrix

In this chapter we study the N/D unitarization method [49] and the analytic structure of the T-matrix. There are several methods which recover the unitarity of the S-matrix, such as solving the Bethe-Salpeter Equation (BSE) [13], Inverse Amplitude Method (IAM) [50], N/D method [22] and so on. In this work, we adopt the N/D method, since this method provides a general form of the T-matrix, using the dispersion relation and the analyticity of the inverse of the T-matrix. Recently the N/D method has been applied to coupled channel meson-baryon scatterings [22, 51]. It was found that the final form of the T-matrix derived from the N/D method is essentially equivalent to the result of Ref. [13], which is derived from the BSE with an approximation. One of the advantages of this method is that we obtain the T-matrix in an analytic form, so that we can perform analytic continuation to the complex energy plane.

In sections 3.1 and 3.2, from general point of view, we derive the optical theorem from the unitarity of the S-matrix, and discuss the analytic structure of the scattering amplitude, where unitarity cut comes from the optical theorem and unphysical cut comes from the optical theorem for crossing diagrams. We also show that the kinematical singularities appear in the case of meson-baryon scatterings with non-relativistic reduction. We then concentrate on the case of the meson-baryon scatterings, and obtain the general form of the T-matrix through the N/D method, neglecting the contribution from the unphysical cut. In section 3.4, we discuss the T-matrix amplitude in the complex plane, performing the analytic continuation of the variable $\sqrt{s}$. Due to the discontinuities of unitarity cut, the complex variable z has two Riemann sheets and the T-matrix amplitude has two branches. In order to search poles, we choose the most relevant branches for scattering line, calculating the loop integral numerically and comparing branches with the value on the scattering line.

3.1 Unitarity of S-matrix

Here we derive the optical theorem from the unitarity condition of the S-matrix for coupled channel scatterings. In order to conserve probability, scattering S-matrix should be a unitary matrix satisfying

$$S^\dagger S = 1 \ . \tag{3.1.1}$$

We define the T-matrix as $S = 1 - iT$, then the unitarity condition requires that

$$\begin{aligned} (1-iT)^\dagger(1-iT) &= 1 \\ 1 + i(T^\dagger - T) + T^\dagger T &= 1 \\ -i(T^\dagger - T) &= T^\dagger T \ . \end{aligned} \tag{3.1.2}$$

In order to compute the matrix element of Eq. (3.1.2), we multiply final and initial states $\langle f|, |i\rangle$, and insert a sum of complete sets for intermediate states which is labeled by k. Since we consider the coupled channel problems, we denote several channels by the labels f, i and k. Then Eq. (3.1.2) becomes

$$-i\big[\langle f|T^\dagger|i\rangle - \langle f|T|i\rangle\big] = \sum_k \left(\prod_{n_k} \int \frac{d^3q_{n_k}}{(2\pi)^3}\frac{1}{2E_{n_k}}\right) \langle f|T^\dagger|k\rangle\langle k|T|i\rangle \ , \tag{3.1.3}$$

where q_{n_k} and E_{n_k} are the momentum and energy of the particle n_k in the intermediate state k. We take product over the label n_k up to the number of particles in the state k, and we take summation for all possible intermediate states k. We introduce the invariant T-matrix amplitude $T_{fi}(2\pi)^4\delta^{(4)}(\sum_{n_f} p_{n_f} - \sum_{n_i} p_{n_i}) = \langle f|T|i\rangle$ and obtain

$$\begin{aligned} -i(T^*_{if} - T_{fi}) &= \sum_k \left(\prod_{n_k} \int \frac{d^3q_{n_k}}{(2\pi)^3}\frac{1}{2E_{n_k}}\right) T^*_{kf}T_{ki}(2\pi)^4\delta^{(4)}\left(\sum_{n_i} p_{n_i} - \sum_{n_k} q_{n_k}\right) \ , \\ &= \sum_k \rho_k T^*_{kf}T_{ki} \ , \end{aligned} \tag{3.1.4}$$

where p_i is the momentum of the particle i in the initial state and we have dropped an overall delta function for momentum conservation of initial and final states. In Eq. (3.1.4), we define the phase space integral ρ_k for an intermediate state k as

$$\rho_k = \int d\Pi_k \equiv \left(\prod_{n_k} \int \frac{d^3q_{n_k}}{(2\pi)^3}\frac{1}{2E_{n_k}}\right) (2\pi)^4\delta^{(4)}\left(\sum_{n_i} p_{n_i} - \sum_{n_k} q_{n_k}\right) \ . \tag{3.1.5}$$

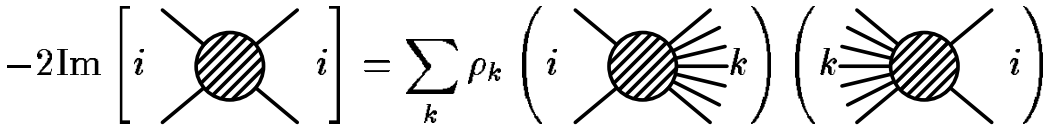

Figure 3.1: Diagrammatic interpretation of the optical theorem. Shaded bubbles denote the T-matrix amplitude. The lines in channel k represent all possible intermediate states.

In the case of $i = f$, where the final state is the same as the initial state, we obtain the optical theorem

$$i[T_{ii} - T_{ii}^*] = \sum_k \rho_k T_{ki}^* T_{ki} \tag{3.1.6}$$

$$-2\mathrm{Im}[T_{ii}] = \sum_k \rho_k |T_{ki}|^2 \ , \tag{3.1.7}$$

The expression (3.1.7) is interpreted diagrammatically as shown in Fig. 3.1. For later convenience, we consider that the T-matrix amplitude is the function of s, the square of the total energy in the center of mass frame, and we define the square of the energy of the threshold of the intermediate state i as $(s_+)_i$. The phase space ρ_i takes non-zero value only above the threshold $s > (s_+)_i$, so that the diagonal elements of the T-matrix amplitude T_{ii} have an imaginary part only above the threshold $s > (s_+)_i$. This result directly comes from the unitarity of S-matrix, namely the conservation of the probability.

3.2 Singularities of the scattering amplitudes

In this section, we discuss the singularities of the scattering amplitudes in the complex energy plane. In general, there are two kinds of cuts in the scattering amplitudes; the unitarity cut, which is required by unitarity condition, and the unphysical left hand cut, which comes from the unitarity condition for the crossing diagrams. In addition, there appear the kinematical singularities when we apply the nonrelativistic reduction for the amplitude of meson-baryon scatterings. In the following, we first discuss general properties of analytic function when the branch cut appears, then consider the singularities of the scattering amplitudes one by one.

3.2.1 Branch point and branch cut

We first consider the branch cut of a general function $f(z)$. In this subsection, we denote the complex variable by z and real variable by x. Let us consider a function $f(x)$ defined on the real axis and

$$\begin{cases} f(x) \in \mathbf{R} & \text{for} \quad x \leq x_b \\ f(x) \in \mathbf{C} & \text{for} \quad x_b < x \end{cases} . \tag{3.2.1}$$

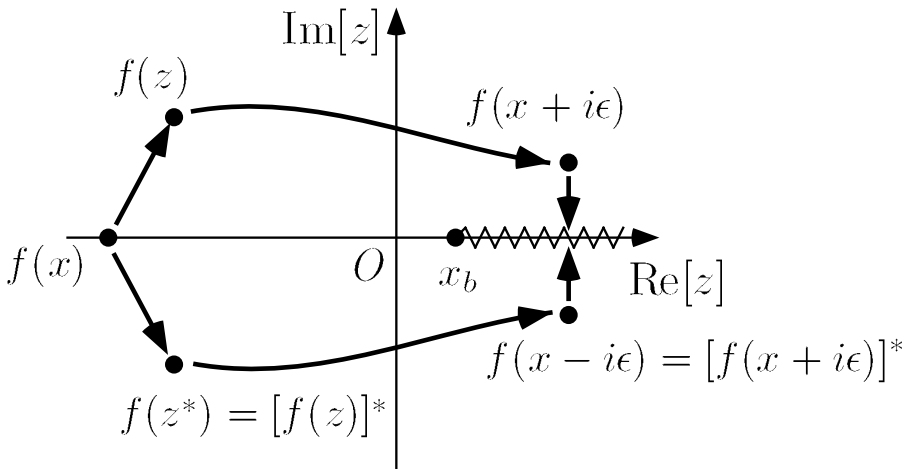

Figure 3.2: Schwarz reflection principle and analytic continuation of the function $f(x)$.

We show that the analytic continuation of $f(x)$ in the whole z plane has a branch point at x_b. If there is no singularity in the complex plane, we can use the Schwarz reflection principle [52];

> If a function $f(z)$ is 1) analytic over some region including the real axis and 2) real when z is real, then
>
> $$[f(z)]^* = f(z^*) \ . \tag{3.2.2}$$

In the present case, we can apply this theorem for the whole complex plane except for the real axis of $x > x_b$, because $f(x)$ is not real there (Fig. 3.2). When $x \leq x_b$, in the vicinity of the real axis, with a small real number ϵ, we have

$$f(x - i\epsilon) = [f(x + i\epsilon)]^* \ . \tag{3.2.3}$$

In the limit $\epsilon \to 0$, $f(x + i\epsilon) \to f(x) \in \mathbf{R}$, such that

$$\begin{aligned} f(x - i0) &= [f(x + i0)]^* \\ &= f(x + i0) \quad \text{for} \quad x \leq x_b \ . \end{aligned} \tag{3.2.4}$$

We see that the upper half plane and lower half plane are continuously connected. However, when $x_b < x$, Eq. (3.2.3) means that in the limit $\epsilon \to 0$, $f(x + i\epsilon) \to f(x) \in \mathbf{C}$, such that

$$\begin{aligned} f(x - i0) &= [f(x + i0)]^* \\ &= f(x + i0) - 2i\mathrm{Im}[f(x + i0)] \quad \text{for} \quad x_b < x \ . \end{aligned} \tag{3.2.5}$$

Eq. (3.2.5) indicates the existence of the branch point at x_b and the discontinuity on the real axis;

$$\mathrm{Disc}[f(x)] \equiv f(x + i0) - f(x - i0) = 2i\mathrm{Im}[f(x)] \quad \text{for} \quad x_b < x \ . \tag{3.2.6}$$

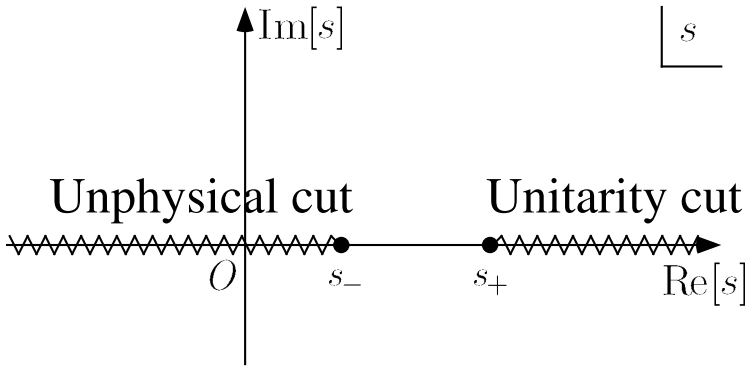

Figure 3.3: Unitarity and unphysical cuts of the T-matrix in the complex s plane.

Usually we choose a branch cut from x_b to $+\infty$, however, in principle the direction of branch cut is arbitrary, once the position of the branch point is fixed. The direction is determined by our definition of the region of the argument of the first Riemann sheet.

3.2.2 Unitarity cut

From Eq. (3.1.7), we see that T_{ii} is

$$\begin{cases} T_{ii}(s) \in \mathbf{R} & \text{for} \quad s \leq (s_+)_i \\ T_{ii}(s) \in \mathbf{C} & \text{for} \quad (s_+)_i < s \end{cases} . \tag{3.2.7}$$

As we have shown in the previous subsection, this implies the existence of a cut which runs from $(s_+)_i$ to $+\infty$ (Fig. 3.3). Since this cut is caused by the unitarity condition, we call it the unitarity cut, or the right hand cut. In later calculations of the chiral unitary model, we take this cut into account in order to incorporate the unitarity condition with ChPT.

3.2.3 Unphysical cut

Next we consider the unphysical cut, which comes form the crossing diagrams. For the sake of simplicity, we discuss the single channel scattering of two particles with the same mass m. In this case the threshold s_+ is $4m^2$, so that we have unitarity cut from $4m^2$ to $+\infty$. The cut comes from the existence of an imaginary part of the T-matrix in the region where the s-channel process becomes on the mass shell

$$s > 4m^2 . \tag{3.2.8}$$

Similarly, the T-matrix amplitude also has imaginary part in the region where the u- and t-channel processes become on the mass shell

$$t > 4m^2 , \quad u > 4m^2 . \tag{3.2.9}$$

In the center of mass frame, the Mandelstam variables s, t and u are given by [53]

$$\begin{aligned} s &= 4(\mathbf{k}^2 + m^2) \\ t &= -2\mathbf{k}^2(1 - \cos\theta) \ , \\ u &= -2\mathbf{k}^2(1 + \cos\theta) \end{aligned} \tag{3.2.10}$$

where θ is the scattering angle and $\mathbf{k}$ is the three momentum in the center of mass frame;

$$|\mathbf{k}| = \frac{\sqrt{s - 4m^2}}{2} \ . \tag{3.2.11}$$

The conditions (3.2.9) require that

$$\begin{aligned} \left(2m^2 - \frac{s}{2}\right)(1 \pm \cos\theta) &> 4m^2 \\ 2m^2 - \frac{s}{2} &> \frac{4m^2}{1 \pm \cos\theta} \\ -\frac{s}{2} &> \frac{4m^2}{1 \pm \cos\theta} - 2m^2 \\ s &< -\frac{8m^2}{1 \pm \cos\theta} + 4m^2 \ , \end{aligned}$$

where $-1 \leq \cos\theta \leq 1$. So we find

$$(3.2.9) \Rightarrow s < 0 \ , \tag{3.2.12}$$

We have shown that the conditions (3.2.9) requires the existence of the cut on $s < 0$. When the mass of the two particles are different, the unphysical cut runs from $s_- \equiv (m - M)^2$ to $-\infty$ [54] as shown in Fig. 3.3.

3.2.4 Kinematical singularities

Here we discuss the kinematical singularities [51], which appear in the meson-baryon scatterings with non-relativistic reduction. The unitarity and unphysical cuts appear for general T-matrix amplitude of scatterings, while this kinematical singularities appear only for the present case. When we take a relativistic approach for the meson-baryon scattering, the scattering amplitudes are generally written as

$$T_{rel}(s,t) = \bar{u}\left[A(s,t) + \frac{1}{2}(q_1 + q_2)^\mu \gamma_\mu B(s,t)\right] u \ , \tag{3.2.13}$$

where q_1 and q_2 are momenta of the incoming and outgoing mesons, respectively. The invariant amplitudes $A(s,t)$ and $B(s,t)$ are functions of s and t, so that there is no kinematical singularity. However, when we apply the nonrelativistic reduction for Eq. (3.2.13), in the

center of mass frame, the T-matrix amplitude is written as [55]

$$T_{NR}(\sqrt{s},t) = \left(\frac{E+M}{2M}\right)\left[g(\sqrt{s},t) + i\boldsymbol{\sigma}\cdot(\mathbf{q}_2\times\mathbf{q}_1)h(\sqrt{s},t)\right] , \tag{3.2.14}$$

$$g(\sqrt{s},t) = \frac{1}{2(M+E)^2}\Big[(4M(E+M)-t)A + \big\{(\sqrt{s}+M)(t+4|\mathbf{q}|^2) + 4Mw(E+M)\big\}B\Big] ,$$

$$h(\sqrt{s},t) = \frac{1}{(M+E)^2}\Big[(\sqrt{s}+M)B - A\Big] ,$$

where M and E are the mass and energy of baryon, and $w = \sqrt{s} - E$ is the energy of meson. Here we use common masses for all baryons and mesons. We see that T_{NR} is now a function of t and $\sqrt{s}$, not s.

Since a point on the s plane corresponds to two points in the $\sqrt{s}$ plane, the unitarity cut on the s plane appears as two cuts in the $\sqrt{s}$ plane, $(-\infty, -\sqrt{s_+})$ and $(\sqrt{s_+}, \infty)$ (Fig. 3.5). We discuss the effects of these singularities later.

3.3 N/D method for meson-baryon scatterings

In the previous section, we have discussed the general structure of the scattering amplitude and found that there are two kinds of cuts in the T-matrix. Now we concentrate on the coupled channel meson-baryon scatterings, and derive a general form of the T-matrix using the N/D method [49]. Let us assume that the intermediate states of the meson-baryon scatterings are composed of one octet meson and one octet baryon. We do not consider multi-mesons and excited baryons, such as $\pi\pi N$ and $\pi\Delta$. In this case, the phase space ρ_i in Eq. (3.1.7) is written as

$$\rho_i(\sqrt{s}) = \frac{2M_i\bar{q}_i(\sqrt{s})}{4\pi\sqrt{s}} \quad \text{for} \quad \sqrt{s_+} < \sqrt{s} , \tag{3.3.1}$$

where $\bar{q}_i(\sqrt{s})$ is the three-momentum of the intermediate meson, which is defined by

$$\bar{q}_i(\sqrt{s}) = \frac{\sqrt{(s-(M_i-m_i)^2)(s-(M_i+m_i)^2)}}{2\sqrt{s}} . \tag{3.3.2}$$

In the N/D method, we divide the T-matrix into numerator (N) and denominator (D) as

$$T(s) = \frac{N(s)}{D(s)} . \tag{3.3.3}$$

The point of the N/D method is that we assign the effect of unitarity cut in the denominator, and the unphysical cut in the numerator. The reason for this is that the inverse of the T-matrix also has a branch cut due to the unitarity condition, as we see by multiplying $(T^*)^{-1}$

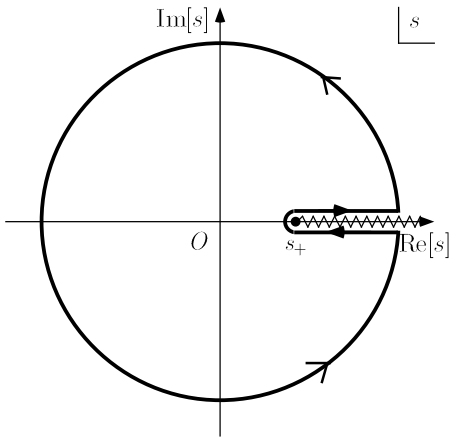

Figure 3.4: Contour of the dispersion integral for $D(s)$ in the complex s plane.

from left and $(T)^{-1}$ from right for Eq. (3.1.6),

$$\begin{aligned} i[(T^*)^{-1}T_{ii}(T)^{-1} - (T^*)^{-1}T^*_{ii}(T)^{-1}] &= \sum_k \rho_k (T^*)^{-1}T^*_{ki}T_{ki}(T)^{-1} \\ i[(T^{-1})^*_{ii} - T^{-1}_{ii}] &= \sum_k \rho_k \delta_{ik} \\ 2\mathrm{Im}[(T)^{-1}_{ii}] &= \rho_i \ . \end{aligned} \tag{3.3.4}$$

Following Ref. [22], we neglect the contribution of the unphysical cut, which means that we take only the s-channel diagrams into account and crossing diagrams are neglected. Using the contour of the integral shown in Fig. 3.4, we apply the dispersion relation to $D(s)$ with a constant subtraction

$$\begin{aligned} N_{ij}(s) &= \delta_{ij} \\ D_{ij}(s) = T^{-1}_{ij}(s) &= \delta_{ij}\Big(\tilde{a}_i(s_0) + \frac{s-s_0}{2\pi}\int_{(s_+)_i}^{\infty} ds' \frac{\rho_i(s')}{(s'-s)(s'-s_0)}\Big) + \mathcal{T}^{-1}_{ij}(s) \ . \end{aligned} \tag{3.3.5}$$

where $(s_+)_i$ is the value of s at the threshold of the channel i, and s_0 is the subtraction point. The parameter $\tilde{a}_i(s_0)$ is a subtraction constant and is a free parameter within the N/D method. The matrix $\mathcal{T}_{ij}(s)$ indicates the contribution from CDD poles [56] and couplings among the channels, which cannot be determined by the unitarity condition only. Later we will determine this $\mathcal{T}_{ij}(s)$ by the chiral perturbation theory.

Note that $D(s)$ is a function of s because so far we have been considering it on the complex s plane. As we have seen in subsection 3.2.4, however there appear kinematical singularities, the two cuts in the complex $\sqrt{s}$ plane, which give different dispersion integrals from Eq. (3.3.5). In Fig. 3.5, we show the contour of the integral in the $\sqrt{s}$ plane. However, it is shown that we can absorb the effects from the kinematical singularities into the same dispersion integrals

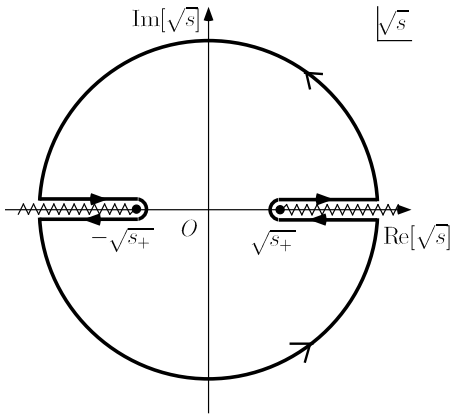

Figure 3.5: Contour of the dispersion integral for $D(\sqrt{s})$ in the complex $\sqrt{s}$ plane. The radius of the enclosing circle is extended to infinity.

in the complex s plane [51]. The contribution from the cut $(\sqrt{s_+}, \infty)$ is

$$\frac{\sqrt{s}-\sqrt{s_0}}{\pi}\int_{(\sqrt{s}_+)_i}^{\infty} d(\sqrt{s}')\frac{\mathrm{Im}T_{ii}^{-1}(\sqrt{s}')}{(\sqrt{s}'-\sqrt{s})(\sqrt{s}'-\sqrt{s}_0)}\ , \tag{3.3.6}$$

and the contribution from the cut $(-\infty, -\sqrt{s_+})$ is

$$\begin{aligned}
&\frac{\sqrt{s}-\sqrt{s_0}}{\pi}\int_{-\infty}^{-(\sqrt{s}_+)_i} d(\sqrt{s}')\frac{\mathrm{Im}T_{ii}^{-1}(\sqrt{s}')}{(\sqrt{s}'-\sqrt{s})(\sqrt{s}'-\sqrt{s}_0)}\\
=&\frac{\sqrt{s}-\sqrt{s_0}}{\pi}\int_{\infty}^{(\sqrt{s}_+)_i} d(-\sqrt{s}')\frac{\mathrm{Im}T_{ii}^{-1}(-\sqrt{s}')}{(-\sqrt{s}'-\sqrt{s})(-\sqrt{s}'-\sqrt{s}_0)}\\
=&\frac{\sqrt{s}-\sqrt{s_0}}{\pi}\int_{(\sqrt{s}_+)_i}^{\infty} d(\sqrt{s}')\frac{\mathrm{Im}T_{ii}^{-1}(-\sqrt{s}')}{(\sqrt{s}'+\sqrt{s})(\sqrt{s}'+\sqrt{s}_0)}\ .
\end{aligned} \tag{3.3.7}$$

From the function (3.3.1), we see that

$$\mathrm{Im}T_{ii}^{-1}(-\sqrt{s}) = -\mathrm{Im}T_{ii}^{-1}(\sqrt{s}) = -\frac{\rho_i(\sqrt{s})}{2}\ . \tag{3.3.8}$$

Summing Eqs. (3.3.6) and (3.3.7) up, and using Eq. (3.3.8), we obtain total dispersion integral as

$$\begin{aligned}
&\frac{\sqrt{s}-\sqrt{s_0}}{2\pi}\int_{(\sqrt{s}_+)_i}^{\infty} d(\sqrt{s}')\rho_i(\sqrt{s}')\left[\frac{1}{(\sqrt{s}'-\sqrt{s})(\sqrt{s}'-\sqrt{s}_0)}-\frac{1}{(\sqrt{s}'+\sqrt{s})(\sqrt{s}'+\sqrt{s}_0)}\right]\\
=&\frac{\sqrt{s}-\sqrt{s_0}}{2\pi}\int_{(\sqrt{s}_+)_i}^{\infty} d(\sqrt{s}')\rho_i(\sqrt{s}')\left[\frac{2\sqrt{s}'(\sqrt{s}-\sqrt{s_0})}{(s'-s)(s'-s_0)}\right]\\
=&\frac{s-s_0}{2\pi}\int_{(\sqrt{s}_+)_i}^{\infty} 2\sqrt{s'}d(\sqrt{s}')\frac{\rho_i(\sqrt{s}')}{(s'-s)(s'-s_0)}\\
=&\frac{s-s_0}{2\pi}\int_{(s_+)_i}^{\infty} ds'\frac{\rho_i(\sqrt{s}')}{(s'-s)(s'-s_0)}\ .
\end{aligned}$$

Then we can use the same dispersion integral by only changing the variables of T-matrix and CDD poles from s to $\sqrt{s}$, and obtain

$$T_{ij}^{-1}(\sqrt{s}) = \delta_{ij}\Big(\tilde{a}_i(s_0) + \frac{s-s_0}{2\pi}\int_{(s_+)_i}^{\infty} ds' \frac{\rho_i(s')}{(s'-s)(s'-s_0)}\Big) + \mathcal{T}_{ij}^{-1}(\sqrt{s}) \ , \tag{3.3.9}$$

This is a general form of the T-matrix in the coupled channel scatterings which satisfies the unitarity condition.

Let us define the G function by

$$G_i(\sqrt{s}) = -\tilde{a}_i(s_0) - \frac{s-s_0}{2\pi}\int_{(s_+)_i}^{\infty} ds' \frac{\rho_i(s')}{(s'-s)(s'-s_0)} \ , \tag{3.3.10}$$

which takes the same form as, up to a constant, the ordinary meson-baryon loop function:

$$G_i(\sqrt{s}) = i\int \frac{d^4q}{(2\pi)^4}\frac{2M_i}{(P-q)^2 - M_i^2 + i\epsilon}\frac{1}{q^2 - m_i^2 + i\epsilon} \ . \tag{3.3.11}$$

This integral should be regularized by an appropriate regularization scheme. In the dimensional regularization, the integral is calculated as

$$\begin{aligned} G_i(\sqrt{s}) = \frac{2M_i}{(4\pi)^2}\Bigg\{ & a_i(\mu) + \ln\frac{M_i^2}{\mu^2} + \frac{m_i^2 - M_i^2 + s}{2s}\ln\frac{m_i^2}{M_i^2} \\ & + \frac{\bar{q}_i}{\sqrt{s}}\Big[\ln(s - (M_i^2 - m_i^2) + 2\sqrt{s}\bar{q}_i) + \ln(s + (M_i^2 - m_i^2) + 2\sqrt{s}\bar{q}_i) \\ & - \ln(-s + (M_i^2 - m_i^2) + 2\sqrt{s}\bar{q}_i) - \ln(-s - (M_i^2 - m_i^2) + 2\sqrt{s}\bar{q}_i)\Big]\Bigg\}, \end{aligned} \tag{3.3.12}$$

where μ is a regularization scale and a_i are the subtraction constants. In the tree level approximation, only the $\mathcal{T}_{ij}$ term survives in Eq. (3.3.9), which is identified with the interactions V obtained by ChPT at the tree level. Therefore, the resulting T-matrix is written as

$$T^{-1} = -G + (V)^{-1} \ , \tag{3.3.13}$$

$$T = [1 - VG]^{-1}V \ . \tag{3.3.14}$$

Since we know the analytic forms of V and G, we can write the T-matrix in analytic way through Eq. (3.3.14). This is one of the advantages of this method, with which we can perform the analytic continuation of the $\sqrt{s}$ to the whole complex plane. Eq. (3.3.14) is rewritten as

$$T = V + VGT \ . \tag{3.3.15}$$

This is the algebraic equation for the T-matrix, which corresponds to the integral BSE. The diagrammatic interpretation of Eq. (3.3.15) is shown in Fig. 3.6.

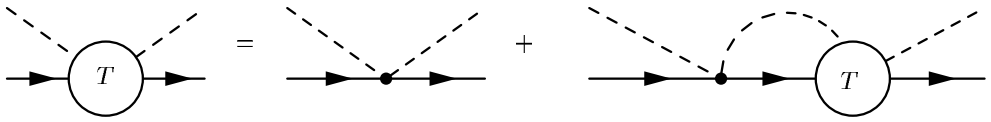

Figure 3.6: Diagrammatic interpretation of Eq. (3.3.15).

3.4 Scattering amplitudes in the complex plane

In this section, we discuss the analytic structure of the T-matrix and the loop function, which are functions of $\sqrt{s}$. When a resonance is well pronounced in the scatterings, the T-matrix amplitude can be approximated by a sum of the Breit-Wigner and background terms around the resonance region [19];

$$T_{ij} \sim \frac{g_i g_j}{\sqrt{s} - M_R + i\Gamma_R/2} + T_{ij}^{BG} \ , \tag{3.4.1}$$

where M_R and Γ_R are the mass and decay width of the resonance, and g_i and g_j are the coupling strength of the resonance R to the channel i and j, respectively. The background T_{ij}^{BG} is assumed to be a slowly varying function. This implies the existence of the pole of the T-matrix amplitude at $z_R = M_R - i\Gamma_R/2$ in complex z plane. However, causality requires the absence of poles in the physical (first Riemann) sheet [57]. Therefore, we search the unphysical sheets for poles. The multivalued nature of T-matrix comes from the unitarity cut of the T-matrix.

In the following, we deal with the case of single channel and drop the index i, for the sake of simplicity. First we see that the formal solution of the T-matrix (3.3.14) satisfies the unitarity condition (3.3.4), considering the loop function (3.3.12) on the real axis. Next we perform the analytic continuation to the complex $\sqrt{s}$ plane, and observe that the analytic structure of $T^{-1}(\sqrt{s})$ is same as the loop function $G(\sqrt{s})$. Using the discontinuity of $G(\sqrt{s})$, we define the Riemann sheets where we search for poles.

Before going into technical details, we briefly note about the words "Riemann sheets" and "branches". Let us consider a multi-valued function $w = f(z)$. In order to avoid multi-valueness, we put a branch cut on the z plane. Then we connect usual z plane, which is defined in the region $0 \leq \theta < 2\pi$, to another "Riemann sheet", which is defined in the region $2\pi \leq \theta < 4\pi$. Although we usually do not distinguish the difference between z_1 and $z_2 = z_1 e^{2\pi i}$, the points z_1 on the first Riemann sheet and $z_2 = z_1 e^{2\pi i}$ on the second Riemann sheet are mapped to the different points $w_1 = f(z_1)$ and $w_2 = f(z_2 = z_1 e^{2\pi i})$, respectively. We call these w_1 and w_2 planes as "branches". We show this schematically in Fig. 3.7. In this way we extend z plane into several Riemann sheets, and the function $w = f(z)$ is uniquely defined on each Riemann sheet.

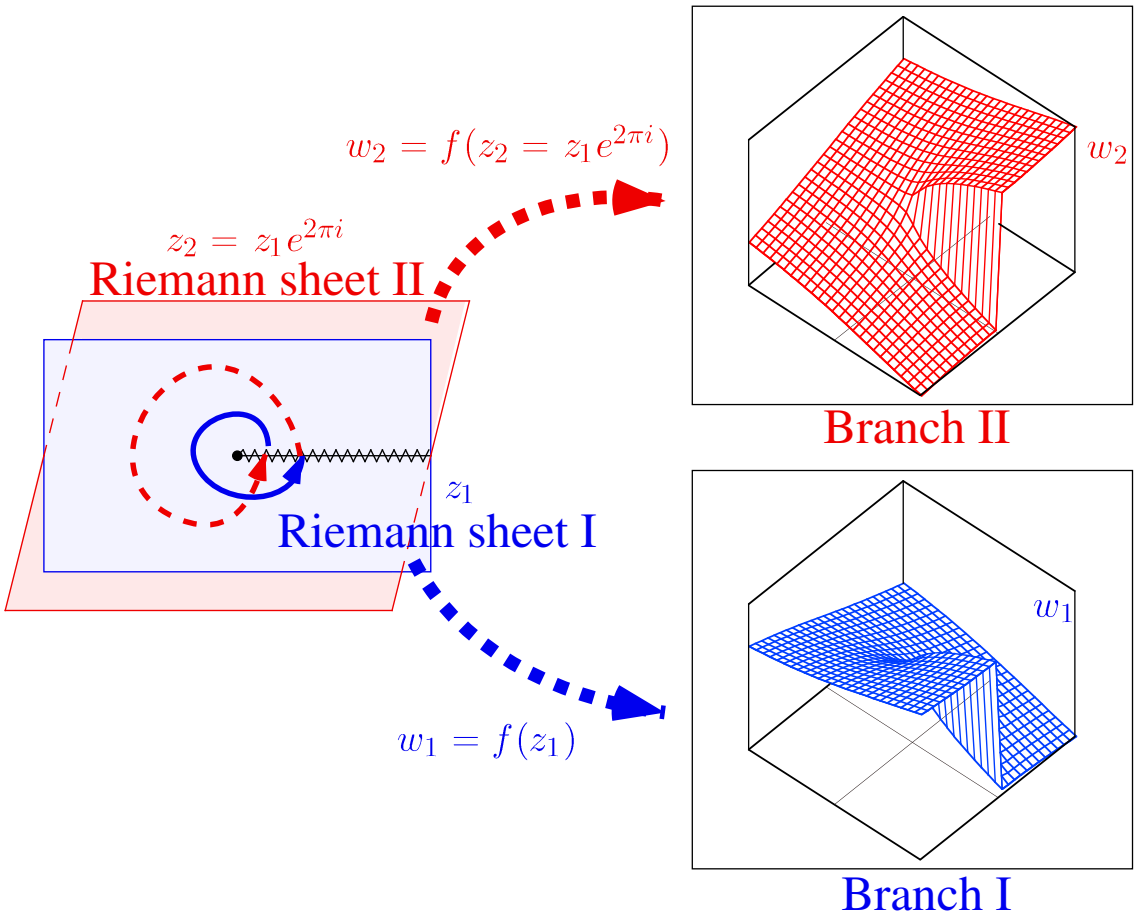

Figure 3.7: Riemann sheets and branches. The points z_1 and $z_2 = z_1 e^{2\pi i}$ are mapped to the different points $w_1 = f(z_1)$ and $w_2 = f(z_2)$

3.4.1 Loop function on the scattering line

Here we consider the loop function (3.3.12) on the real axis. Since $G(\sqrt{s})$ is a multivalued function even on the real axis due to the logarithmic and square root functions, we define the value with respect to the first Riemann sheet, namely we restrict the arguments of the variable $0 \leq \theta < 2\pi$. We referred to this values as "on the scattering line", which is used in the practical calculation of the scattering problem. For convenience, we rewrite the loop function as

$$\begin{aligned} G(\sqrt{s}) =& \frac{2M}{16\pi^2}\Big\{a(\mu) + \ln\frac{M^2}{\mu^2} + \frac{m^2 - M^2 + s}{2s}\ln\frac{m^2}{M^2} \\ &+ \frac{\lambda^{1/2}}{2s}\Big[\ln(s - (M^2 - m^2) + \lambda^{1/2}) + \ln(s + (M^2 - m^2) + \lambda^{1/2}) \\ &- \ln(-s + (M^2 - m^2) + \lambda^{1/2}) - \ln(-s - (M^2 - m^2) + \lambda^{1/2})\Big]\Big\}, \end{aligned} \tag{3.4.2}$$

with the Källen function

$$\begin{aligned}\lambda^{1/2}(s,M^2,m^2) &= \sqrt{s^2+M^4+m^4-2sM^2-2sm^2-2m^2M^2} \\ &= \sqrt{(s-(M-m)^2)(s-(M+m)^2)} = 2\sqrt{s}\bar{q}\ .\end{aligned} \tag{3.4.3}$$

In Eq. (3.4.2), the terms in the first line are always real for real values of $\sqrt{s}$. The imaginary part of the loop function is produced from the terms

$$\frac{\lambda^{1/2}}{2s}[\ln(A)+\ln(B)-\ln(C)-\ln(D)]\ ,$$

where we define

$$\begin{aligned}A &= s-(M^2-m^2)+\lambda^{1/2}\ ,\\ B &= s+(M^2-m^2)+\lambda^{1/2}\ ,\\ C &= -s+(M^2-m^2)+\lambda^{1/2}\ ,\\ D &= -s-(M^2-m^2)+\lambda^{1/2}\ .\end{aligned}$$

Below the threshold, $\lambda^{1/2}$ is pure imaginary, so that $A\sim D$ are complex numbers. In this case, we define $\log(z)$ on the first Riemann sheet, namely, we restrict the argument of z within $0\le\theta<2\pi$. Then we see that $[\ln(A)+\ln(B)-\ln(C)-\ln(D)]$ becomes pure imaginary. But $\lambda^{1/2}$ is also pure imaginary, and hence, we obtain the real $G(\sqrt{s})$ below the threshold.

Above the threshold, $\lambda^{1/2}$ is real, so that $A\sim D$ are real numbers. The real logarithmic function is defined in the region $0\le x<\infty$. In order to avoid this multivalued nature, we then consider whether $A\sim D$ are positive or negative. If x is real negative number, we rewrite $\log(x)$ as $\log(-x)+i\pi$, because $-1=e^{i\pi}$ and we restrict the argument of z within $0\le\theta<2\pi$. When $\sqrt{s}>\sqrt{s_+}$, we see that

$$\begin{aligned}&A>0\ ,\quad B>0\ ,\\ &C<0\ ,\quad D<0\ ,\end{aligned}\quad \text{for}\quad \sqrt{s}>\sqrt{s_+}\ . \tag{3.4.4}$$

Then we define Eq. (3.4.2) as

$$\begin{aligned}G(\sqrt{s}) =& \frac{2M}{16\pi^2}\Big\{a(\mu)+\ln\frac{M^2}{\mu^2}+\frac{m^2-M^2+s}{2s}\ln\frac{m^2}{M^2} \\ &+\frac{\lambda^{1/2}}{2s}\left[\ln(A)+\ln(B)-\ln(-C)-\ln(-D)-2\pi i\right]\Big\}\ ,\quad \text{for}\quad \sqrt{s}>\sqrt{s_+}\ ,\end{aligned} \tag{3.4.5}$$

without multivalued nature. In the expression (3.4.5), $\lambda^{1/2}$ and all logarithmic function are real, so we extract the imaginary part of the G function as

$$\begin{aligned}\mathrm{Im}[G(\sqrt{s})] &= -\frac{M\lambda^{1/2}(s,M^2,m^2)}{8s\pi} \\ &= -\frac{1}{2}\cdot\left(\frac{2M|\bar{q}|}{4\pi\sqrt{s}}\right) = -\frac{\rho(\sqrt{s})}{2}\ ,\end{aligned} \tag{3.4.6}$$

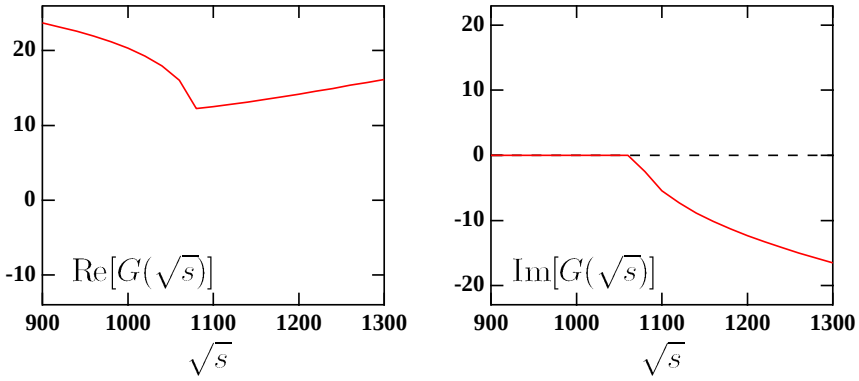

Figure 3.8: Real and imaginary parts of the loop function on the scattering line. Here we plot the loop function of the πN channel.

for $\sqrt{s} > \sqrt{s_+}$. This result guarantees the unitarity condition, as we will see later. In Fig. 3.8, we show the value of the loop function for the πN channel on the scattering line.

3.4.2 Loop function in the complex plane

Here we compute the loop function numerically, and see which branch of the T-matrix is closest to the scattering line. When we deal with multi-valued functions, several Riemann sheets appear and the value on the first Riemann sheet is defined by the restriction of the arguments $0 \leq \theta < 2\pi$. Eq. (3.3.4) represents the discontinuity of the inverse of the T-matrix due to the unitarity cut, which runs from $\sqrt{s^+}$ to $+\infty$. Using Eqs. (3.2.6) and (3.3.4), above the threshold, the discontinuity of the inverse of the T-matrix is given by

$$\mathrm{Disc}[T^{-1}(\sqrt{s})] \equiv T_I^{-1}(\sqrt{s}+i0) - T_I^{-1}(\sqrt{s}-i0) = i\rho(\sqrt{s}), \tag{3.4.7}$$

where $T_I(z)$ is the branch whose variable z is on the first Riemann sheet. The definition of the second branch $T_{II}^{-1}(z)$ with z on the second Riemann sheet is

$$T_{II}^{-1}(\sqrt{s}+i0) \equiv T_I^{-1}(\sqrt{s}-i0), \quad \text{for} \quad \sqrt{s} > \sqrt{s^+}\ . \tag{3.4.8}$$

According to the result of the N/D method (3.3.13), the relation between the T-matrix and the G function is given by

$$T^{-1} = V^{-1} - G\ . \tag{3.4.9}$$

Now V is a tree vertex, so that it is always real. Using the unitarity condition (3.3.4) and Eq. (3.4.9), we find

$$2\mathrm{Im}G(\sqrt{s}) = -\rho(\sqrt{s}), \quad \text{for} \quad \sqrt{s} > \sqrt{s^+}\ . \tag{3.4.10}$$

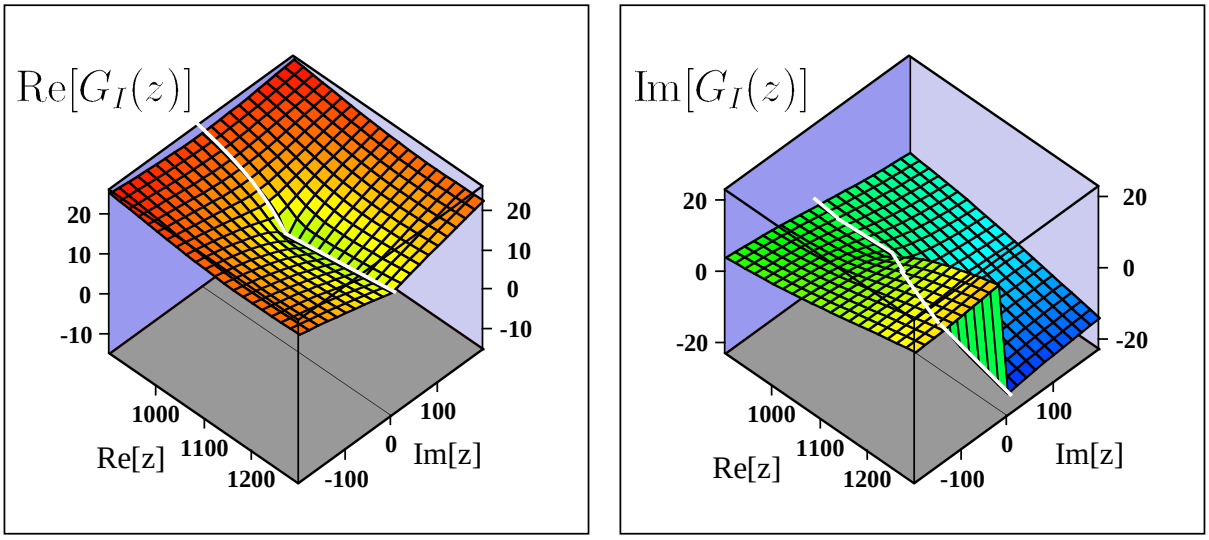

Figure 3.9: Real and imaginary parts of the $G_I(z)$ function. Here we plot the loop function of the πN channel. White line in the figure denotes the values on the scattering line (real axis).

This relation is valid above the threshold and consistent with the result (3.4.6). Since the T-matrix amplitude has the same branch cut as the G function, we investigate the G function instead of the T-matrix. We perform analytic continuation of $G(\sqrt{s})$ to the whole complex z plane. In Fig. 3.9, real and imaginary parts of the G function for πN channel on the first Riemann sheet are shown, where we see the discontinuity of the imaginary part. The origin of this discontinuity lies in the square root in the function $\rho(\sqrt{s})$. In the complex z plane, $\rho(z)$ is a double-valued function with the cut along the real axis $(\sqrt{s^+}, +\infty)$ due to square root

$$\rho(\sqrt{s}+i0) = -\rho(\sqrt{s}-i0), \quad \text{for} \quad \sqrt{s} > \sqrt{s^+}\ , \tag{3.4.11}$$

Therefore the discontinuity of the loop function G and relation between branches of G on the first and second Riemann sheets are given as

$$\begin{aligned} G_I(\sqrt{s}+i0) &= G_I(\sqrt{s}-i0) - i\rho(\sqrt{s}+i0) \\ G_{II}(\sqrt{s}+i0) &= G_I(\sqrt{s}-i0) \end{aligned}, \quad \text{for} \quad \sqrt{s} > \sqrt{s^+}\ , \tag{3.4.12}$$

where $G_I(z)$ and $G_{II}(z)$ represent the first and second branches, respectively. Using Eq. (3.4.12), we obtain the expression of the second branch

$$G_{II}(z) = G_I(z) + i\rho(z)\ . \tag{3.4.13}$$

In Fig. 3.10, real and imaginary parts of the G_{II} function for the πN channel, where we again

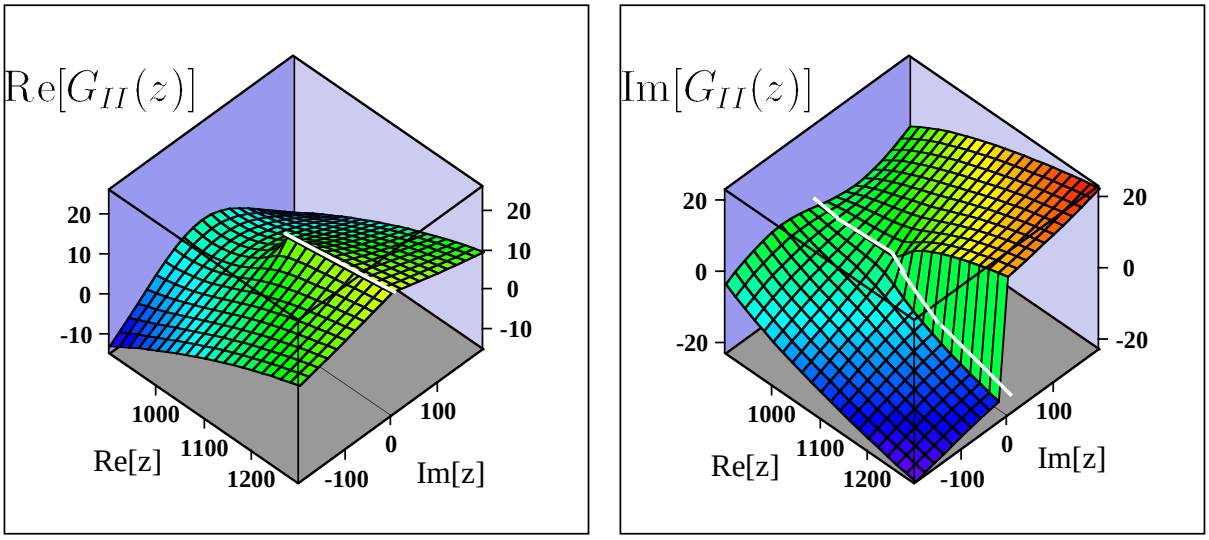

Figure 3.10: Real and imaginary parts of the $G_{II}(z)$ function. Here we plot the loop function of the πN channel. White line in the figure denotes the values on the scattering line (real axis).

see the discontinuity of imaginary part. From Eqs. (3.4.5) and (3.4.13), the explicit form of the function $G_{II}(z)$ is given as

$$G_{II}(z) = \frac{2M}{16\pi^2}\Big\{a(\mu) + \ln\frac{M^2}{\mu^2} + \frac{m^2 - M^2 + z^2}{2z^2}\ln\frac{m^2}{M^2} + \frac{\lambda^{1/2}(z)}{2z^2}\left[\ln(A) + \ln(B) - \ln(-C) - \ln(-D) + 2\pi i\right]\Big\}\,, \tag{3.4.14}$$

for $\mathrm{Re}[z] > \sqrt{s_+}$.

From Eqs. (3.4.13) and (3.4.10), on the real axis and above the threshold, it seems to be valid to write

$$G_{II}(\sqrt{s}) = G_I(\sqrt{s})^*.$$

However, Eq. (3.4.10) is valid only on the real axis. We must not use this form for complex plane, because, when we extend $\sqrt{s}$ to complex value, the loop function (3.4.2) can have imaginary part at s and so on. We should define the analytic form on the real axis first, then we can extend $\sqrt{s}$ to complex value. This is due to the fact that the operation of taking imaginary is not an analytic operation.

In practical calculations to find poles, we use the most relevant branches for scattering line (Fig. 3.8). The white lines in Figs. 3.9 and 3.10 indicates the corresponding values. From these lines, we see that

- below the threshold, the first branch contains the scattering line.

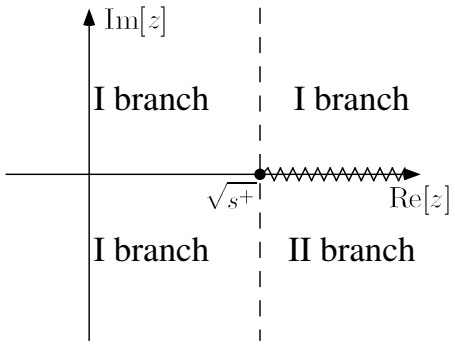

Figure 3.11: Diagrammatic expression of the definition of G_{pole}.

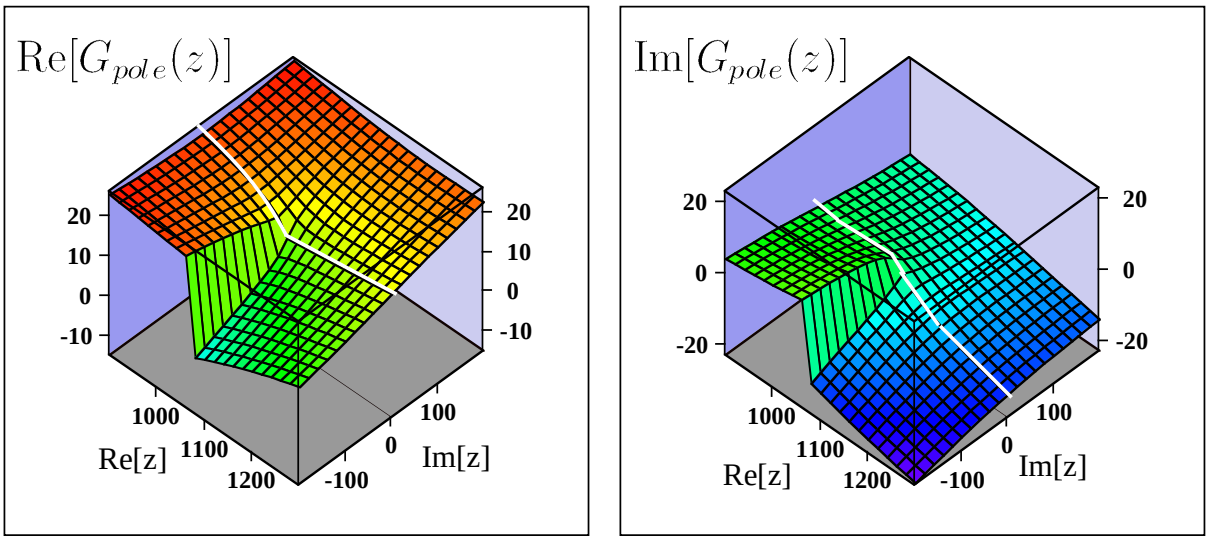

Figure 3.12: Real and imaginary parts of the $G_{pole}(z)$ function. Here we plot the loop function of the πN channel. White line in the figure denotes the values on the scattering line (real axis).

- above the threshold and Im$z > 0$, the first branch is connected with the scattering line.
- above the threshold and Im$z < 0$, the second branch is connected with the scattering line.

For this purpose, we define the function $G_{pole}(z)$ as

$$G_{pole}(z) = \begin{cases} G_I(z) & \text{for} \quad \mathrm{Re}[z] \leq \sqrt{s^+} \\ G_I(z) & \text{for} \quad \mathrm{Re}[z] > \sqrt{s^+} \quad \text{and} \quad \mathrm{Im}[z] > 0 \\ G_{II}(z) & \text{for} \quad \mathrm{Re}[z] > \sqrt{s^+} \quad \text{and} \quad \mathrm{Im}[z] < 0 \end{cases} . \tag{3.4.15}$$

The function G_{pole} is shown diagrammatically in Fig. 3.11 and is plotted in Fig. 3.12, where we see that the scattering line is included in the sheet. In this way we search poles in the branch which is the closest to the scattering line, namely which includes the scattering line.

Finally we consider the third branch, which is defined as

$$G_{III}(\sqrt{s}+i0) \equiv G_{II}(\sqrt{s}-i0), \quad \text{for} \quad \sqrt{s} > \sqrt{s^+} \ . \tag{3.4.16}$$

However, using Eqs. (3.4.11) and (3.4.12), if we go through the unitarity cut once again,

$$\begin{aligned} G_{III}(\sqrt{s}+i0) &= G_I(\sqrt{s}-i0) + i\rho(\sqrt{s}-i0) \\ &= G_I(\sqrt{s}+i0) + i\rho(\sqrt{s}+i0) + i\rho(\sqrt{s}-i0) \\ &= G_I(\sqrt{s}+i0) - i\rho(\sqrt{s}-i0) + i\rho(\sqrt{s}-i0) \\ &= G_I(\sqrt{s}+i0) \ , \end{aligned}$$

we back to the first branch. This means that there are only two Riemann sheets. Note that this result is expected from the fact that $\lambda^{1/2}(\sqrt{s})$ is double-valued function (3.4.11).

Chapter 4

Chiral unitary model

In this chapter we review the formulation of the chiral unitary model, and show the numerical results. Since we are interested in $1/2^-$ resonances, we calculate s wave meson-baron scatterings throughout this thesis. We derive the basic interaction of meson-baryon scatterings from the lowest order chiral Lagrangian (2.6.12), and construct the S-matrix using the N/D method keeping the unitarity condition. In order to see the role of channel dependence in the subtraction constants, we study the chiral unitary model with a single subtraction constant a. We calculate T-matrix amplitudes, total cross sections and invariant mass distributions numerically. In section 4.3, we discuss the properties of the T-matrix around the resonance regions. We perform analytic continuation to the complex energy plane, and search poles which indicate resonances.

4.1 Formulation

As shown in section 2.6, the chiral Lagrangian for baryons in the lowest order of the chiral expansion is given by

$$\begin{aligned} \mathcal{L}_1^{MB} =& \mathrm{Tr}\Big(\bar{B}(i\not{\mathcal{D}} - M_0)B - D(\bar{B}\gamma^\mu\gamma_5\{A_\mu, B\}) - F(\bar{B}\gamma^\mu\gamma_5[A_\mu, B])\Big) \ , \\ & \mathcal{D}_\mu B = \partial_\mu B + i[V_\mu, B] \ . \end{aligned} \tag{4.1.1}$$

In the Lagrangian (4.1.1), M_0 denotes a common mass of the octet baryons. However, we use the observed values of the baryon masses in the following calculations. The mass splitting among the octet baryons in the Lagrangian level will be introduced consistently with the $SU(3)$ breaking in section 5.2.

The s wave interaction at the tree level is described by the Weinberg-Tomozawa (WT) interaction, which is in the vector coupling term $V_\mu = -i(\xi^\dagger\partial_\mu\xi + \xi\partial_\mu\xi^\dagger)/2$ in the covariant derivative;

$$\mathcal{L}_{WT} = \mathrm{Tr}\Big(\bar{B}i\gamma^\mu\frac{1}{4f^2}\big[(\Phi\partial_\mu\Phi - \partial_\mu\Phi\Phi), B\big]\Big) \ . \tag{4.1.2}$$

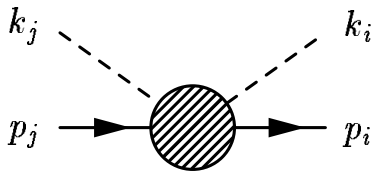

Figure 4.1: Definition of the momentum variables. Dashed and solid lines represent mesons and baryons, respectively.

We do not include diagrams with meson-baryon Yukawa terms in the axial couplings in the Lagrangian (4.1.1), because they are p wave couplings. From the Lagrangian (4.1.2), the meson-baryon scattering amplitude at the tree level is given by

$$\begin{aligned} V_{ij}^{(WT)} &= -\frac{C_{ij}}{4f^2}\bar{u}(p_i)(\not{k}_i + \not{k}_j)u(p_j) \\ &= -\frac{C_{ij}}{4f^2}(2\sqrt{s} - M_i - M_j)\sqrt{\frac{E_i + M_i}{2M_i}}\sqrt{\frac{E_j + M_j}{2M_j}}, \end{aligned} \tag{4.1.3}$$

where the indices (i, j) denote the channels of the meson-baryon scatterings and M_i and E_i are the observed mass and the energy of the baryon in the channel i, respectively. The kinematics of this vertex is shown in Fig. 4.1 and s in Eq. (4.1.3) is defined as $s = (k + p)^2$. The channels (i, j) are shown in Table B.1 in Appendix B. The coefficient C_{ij} is fixed by chiral symmetry and the explicit form of C_{ij} is shown in Tables C.3∼C.7 in Appendix C. The last line is obtained in the center of mass frame with the nonrelativistic reduction.

Following the result of N/D method (3.3.9), the resulting T-matrix is written as

$$T = [1 - VG]^{-1}V \ , \tag{4.1.4}$$

with a tree level vertex V and the loop function G, which is defined as

$$\begin{aligned} G_i(\sqrt{s}) = \frac{2M_i}{(4\pi)^2}\Bigg\{ & a_i(\mu) + \ln\frac{M_i^2}{\mu^2} + \frac{m_i^2 - M_i^2 + s}{2s}\ln\frac{m_i^2}{M_i^2} \\ & + \frac{\bar{q}_i}{\sqrt{s}}\Big[\ln(s - (M_i^2 - m_i^2) + 2\sqrt{s}\bar{q}_i) + \ln(s + (M_i^2 - m_i^2) + 2\sqrt{s}\bar{q}_i) \\ & - \ln(-s + (M_i^2 - m_i^2) + 2\sqrt{s}\bar{q}_i) - \ln(-s - (M_i^2 - m_i^2) + 2\sqrt{s}\bar{q}_i)\Big]\Bigg\}, \end{aligned} \tag{4.1.5}$$

In this section we identify V as the WT interaction (4.1.3), and obtain

$$T = [1 - V^{(WT)}G]^{-1}V^{(WT)} \ . \tag{4.1.6}$$

This is a solution of the algebraic equation for the T-matrix, which corresponds to the integral Bethe-Salpeter equation.

channel	$\bar{K}N$	$\pi\Sigma$	$\pi\Lambda$	$\eta\Lambda$	$\eta\Sigma$	$K\Xi$
a_i	-1.84	-2.00	-1.83	-2.25	-2.38	-2.67

channel	πN	ηN	$K\Lambda$	$K\Sigma$
a_i	0.711	-1.09	0.311	-4.09

Table 4.1: Channel dependent subtraction constants a_i used in Refs. [19, 20] with the regularization scale $\mu = 630$ MeV. For the $S = 0$ channel, although the original values of a_i are shown with $\mu = 1200$ MeV, here we show the values of a_i corresponding to $\mu = 630$ MeV by using the relation $a(\mu') = a(\mu) + 2\ln(\mu'/\mu)$.

The subtraction constants $a_i(\mu)$ in Eq. (4.1.5), in principle, would be related to the counter terms in the higher order terms in the chiral perturbation Lagrangian. In the previous works [19, 20], they hae fitted these subtraction constants(a_i) by using the data of $\bar{K}N(S = -1)$ and $\pi N(S = 0)$ scatterings. In Table 4.1 we show the subtraction constants used in Refs. [19, 20]. In the table, in order to compare the channel dependence of the subtraction constants, we take the regularization scale at $\mu = 630$ MeV in the both channels. Changing the regularization scale, the subtraction constants are simply shifted by $a(\mu') = a(\mu) + 2\ln(\mu'/\mu)$, as we see in Eq. (4.1.5). From this table we see that the values of a_i in $S = 0$ are very much different from each other. In the rest of this thesis, we refer to these parameter sets as " channel dependent a_i ".

4.2 Calculation with a common subtraction constant

In this section, we show calculations in which a single subtraction constant a is commonly used in the meson-baryon loop function (3.3.12), in order to see the role of the channel dependent a_i to reproduce the observed cross sections and the resonance properties. First, we discuss the case of $S = -1$, where the subtraction constants a_i are not very dependent on the channels as shown in Table 4.1. Therefore, it is expected that the calculation with a common a gives a good description by choosing a suitable value. Next we study the $S = 0$ channel using a common subtraction constant. Here we will find that the common a cannot reproduce simultaneously the resonance properties and the S_{11} amplitude at low energy region.

In order to concentrate on the role of the subtraction constants and to see the channel dependence, we assume the following simplifications for the calculations of the $S = -1$ and $S = 0$ channels;

- We use an averaged value for the meson decay constants, $f = 1.15 f_\pi = 106.95$ MeV, while in Ref. [20] physical values were taken as $f_\pi = 93$ MeV, $f_K = 1.22 f_\pi$, $f_\eta = 1.3 f_\pi$.
- We do not include the effect of vector meson exchanges and $\pi\pi N$ channels to reproduce

	γ	R_c	R_n
experiment	2.36 ± 0.04	0.664 ± 0.011	0.189 ± 0.015
channel dependent a_i	1.73	0.629	0.195
common $a = -1.96$	1.80	0.624	0.225
common $a = -2.6$	2.41	0.569	0.759

Table 4.2: Threshold branching ratios calculated with the channel dependent a_i, the common $a = -1.96$ and the common $a = -2.6$. The experimental values are take from Refs. [58, 59].

the $\Delta(1620)$ resonance, which were considered in Ref. [20].

With these simplifications, the calculations in the $S = -1$ and $S = 0$ channels are based on exactly the same formulation; the differences are in the flavor $SU(3)$ coefficients C_{ij} in Eq. (4.1.3) and in the channel dependent subtraction constants.

4.2.1 The $S = -1$ channel ($\bar{K}N$ scattering)

In the $S = -1$ channel, the subtraction constants a_i obtained in Ref. [19] are not very much dependent on the channels, as shown in Table 4.1. In Ref. [22], they used a common $a \sim -2$ with $\mu = 630$ MeV, which was "naturally" obtained from the matching with the three-momentum cut-off regularization with $\Lambda_3 = 630$ MeV. In the both works, they reproduced very well the total cross sections of the $K^- p$ scatterings and the mass distribution of the $\pi\Sigma$ channel with $I = 0$, where the $\Lambda(1405)$ resonance is seen. In Ref. [19], the $\Lambda(1670)$ resonance was also obtained with the channel dependent subtraction constants, and its property was discussed by analyzing the speed plots in the $I = 0$ channels.

Here we search one common a to be used in all channels in $S = -1$. In order to fix the common a, we use threshold properties of the $\bar{K}N$ scatterings, which are well observed in the branching ratios [58, 59]:

$$\begin{aligned} \gamma =& \frac{\Gamma(K^- p \to \pi^+ \Sigma^-)}{\Gamma(K^- p \to \pi^- \Sigma^+)} \sim 2.36 \pm 0.04 \ , \\ R_c =& \frac{\Gamma(K^- p \to \text{charged particles})}{\Gamma(K^- p \to \text{all})} \sim 0.664 \pm 0.011 \ , \\ R_n =& \frac{\Gamma(K^- p \to \pi^0 \Lambda)}{\Gamma(K^- p \to \text{neutral particles})} \sim 0.189 \pm 0.015 \ . \end{aligned} \tag{4.2.1}$$

After fitting, we find the optimal value $a = -1.96$, with which the threshold branching ratios are obtained as shown in Table 4.2. The result using the common $a = -1.96$ does not differ very much from that of channel dependent ones, and also the value $a = -1.96$ is close to an averaged value of the channel dependent subtraction constants a_i, namely ~ -2.15. Therefore, the threshold properties are not sensitive to such a fine tuning of the subtraction constants.

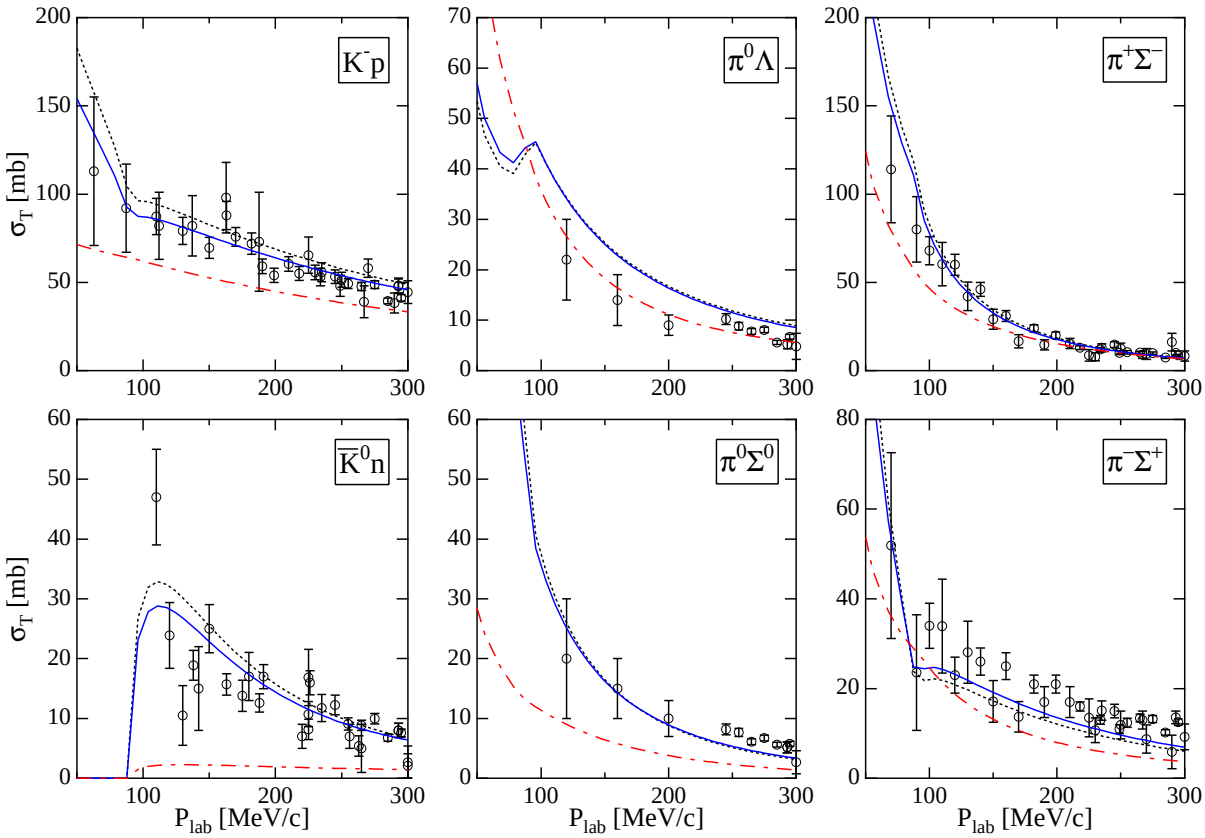

Figure 4.2: Total cross sections of K^-p scatterings ($S = -1$) as functions of $P_{\rm lab}$, the three-momentum of initial K^- in the laboratory frame. Dotted lines show the results with the channel dependent a_i, solid lines show the results with the common $a = -1.96$, and dash-dotted lines show the results with the common $a = -2.6$. Open circles with error bars are experimental data taken from Refs. [58, 59, 60, 61, 62, 63, 64, 65, 66, 67, 68, 69, 70, 71].

Using the common $a = -1.96$, we calculate the total cross sections of the K^-p scatterings (Fig. 4.2, solid lines), the T-matrix amplitude of the $\bar{K}N$ scattering with $I = 0$ and the mass distributions of the $\pi\Sigma$ channel with $I = 0$ (Fig. 4.3, solid lines). We also plot the calculations with the channel dependent a_i obtained in Ref. [19] in Figs. 4.2 and 4.3 as the dotted lines. Here we find that the present calculations are slightly different from the calculations with the channel dependent a_i in the total cross sections and the $\pi\Sigma$ mass distributions. Therefore, the $\Lambda(1405)$ resonance is well reproduced with the common $a = -1.96$, which is consistent with the results in Ref. [22]. However, the resonance $\Lambda(1670)$ disappears when the common a is used, as we see in the T-matrix amplitude of $\bar{K}N \to \bar{K}N$ with $I = 0$ in Fig. 4.3. As pointed out in Ref. [19], the $\Lambda(1670)$ resonance structure is very sensitive to the value of $a_{K\Xi}$. Indeed we have checked that the $\Lambda(1670)$ resonance is reproduced when we choose $a_{K\Xi} \sim -2.6$ with the other a_i unchanged, -1.96.

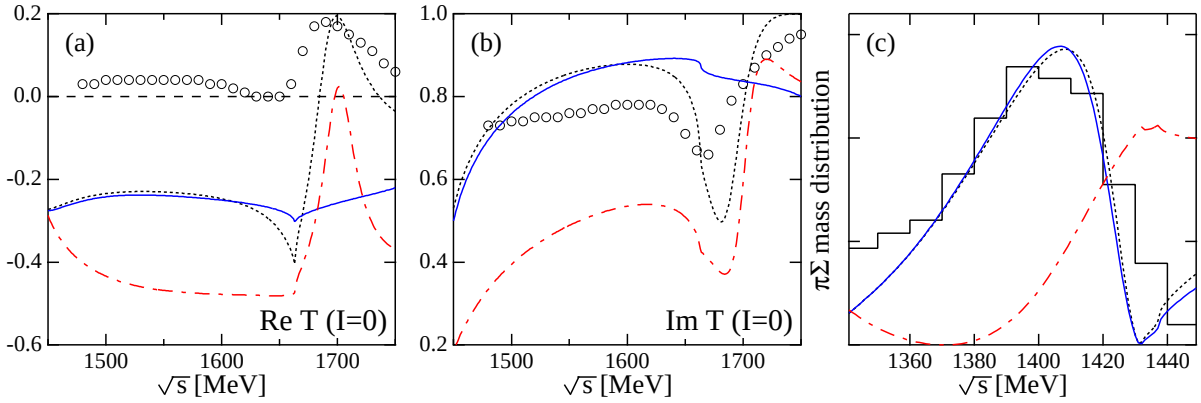

Figure 4.3: Real and imaginary parts of the T-matrix amplitude of $\bar{K}N \to \bar{K}N$ with $I = 0$ (a,b) and mass distributions of the $\pi\Sigma$ channel with $I = 0$ (c). Dotted lines show the results with the channel dependent a_i, solid lines show the results with the common $a = -1.96$, and dash-dotted lines show the results with the common $a = -2.6$. Open circles and histogram are experimental data taken from Ref. [72, 73].

If we choose $a = -2.6$ for all subtraction constants, the threshold branching ratios are calculated as in Table 4.1, and the agreement with the experimental data becomes poor, as shown in Figs. 4.2 and 4.3. In particular, the $K^-p \to \bar{K}^0 n$ cross section is underestimated, and also the resonance structure of $\Lambda(1405)$ disappears in the $\pi\Sigma$ mass distribution (Fig. 4.3). As we change all subtraction constants from $a = -1.96$ to $a = -2.6$ gradually, the position of the peak of $\Lambda(1405)$ moves to lower energy side and finally disappears under the $\pi\Sigma$ threshold. Therefore, taking common $a \sim -2$ is essential to reproduce the resonance properties of $\Lambda(1405)$ and the total cross sections of the K^-p scatterings in the low energy region.

4.2.2 The $S = 0$ channel (πN scattering)

In Ref. [20], the total cross sections of the π^-p inelastic scatterings and the resonance properties of the $N(1535)$ were reproduced well by using the channel dependent a_i. After the simplification for f and inelastic channels, the agreement with the data is still acceptable, as shown in Figs. 4.4 and 4.5 by dotted lines, as long as the channel dependent a_i are employed. In the T-matrix elements of the πN scattering in the S_{11} channel, we see a kink structure around the energy $\sqrt{s} \sim 1500$ MeV, which corresponds to the $N(1535)$ resonance [20].

In the previous subsection, we obtained the common subtraction constant $a = -1.96$ with which the $\bar{K}N$ total cross sections and the $\Lambda(1405)$ properties are reproduced well. First, we use this common a for the $S = 0$ channel. Shown in Figs. 4.4 and 4.5 by dash-dotted lines are the results with $a = -1.96$ for the total cross sections of the $\pi^-p \to \pi^0\eta$, $K^0\Lambda$ and $K^0\Sigma$ scatterings, and the S_{11} T-matrix amplitude of $\pi N \to \pi N$. As can be seen in Figs. 4.4

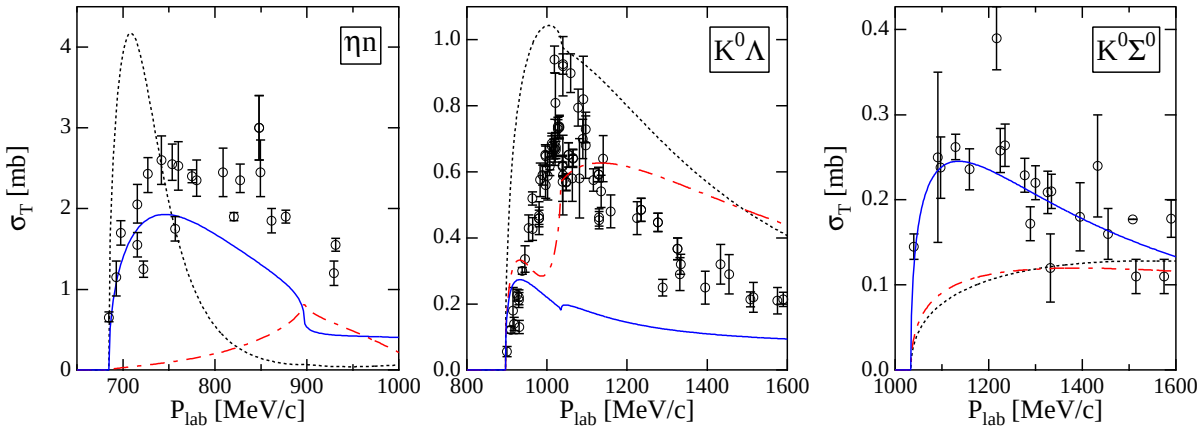

Figure 4.4: Total cross sections of $\pi^- p$ scatterings ($S = 0$) as functions of $P_{\rm lab}$, the three-momentum of initial π^- in the laboratory frame. Dotted lines show the results with channel dependent a_i, dash-dotted lines show the results with the common $a = -1.96$, obtained in $S = -1$, and solid lines show the results with the common $a = 0.53$. Open circles with error bars are experimental data taken from Refs. [74, 75, 76, 77, 78, 79, 80, 81, 82, 83, 84, 85, 86, 87, 88, 89, 90, 91, 92, 93].

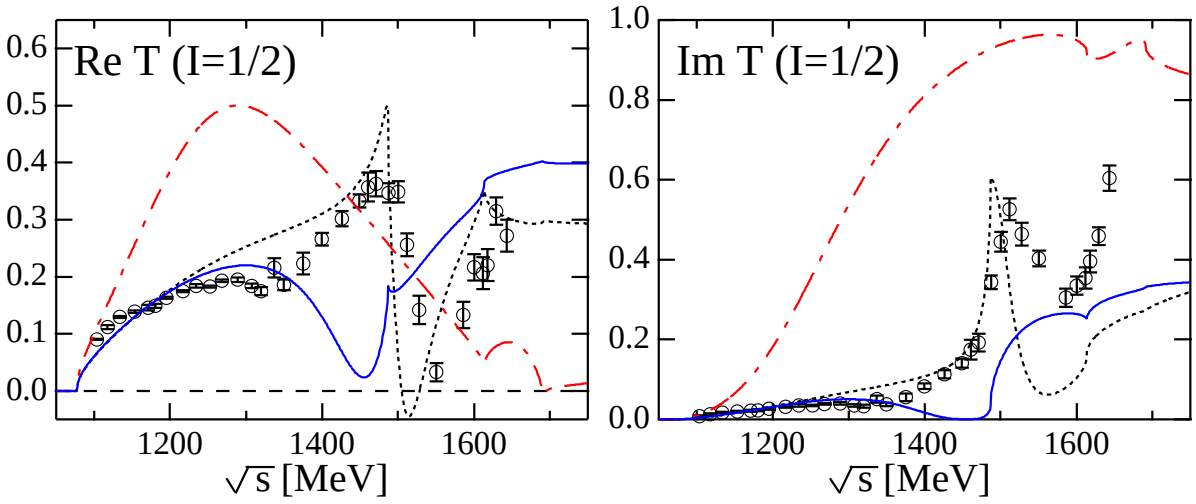

Figure 4.5: Real and imaginary parts of the S_{11} T-matrix amplitudes of $\pi N \to \pi N (I = 1/2)$. Dotted lines show the results with channel dependent a_i, dash-dotted lines show the results with the common $a = -1.96$, same as the $S = -1$ channel. Solid lines show the results with the common $a = 0.53$. Open circles with error bars are experimental data taken from Refs. [94].

and 4.5, the results with $a = -1.96$ in the $S = 0$ channel are far from the experimental data. In particular, in the $\pi^- p \to \eta n$ cross section, the threshold behavior disagrees with the experiment, and the resonance structure of $N(1535)$ disappears. In addition, as shown in Fig. 4.5, the T-matrix amplitude of the S_{11} πN channel is overestimated and an unexpected resonance has been generated at around $\sqrt{s} \sim 1250$ MeV.

Next we search the single optimal subtraction constant within the $S = 0$ channel, since the unnecessary resonance are obtained with $a = -1.96$ at low energy. In order to avoid the appearance of such an unphysical resonance, we determine the common subtraction constant a so as to reproduce observed data up to $\sqrt{s} = 1400$ MeV. The optimal value is found to be $a = 0.53$. The calculated S_{11} amplitude as well as the total cross sections are plotted in Figs. 4.4 and 4.5 by the solid lines. With this subtraction constant, the low energy behavior of the S_{11} amplitude of πN scatterings ($\sqrt{s} < 1400$ MeV) is well reproduced, while, however, the $N(1535)$ resonance structure is not still generated. We have also checked that there is no pole in the scattering amplitudes in the second Riemann sheet. Therefore, we conclude that in the $S = 0$ channel we cannot reproduce simultaneously the $N(1535)$ resonance and the S_{11} amplitude at low energy if a single subtraction constant is used.

4.3 Resonance in the scattering amplitude

In this section, we show the way to extract the information of the resonance from the scattering amplitude. We study the behavior of the T-matrix around the pole on the real axis. Then we perform the analytic continuation of the variable $\sqrt{s}$, and search poles in the complex z plane by calculating the T-matrix in the complex plane numerically. In order to estimate the coupling strength to each channel, we calculate the residues of the poles for each channel.

From Eq. (3.4.1), around a resonance, the T-matrix amplitude is written as

$$T_{ij}(\sqrt{s}) \sim \frac{g_i g_j}{\sqrt{s} - M_R + i\Gamma_R/2} + T_{ij}^{BG} \ , \tag{4.3.1}$$

which indicates the existence of a pole at

$$z_R = M_R - i\frac{\Gamma_R}{2} \ . \tag{4.3.2}$$

In this way, through the Breit-Wigner term, the position of the pole z_R gives the mass M_R and the width Γ_R of the corresponding resonance.

We first discuss the property of the T-matrix amplitude on the real axis around the resonance region. Eq. (4.3.1) can be written as

$$T_{ij}(\sqrt{s}) \sim \frac{g_i g_j(\sqrt{s} - M_R - i\Gamma_R/2)}{(\sqrt{s} - M_R)^2 - (\Gamma_R/2)^2} + T_{ij}^{BG} \ , \tag{4.3.3}$$

which imply that if the background term is negligible, $T_{ij}(\sqrt{s})$ becomes pure imaginary when $\sqrt{s} = M_R$. When we differentiate $T_{ij}(\sqrt{s})$ in terms of $\sqrt{s}$, we have

$$\begin{aligned}
\frac{\partial}{\partial\sqrt{s}}T_{ij}(\sqrt{s}) &= -\frac{g_i g_j}{(\sqrt{s} - M_R + i\Gamma_R/2)^2} + \frac{\partial}{\partial\sqrt{s}}T_{ij}^{BG} \\
&= -\frac{g_i g_j}{(\sqrt{s} - M_R)^2 - (\Gamma_R/2)^2 + i\Gamma_R(\sqrt{s} - M_R)} + \frac{\partial}{\partial\sqrt{s}}T_{ij}^{BG} \\
&= -\frac{g_i g_j(\sqrt{s} - M_R)^2 - (\Gamma_R/2)^2 - i\Gamma_R(\sqrt{s} - M_R)}{[(\sqrt{s} - M_R)^2 - (\Gamma_R/2)^2]^2 - [\Gamma_R(\sqrt{s} - M_R)]^2} + \frac{\partial}{\partial\sqrt{s}}T_{ij}^{BG}
\end{aligned} \tag{4.3.4}$$

which imply that if the first derivative of the background term is negligible, $\frac{\partial}{\partial\sqrt{s}}T_{ij}(\sqrt{s})$ becomes pure real when $\sqrt{s} = M_R$. Since the derivative of the imaginary part is zero, $\mathrm{Im}[T_{ij}]$ has an extreme value at $\sqrt{s} = M_R$. Hence, if the background term and its first derivative are negligible, or in the other words, if the Breit-Wigner term is dominant, the T-matrix has the following properties;

- $\mathrm{Re}[T]$ becomes zero at $\sqrt{s} = M_R$.
- $\mathrm{Im}[T]$ has an extreme value at $\sqrt{s} = M_R$.

As an example, in Fig. 4.3, we see that zero of the real part and extreme value of imaginary part of dotted lines are around $\sqrt{s} = 1670$ MeV, which corresponds to the mass of the $\Lambda(1670)$ resonance. Since the background term is assumed to be slowly varying function of $\sqrt{s}$, its first derivative seems to be negligible. However, it is not always true that the background term itself is negligible. Therefore, in general, the zero of the real part and the extreme value of imaginary part might not coincide. This discrepancy is referred to as the background effects.

As we have seen, the use of the channel dependent subtraction constants gives reasonable results on the scattering line. Using the method presented in section 3.4.2, we plot the absolute value of the T-matrix amplitudes $|T|$ of $\bar{K}N \to \bar{K}N$ in Fig. 4.6 and of $\pi N \to \pi N$ with $I = 1/2$ in Fig. 4.7. In the $S = -1$ channel, around the energy region of $\Lambda(1405)$, we find two poles at

$$z_1 = 1428.98 - 13.81i\ , \quad z_2 = 1396.50 - 73.35i\ . \tag{4.3.5}$$

As reported in Refs. [22, 28, 95], there are two poles around this energy region. They seem to construct a distorted shape in the $\pi\Sigma$ mass distribution (Fig. 4.3). Around the energy region of $\Lambda(1670)$, we also find a pole and the position of the pole is

$$z = 1689.59 - 21.82i\ . \tag{4.3.6}$$

The values in Eqs. (4.3.5) and (4.3.6) are different from the values in Ref. [19], because here we use $f = 1.15 \times 93$ [MeV] for the meson decay constant, while $f = 1.123 \times 93$ [MeV] is used in Ref. [19]. In the $S = 0$ channel, we find a pole at

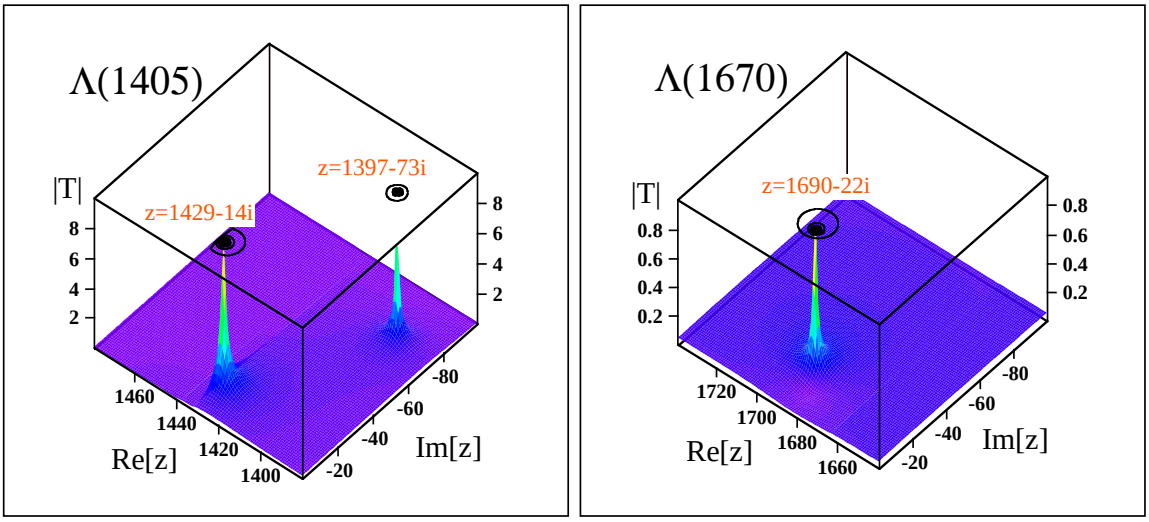

Figure 4.6: Poles in the complex z plane. Here we plot the absolute value of the T-matrix amplitudes of $\bar{K}N \to \bar{K}N$ with $I = 0$.

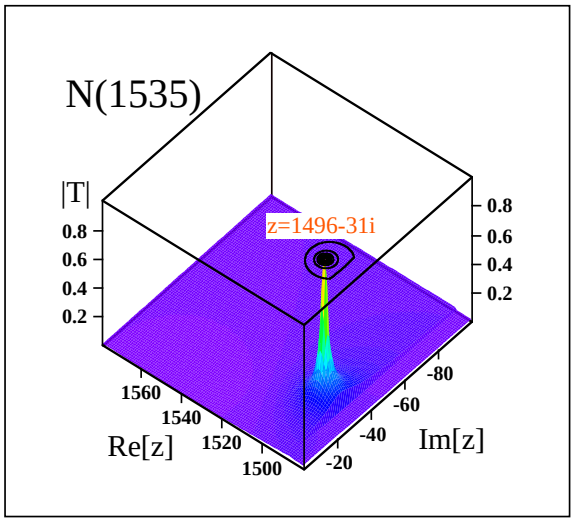

Figure 4.7: Poles in the complex z plane. Here we plot the absolute value of the T-matrix amplitude of $\pi N \to \pi N$ with $I = 1/2$.

$$z = 1495.89 - 31.29i \ , \tag{4.3.7}$$

which corresponds to the $N(1535)$ resonance.

Next we calculate residues of the poles,

$$\begin{aligned} \lim_{z\to z_R} \left[(z - z_R)T_{ij}(z)\right] &\sim \lim_{z\to z_R} \left[(z - z_R)\frac{g_i g_j}{z - z_R} + (z - z_R)T_{ij}^{BG}\right] \\ &\sim \lim_{z\to z_R} \left[g_i g_j + (z - z_R)T_{ij}^{BG}\right] \\ &\sim g_i g_j \ . \end{aligned} \tag{4.3.8}$$

		$\lvert g_{\bar{K}N}\rvert^2$	$\lvert g_{\pi\Sigma}\rvert^2$	$\lvert g_{\eta\Lambda}\rvert^2$	$\lvert g_{K\Xi}\rvert^2$
$\Lambda(1405)$	z_1	6.57	1.88	1.74	0.100
	z_2	3.83	8.20	0.497	0.383
$\Lambda(1670)$		0.585	0.725	1.10	11.3

Table 4.3: Coupling strengths of the $\Lambda(1405)$ and $\Lambda(1670)$ resonances to meson-baryon channels. All channels are in $I = 0$. Around the $\Lambda(1405)$ resonance, there are two poles z_1 and z_2 (4.3.5).

	$\lvert g_{\pi N}\rvert^2$	$\lvert g_{\eta n}\rvert^2$	$\lvert g_{K\Lambda}\rvert^2$	$\lvert g_{K\Sigma}\rvert^2$
N(1535)	0.895	2.65	2.11	8.61

Table 4.4: Coupling strengths of the $N(1535)$ resonance to meson-baryon channels. All channels are in $I = 1/2$.

These values determine the coupling strengths g_i and g_j of the resonance to meson-baryon states, which are well defined even if these states are closed in the decay of the resonance. From Eq. (4.3.8), we evaluate

$$|g_i|^2 = \lim_{z \to z_R} |(z - z_R) \times T_{ii}(z)| \ . \tag{4.3.9}$$

Mathematically, this quantity is well defined. However, numerically it is unstable if z approaches z_R too much. Therefore it is important to fix the position of the pole precisely, and we should check that Eq. (4.3.9) gives a stable value when z approach in different directions. The values of $|g_i|^2$ are shown in Tables 4.3 and 4.4.

From the Table 4.3, we see that $\Lambda(1670)$ strongly couples to the $K\Xi$ channel, and this agrees with the fact that the position of the $\Lambda(1670)$ structure is dominated by $a_{K\Xi}$ parameter (Fig. 4.3). Concerning with the $N(1535)$ resonance, the πN and ηN channels are opened at the energy of resonance. Therefore, the decay of $N(1535)$ is dominated by ηN channel, which also corresponds to the experimental fact.

Chapter 5

Flavor $SU(3)$ breaking effects in the chiral unitary model

In this chapter, we first derive the masses of mesons and baryons from flavor $SU(3)$ breaking terms in the chiral Lagrangian, and see the mass relations among them. Next we extract the meson-baryon interaction including the $SU(3)$ breaking effects, and combine it with the previous WT interaction. The numerical results with the $SU(3)$ breaking interaction are also presented.

5.1 Flavor $SU(3)$ breaking terms in the chiral Lagrangian

Here we introduce the flavor $SU(3)$ breaking effects in the chiral Lagrangian by the quark masses up to order $\mathcal{O}(m_q)$. From the second order chiral Lagrangian (2.5.9), these terms for mesons are

$$\mathcal{L}_{SB}^{M} = \frac{f^2}{4}\mathrm{Tr}(U^\dagger\chi + \chi^\dagger U) \ , \quad \chi = 2B_0\mathbf{m} \ , \tag{5.1.1}$$

and the $SU(3)$ breaking terms for baryons in Eq. (2.6.14) can be written as

$$\begin{aligned}\mathcal{L}_{SB}^{MB} =& -\frac{Z_0}{2}\mathrm{Tr}\Big(d_m\bar{B}\{\xi\mathbf{m}\xi + \xi^\dagger\mathbf{m}\xi^\dagger, B\} + f_m\bar{B}[\xi\mathbf{m}\xi + \xi^\dagger\mathbf{m}\xi^\dagger, B]\Big) \\ & -\frac{Z_1}{2}\mathrm{Tr}(\bar{B}B)\mathrm{Tr}(\mathbf{m}U + U^\dagger\mathbf{m}) \ ,\end{aligned} \tag{5.1.2}$$

where $f_m + d_m = 1$ and the quark mass matrix $\mathbf{m}$ is defined by

$$\mathbf{m} = \begin{pmatrix} m_u & & \\ & m_d & \\ & & m_s \end{pmatrix} . \tag{5.1.3}$$

Here we follow the notation in Ref. [43].

5.2 Mass relations

If there is no quark mass term in ChPT, chiral symmetry is not broken explicitly, where all mesons are massless and baryons have a common mass M_0 in the Lagrangian (2.6.12). Introduction of the quark mass term generates meson masses and baryon mass splittings. In ChPT, the masses derived from the terms (5.1.1) and (5.1.2) automatically satisfy the Gell-Mann Okubo (GMO) mass relations [96, 97].

5.2.1 Mesons

In order to derive the meson masses, we need terms which is proportional to Φ^2. Expanding Eq. (5.1.1) and taking these terms,

$$\begin{aligned}
\mathcal{L}^M_{mass} =& \frac{2B_0 f^2}{4}\mathrm{Tr}\left(-\frac{1}{f^2}\Phi^2\mathbf{m} - \mathbf{m}^\dagger\frac{1}{f^2}\Phi^2\right) \\
=& -\frac{B_0}{2}\mathrm{Tr}\big(\Phi^2\mathbf{m} + \mathbf{m}\Phi^2\big) \\
=& -B_0\mathrm{Tr}(\Phi^2\mathbf{m}) \\
=& -B_0\Big(\pi^+\pi^-(m_u+m_d) + K^+K^-(m_u+m_s) + \bar{K}^0K^0(m_d+m_s) \\
&+ \frac{1}{2}\pi^0\pi^0(m_u+m_d) + \frac{1}{6}\eta\eta(m_u+m_d+4m_s) + \frac{1}{\sqrt{3}}\pi^0\eta(m_u-m_d)\Big)\ . \qquad (5.2.1)
\end{aligned}$$

If we break isospin symmetry($m_u \neq m_d$), there appear mixing terms such as $\pi^0\eta$, because the basis that we adopt does not diagonalize the mass term of Hamiltonian. Physical π^0_{phys} and η_{phys} are linear combinations of π^0 and η in Eq. (5.2.1).

Among octet mesons, π^0, η are real fields and the others are complex fields. The definition of the mass term for real boson field ϕ_R and complex boson field ϕ_C are

$$-\frac{1}{2}m_R^2\phi_R^2\ , \quad -m_C^2\phi_C\phi_C^\dagger\ , \qquad (5.2.2)$$

where ϕ_C and $\phi_C^\dagger$ have the same mass m_c. Using Eqs. (5.2.1) and (5.2.2), the masses of the octet mesons are

$$\begin{aligned}
M^2_{\pi^0} &= B_0(m_u+m_d)\ , \\
M^2_{\eta} &= \frac{1}{3}B_0(m_u+m_d+4m_s)\ , \\
M^2_{\pi^+} = M^2_{\pi^-} &= B_0(m_u+m_d)\ , \\
M^2_{K^+} = M^2_{K^-} &= B_0(m_u+m_s)\ , \\
M^2_{K^0} = M^2_{\bar{K}^0} &= B_0(m_d+m_s)\ .
\end{aligned} \qquad (5.2.3)$$

These masses satisfy the Gell-Mann-Oakes-Renner (GMOR) mass relation [41]

$$\frac{M^2_{\pi^\pm}}{m_u+m_d} = \frac{M^2_{K^\pm}}{m_u+m_s} = \frac{M^2_{K^0}}{m_d+m_s} = \frac{3M_\eta}{m_u+m_d+4m_s}\ . \qquad (5.2.4)$$

If we assume the isospin symmetry ($m_u = m_d = \hat{m}$), the masses of mesons are

$$\begin{aligned} M_\pi^2 &= 2B_0\hat{m} \ , \\ M_K^2 &= B_0(\hat{m} + m_s) \ , \\ M_\eta^2 &= \frac{2}{3}B_0(\hat{m} + 2m_s) \ , \end{aligned} \tag{5.2.5}$$

which satisfy the GMO mass relation for mesons [30]

$$3M_\eta^2 = 2B_0(\hat{m} + 2m_s) \tag{5.2.6}$$

$$= 4B_0(\hat{m} + m_s) - 2B_0\hat{m} \tag{5.2.7}$$

$$= 4M_K^2 - M_\pi^2 \ . \tag{5.2.8}$$

From Eqs. (5.2.5) we also derive the quark mass ratio

$$\frac{\hat{m}}{m_s} = \frac{m_\pi^2}{2m_K^2 - m_\pi^2} \sim 26 \ , \tag{5.2.9}$$

with the physical meson masses.

5.2.2 Baryons

Up to order $\mathcal{O}(p^2)$, the terms which contribute to the baryon masses are

$$\begin{aligned} \mathcal{L}^B_{mass} = &- M_0 \mathrm{Tr}(\bar{B}B) - \frac{Z_1}{2}\mathrm{tr}(\bar{B}B)\mathrm{tr}(\mathbf{m}) \\ &- \frac{Z_0}{2}\mathrm{tr}\left(d_m\big(\bar{B}\mathbf{m}B + \bar{B}B\mathbf{m}\}\big) + f_m\big(\bar{B}\mathbf{m}B - \bar{B}B\mathbf{m}\big)\right) \end{aligned} \ . \tag{5.2.10}$$

Under the isospin symmetry, the baryon masses derived from the Lagrangian (5.2.10) are

$$\begin{aligned} M_N &: M_0 + Z_0 d_m(\hat{m} + m_s) + Z_0 f_m(\hat{m} - m_s) + Z_1(2\hat{m} + m_s) \ , \\ M_\Sigma &: M_0 + 2Z_0 d_m \hat{m} + Z_1(2\hat{m} + m_s) \\ M_\Xi &: M_0 + Z_0 d_m(\hat{m} + m_s) + Z_0 f_m(m_s - \hat{m}) + Z_1(2\hat{m} + m_s) \ , \\ M_\Lambda &: M_0 + \frac{2}{3}Z_0 d_m(\hat{m} + 2m_s) + Z_1(2\hat{m} + m_s) \ , \end{aligned}$$

which satisfy the GMO mass formula

$$\begin{aligned} \frac{1}{2}(M_\Xi - M_N) + \frac{3}{4}(M_\Sigma - M_\Lambda) &= \frac{1}{2}2Z_0 f_m(m_s - \hat{m}) + \frac{3}{4}\left[-\frac{4}{3}Z_0 d_m(m_s - \hat{m})\right] \\ &= Z_0(f_m - d_m)(m_s - \hat{m}) \\ &= M_\Sigma - M_N \ . \end{aligned}$$

5.3 Flavor $SU(3)$ breaking interactions

In the previous chapter, it has been found that the channel dependent subtraction constants a_i are crucial in order to reproduce important features of experimental data. In this section, we consider $SU(3)$ breaking interactions of the chiral Lagrangian in order to see if the channel dependence in the subtraction constants can be absorbed into those terms. In this way, we are hoping that the number of free parameters could be reduced and that the origin of the channel dependence would be clarified. According to the chiral counting rule, these quark mass terms are regarded as quantities of order $\mathcal{O}(p^2)$. In this study, since we concentrate on the $SU(3)$ breaking effect, we take into account only the terms of Eq. (5.1.2), and other terms of order $\mathcal{O}(p^2)$ are not included. From the mass splitting among the octet baryons and the πN sigma term, which we take here $\sigma_{\pi N} = 36.4$ MeV, all the parameters in the Lagrangian (5.1.2) are determined as

$$Z_0 = 0.528 \ , \quad Z_1 = 1.56 \ , \quad f_m/d_m = -0.31 \ , \tag{5.3.1}$$

and $M_0 = 759$ MeV in the Lagrangian (2.6.12).

The meson-baryon interaction Lagrangian with the $SU(3)$ breaking is obtained by picking up the terms with two meson fields. We find

$$\begin{aligned}\mathcal{L}^{(2)}_{SB} =& \frac{Z_0}{4f^2}\mathrm{Tr}\Big(d_m\bar{B}\big\{(2\Phi\mathbf{m}\Phi + \Phi^2\mathbf{m} + \mathbf{m}\Phi^2), B\big\} + f_m\bar{B}\big[(2\Phi\mathbf{m}\Phi + \Phi^2\mathbf{m} + \mathbf{m}\Phi^2), B\big]\Big) \\ &+ \frac{Z_1}{f^2}\mathrm{Tr}(\bar{B}B)\mathrm{Tr}(\mathbf{m}\Phi^2) \ .\end{aligned} \tag{5.3.2}$$

From this Lagrangian the basic interaction is given by

$$\begin{aligned}V^{(SB)}_{ij} =& -\frac{1}{f^2}\Big[Z_0\Big((A^d_{ij}d_m + A^f_{ij}f_m)\hat{m} + (B^d_{ij}d_m + B^f_{ij}f_m)m_s\Big) \\ &+ Z_1\delta_{ij}D_i^{Z_1}\Big]\sqrt{\frac{E_i + M_i}{2M_i}}\sqrt{\frac{E_j + M_j}{2M_j}}.\end{aligned} \tag{5.3.3}$$

The explicit forms of the coefficients A_{ij} and B_{ij} are given in Appendix C. These interaction terms are independent of the meson momenta unlike the WT interaction (4.1.3).

Adding Eq. (5.3.3) to Eq. (4.1.3) and substituting them into Eq. (3.3.14), we obtain the unitarized T-matrix with the flavor $SU(3)$ breaking effects as

$$T = \Big[1 - \Big(V^{(WT)} + V^{(SB)}\Big)\,G\Big]^{-1}\Big(V^{(WT)} + V^{(SB)}\Big) \, . \tag{5.3.4}$$

Since we have already fitted the all parameters in the chiral Lagrangian from physical quantities, the free parameters in the chiral unitary model with the $SU(3)$ breaking effects are only the subtraction constants.

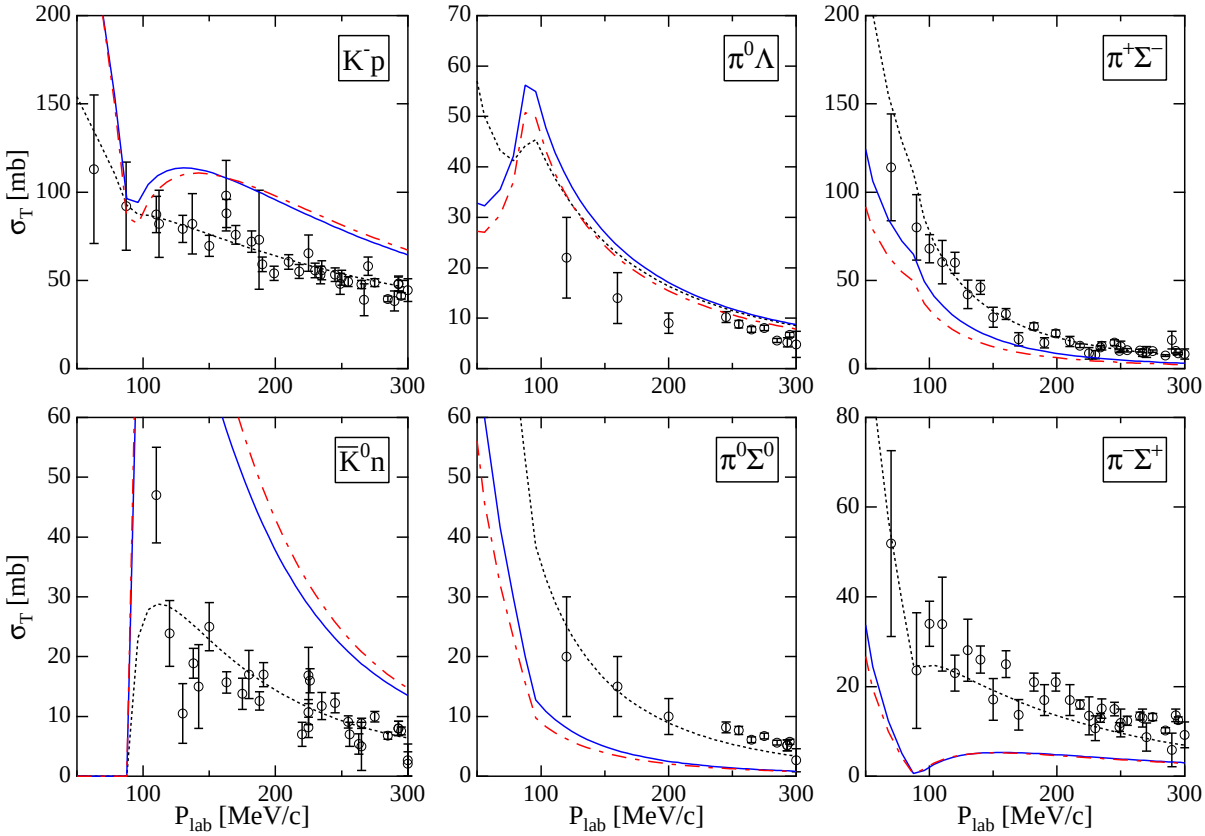

Figure 5.1: Total cross sections of K^-p scatterings ($S = -1$) as functions of $P_{\rm lab}$, the three-momentum of initial K^- in the laboratory frame. Dotted lines show the results with the common $a = -1.96$, dash-dotted lines show the results including the $SU(3)$ breaking with the common $a = -1.59$, and solid lines show the results including the $SU(3)$ breaking and the physical f with the common $a = -1.68$. Open circles with error bars are experimental data taken from Refs. [58, 59, 60, 61, 62, 63, 64, 65, 67, 68, 66, 69, 70, 71].

5.3.1 The $S = -1$ channel

We follow the same procedures as in the calculations without the $SU(3)$ breaking terms. First of all, we determine a common subtraction constant a from the threshold branching ratios (4.2.1). Then the optimal value is found to be $a = -1.59$. With this value, the total cross sections of the K^-p scatterings, the $\pi\Sigma$ mass distribution and the scattering amplitude of $\bar{K}N \to \bar{K}N$ with $I = 0$ are plotted in Figs. 5.1 and 5.2 by dash-dotted lines. As seen in the Fig. 5.1, for all the total cross sections, the inclusion of the $SU(3)$ breaking terms with the common a makes the agreement with data worse, although the threshold branching ratios are produced much better than the previous works, as seen in Table 5.1.

In the $\pi\Sigma$ mass distribution shown in Fig.5.2 (dash-dotted line), a sharp peak is seen, in

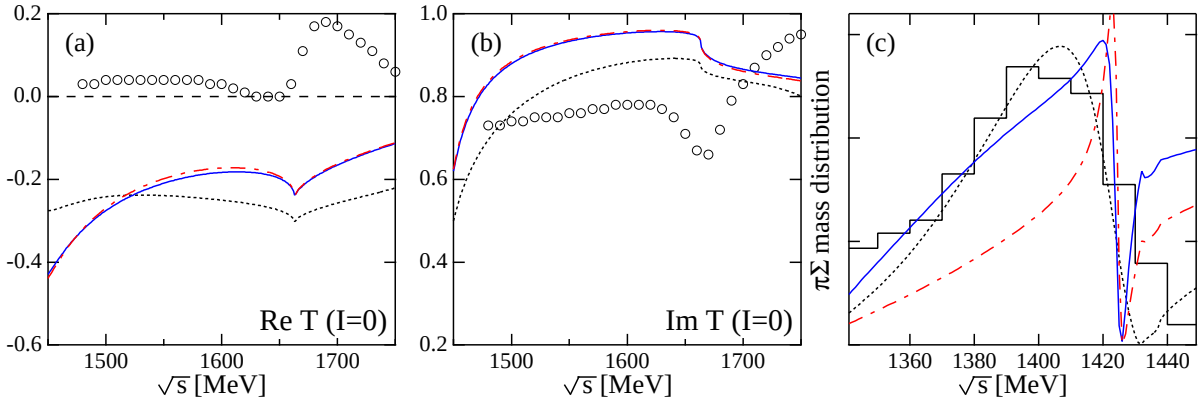

Figure 5.2: Real and imaginary parts of the T-matrix amplitude of $\bar{K}N \to \bar{K}N$ with $I = 0$ (a,b) and mass distributions of the $\pi\Sigma$ channel with $I = 0$ (c). Dotted lines show the results with the common $a = -1.96$, dash-dotted lines show the results including the $SU(3)$ breaking with the common $a = -1.59$, and solid lines show the results including the $SU(3)$ breaking and the physical f with the common $a = -1.68$. Open circles are experimental data taken from Ref. [72, 73].

	γ	R_c	R_n
experiment	2.36 ± 0.04	0.664 ± 0.011	0.189 ± 0.015
common $a = -1.96$	1.80	0.624	0.225
$SU(3)$ breaking with $a = -1.59$	2.19	0.623	0.179
$SU(3)$ breaking with $a = -1.68$, physical f	2.35	0.626	0.172

Table 5.1: Threshold branching ratios calculated with common $a = -1.96$, $a = -1.59$ with the $SU(3)$ breaking interaction, and $a = -1.68$ with the $SU(3)$ breaking interaction using the physical meson decay constants. The experimental values are take from Refs. [58, 59].

obvious contradiction with the observed spectrum, which means that the important resonance structure of $\Lambda(1405)$ has been lost. However, we find two poles of the T-matrix amplitude at $z_1 = 1424 + 1.6i$ and $z_2 = 1389 + 135i$ in the second Riemann sheet. It is reported that there are two poles in the T-matrix amplitude around the energy region of $\Lambda(1405)$ in Refs. [22, 28, 95]. The inclusion of the $SU(3)$ breaking terms does not change this conclusion, although the positions of the poles change.

We also calculate the total cross sections and the $\pi\Sigma$ mass distribution with the physical values of the meson decay constants, $f_\pi = 93$ MeV, $f_K = 1.22 f_\pi$, $f_\eta = 1.3 f_\pi$. The calculated results are shown in Figs. 5.1 and 5.2 by solid lines. The optimal value of the subtraction constants is $a = -1.68$ to reproduce the threshold branching ratios as shown in Table 5.1. The $SU(3)$ breaking effect on the meson decay constants is not so large in the total cross sections, as seen in the figures. However, the shape of the peak seen in the $\pi\Sigma$ mass distribution becomes wider than that in the calculation with the averaged meson decay constant.

Indeed we find again two poles in the scattering amplitudes at $z_1' = 1424 + 2.6i$ and $z_2' = 1363 + 87i$ in the second Riemann sheet. Compared with the poles z_1 and z_2 obtained in the above calculation, the position of the pole z_2' moves to lower energy side and approaches the real axis. The reason why the position of z_2' changes is understood as follows. Since z_2 has large imaginary part, which means large width, and only the $\pi\Sigma$ channel opens in this energy region, the resonance represented by the pole z_2 has strong coupling to the $\pi\Sigma$ channel. This fact implies that the position of the pole z_2 is sensitive to the $\pi\Sigma$ interaction. In the present calculation, the pion decay constant (93 MeV) is smaller than the averaged value (106.95 MeV) used in the above calculation, so that the attractive interaction of $\pi\Sigma$ becomes stronger. It shifts the position of the pole z_2 to lower energy side. Simultaneously, this suppresses the phase space of the decay of the resonance to the $\pi\Sigma$ channel, and hence, the position of the pole approaches the real axis.

5.3.2 The $S = 0$ channel

Here we show calculations in the $S = 0$ channel with the $SU(3)$ breaking terms. With a common $a \sim -1.5$, in which the threshold properties are reproduced well in the $S = -1$ channel, we obtain still the large contribution in the S_{11} πN scattering amplitude at the low energy as in the calculation without the $SU(3)$ breaking effects. From this analysis, it is found that the low energy behavior of the πN scatterings cannot be reproduced as long as we use the common $a \sim -2$, even if we introduce the $SU(3)$ breaking effects.

In order to search the optimal value of the common subtraction constant within the $S = 0$ channel, we perform fitting of the T-matrix elements in the πN S_{11} channel in low energy region up to 1400 MeV. We find $a = 1.33$. The results including the $SU(3)$ breaking effects with $a = 1.33$ are shown as dash-dotted lines in Figs. 5.3 and 5.4. As seen in Fig. 5.4, the fitting is well performed up to $\sqrt{s} \sim 1400$ MeV, while, however, the resonance structure does not appear around the energies of $N(1535)$.

Finally we show the calculations with the physical values of the meson decay constants in Figs. 5.3 and 5.4 (solid lines). The optimal value of the common subtraction constant is found to be $a = 2.24$. The results with the physical meson decay constants and $a = 2.24$ are very similar to the calculation with the averaged value of the decay constants and $a = 1.33$. In this sense, the $SU(3)$ breaking effect of the meson decay constant f is absorbed into the change of the common subtraction constant a.

In closing this section, we conclude that even if we introduce the $SU(3)$ breaking effects in the Lagrangian level, the $SU(3)$ breaking in the channel dependent subtraction constants a_i cannot be absorbed into the $SU(3)$ breaking effects in the fundamental interactions in the both $S = -1$ and $S = 0$ channels.

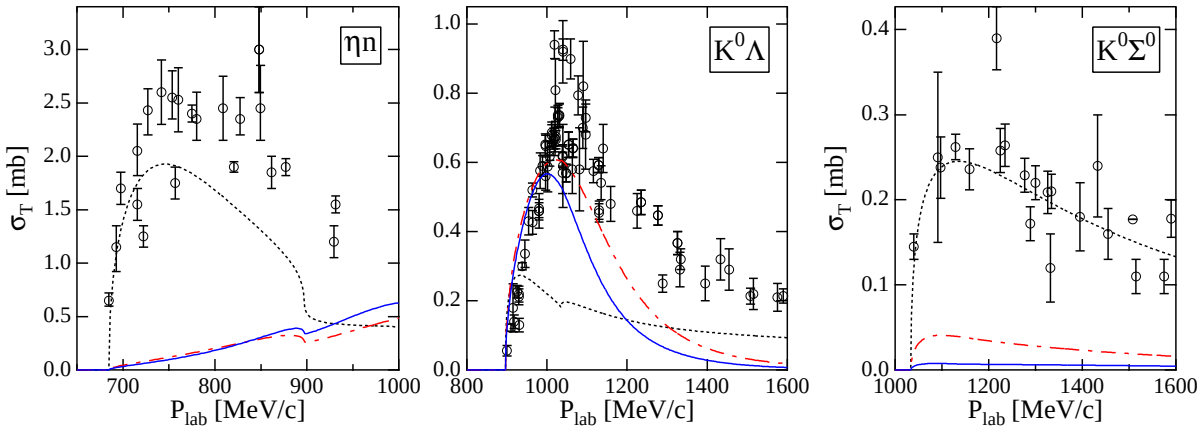

Figure 5.3: Total cross sections of $\pi^- p$ scatterings ($S = 0$) as functions of $P_{\rm lab}$, the three-momentum of initial π^- in the laboratory frame. Dotted lines show the results with the common $a = 0.53$, dash-dotted lines show the results including the $SU(3)$ breaking interaction with the common $a = 1.33$, and solid lines show the results including the $SU(3)$ breaking and the physical f with the common $a = 2.24$. Open circles with error bars are experimental data taken from Refs. [74, 75, 76, 77, 78, 79, 80, 81, 82, 83, 84, 85, 86, 87, 88, 89, 90, 91, 92, 93].

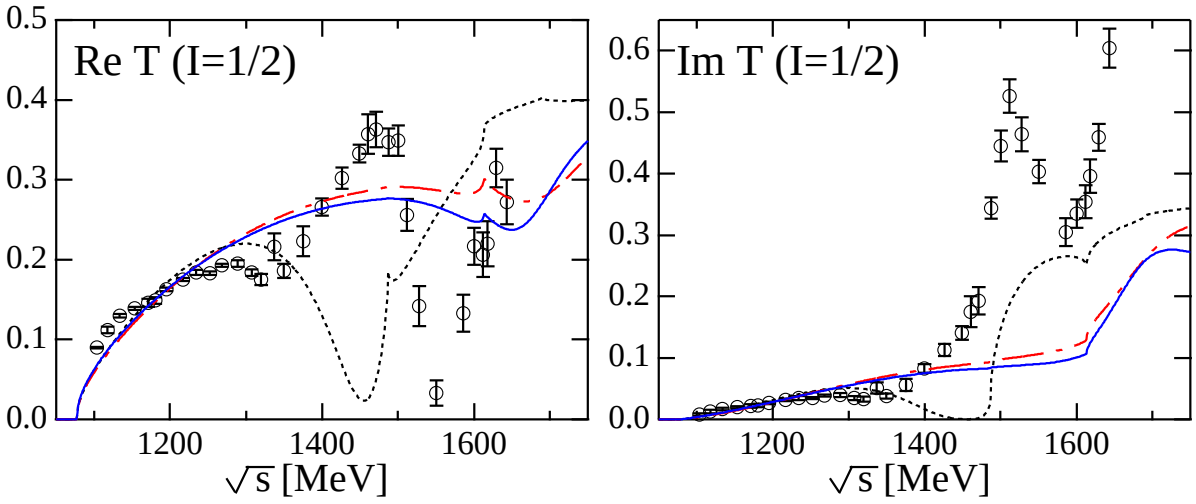

Figure 5.4: Real and imaginary parts of the S_{11} T-matrix amplitudes of $\pi N \to \pi N$. Dotted lines show the results with the common $a = 0.53$, dash-dotted lines show the results including the $SU(3)$ breaking interaction with the common $a = 1.33$, and solid lines show the results including the $SU(3)$ breaking and the physical f with the common $a = 2.24$. Open circles with error bars are experimental data taken from Refs. [94].

Chapter 6

Magnetic moments of the baryon resonances

In this chapter, we study the magnetic moments of baryons. First, using the chiral Lagrangian, we calculate the magnetic moments of the ground state baryons. Then we formulate a method to calculate the magnetic moments of the resonances, following the procedure of Ref. [28], where the magnetic moments of $\Lambda(1405)$ and $\Lambda(1670)$, and the transition moment between them are calculated within the chiral unitary model. Since our final goal is to calculate the magnetic moments of the $N(1535)$ resonance, we choose a parameter set with which the generated resonance has proper mass and width. Here we do not include the $SU(3)$ breaking effects. We calculate in both the $Q = 1$ and $Q = 0$ channels, in which there appear the proton and neutron resonances. Using coupling strengths of the resonance to meson-baryon channels and the magnetic moments of the ground state baryons, we estimate the magnetic moments of the resonances. In the present case of $N(1535)$, the $\Sigma_0\Lambda$ transition magnetic moment has moderate effects, which were almost negligible in $S = -1$, because of the isospin of the Λ resonances. We calculate the magnetic moments of the $N(1535)$ resonance in two different ways, on the real axis and in the complex plane. Combining both the results, we determine the values of the magnetic moments of the $N(1535)$ resonance.

6.1 Magnetic moments of the ground state baryons in ChPT

In this section we calculate the magnetic moments of the ground state baryons in the framework of the chiral perturbation theory. For the octet baryons, there are eight magnetic moments of eight baryons and one $\Sigma_0\Lambda$ transition magnetic moment, which have been measured experimentally with high precision. At the tree level, the results are in good agreement with data, and also satisfy the Coleman-Glashow relations [98], which is derived from the $SU(3)$ symmetry.

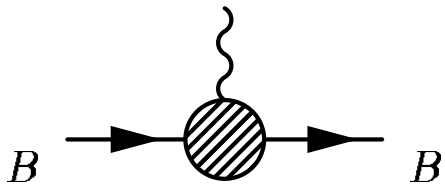

Figure 6.1: Electromagnetic vertex for a fermion. Solid and wave lines represent fermions and photon.

In general, the electromagnetic interaction vertex for a spin 1/2 fermion (Fig. 6.1) is written in terms of two form factors $F_1(q^2)$ and $F_2(q^2)$ [53];

$$\bar{u}(p')\left[\gamma^\mu F_1(q^2) + \frac{i\sigma^{\mu\nu}q_\nu}{2m}F_2(q^2)\right]u(p)\ , \tag{6.1.1}$$

where $\sigma^{\mu\nu} = i[\gamma^\mu, \gamma^\nu]/2$, u and $\bar{u}$ are the spinors of initial and final fermions, p and p' are the momenta of the initial and final fermions, and m is the mass of the fermion. The magnetic moment is calculated as

$$\mu = \frac{e}{2m}[F_1(0) + F_2(0)] = \frac{e}{2m}[1 + F_2(0)]\ . \tag{6.1.2}$$

We refer to $\frac{e}{2m}$ as the normal magnetic moment and $\frac{e}{2m}\cdot F_2(0)$ as the anomalous magnetic moment.

In the ChPT, we have electromagnetic couplings in the covariant derivative of baryon kinetic term in the chiral Lagrangian (2.6.13). In the order $\mathcal{O}(p^2)$ chiral Lagrangian (2.6.15), the photon coupling terms can be rewritten as

$$\mathcal{L}^{MB}_{(\gamma)} = -\frac{i}{4M_P}b_6^F \mathrm{Tr}\left(\bar{B}[S^\mu, S^\nu][F^+_{\mu\nu}, B]\right) - \frac{i}{4M_P}b_6^D \mathrm{Tr}\left(\bar{B}[S^\mu, S^\nu]\{F^+_{\mu\nu}, B\}\right)\ , \tag{6.1.3}$$

where $F^+_{\mu\nu} = -e(\xi^\dagger Q F_{\mu\nu}\xi + \xi Q F_{\mu\nu}\xi^\dagger)$, $Q = \mathrm{diag}(2,-1,-1)/3$ and S^μ is a covariant baryon spin operator, which is defined in Eq. (2.6.21). This Lagrangian has contributions to anomalous magnetic moments. In the rest frame of a baryon, a commutation relation of spin operators takes the form

$$[S^\mu, S^\nu]F_{\mu\nu} \to -(\boldsymbol{\sigma}\times\boldsymbol{q})\cdot\boldsymbol{\epsilon} \tag{6.1.4}$$

Thus the Lagrangian (6.1.3) is written as

$$\mathcal{L}^{MB}_{(\gamma)} = e\frac{\boldsymbol{\sigma}\times\boldsymbol{q}}{2M_P}\cdot\boldsymbol{\epsilon}\left(-\frac{i}{2}b_6^F \mathrm{Tr}\bar{B}[(u^\dagger Q u + u Q u^\dagger), B] - \frac{i}{2}b_6^D \mathrm{Tr}\bar{B}\{(u^\dagger Q u + u Q u^\dagger), B\}\right) \tag{6.1.5}$$

For the magnetic moments of the ground state baryons, we take $u = 1$ to obtain the vertex of Fig. 6.1. We then obtain

$$\mathcal{L}^{BB\gamma} = -ie\frac{\boldsymbol{\sigma}\times\boldsymbol{q}}{2M_P}\cdot\boldsymbol{\epsilon}\left(b_6^F \mathrm{Tr}\bar{B}[Q, B] + b_6^D \mathrm{Tr}\bar{B}\{Q, B\}\right). \tag{6.1.6}$$

baryon	$\mu_{\rm th}$		$\mu_{\rm exp}$
p	$\frac{1}{3}b_6^D + b_6^F$	2.56	$2.792847337 \pm 0.000000029$
n	$-\frac{2}{3}b_6^D$	-1.60	-1.9130427 ± 0.0000005
Σ^+	$\frac{1}{3}b_6^D + b_6^F$	2.56	2.458 ± 0.010
Σ^-	$\frac{1}{3}b_6^D - b_6^F$	-0.97	-1.160 ± 0.025
Σ^0	$\frac{1}{3}b_6^D$	0.80	
Λ	$-\frac{1}{3}b_6^D$	-0.80	-0.613 ± 0.004
Ξ^-	$\frac{1}{3}b_6^D - b_6^F$	-0.97	-0.6507 ± 0.0025
Ξ^0	$-\frac{2}{3}b_6^D$	-1.60	-1.250 ± 0.014
$\Sigma^0\Lambda$	$\frac{1}{\sqrt{3}}b_6^D$	1.38	$\pm 1.61 \pm 0.08$

Table 6.1: The magnetic moments of the ground state baryons. The left column of $\mu_{\rm th}$ are extracted from the tree graph with the term (6.1.6), and the values in the right column of $\mu_{\rm th}$ are obtained with the parameters in Eq. (6.1.8). $\mu_{\rm exp}$ are experimental data taken from Ref. [99]

Therefore, after taking trace of Eq. (6.1.6), the magnetic moments of the ground state baryons are obtained as shown in Table 6.1 (left column of $\mu_{\rm th}$). From the table, we see the following Coleman-Glashow relations are satisfied

$$\begin{aligned} &\mu_{\Sigma^+} = \mu_p \ , \quad 2\mu_\Lambda = \mu_n \ , \quad \mu_{\Sigma^-} = \mu_{\Xi^-} \ , \quad \mu_{\Xi^0} = \mu_n \ , \\ &\mu_{\Sigma^-} + \mu_n = -\mu_p \ , \quad 2\mu_{\Sigma^0\Lambda} = -\sqrt{3}\mu_n \ , \quad 2\mu_{\Sigma^0} = \mu_{\Sigma^+} + \mu_{\Sigma^-} \ . \end{aligned} \tag{6.1.7}$$

There are only two parameters, b_6^D and b_6^F.

Recall that the magnetic moments derived from the Lagrangian (6.1.3) are the anomalous magnetic moments, while the normal magnetic moments come from the vector current coupling in the covariant derivative. However, the contributions from the normal magnetic moments are exactly the same as the first term of Eq. (6.1.6). Indeed the normal magnetic moments just shift $b_6^F \to b_6^F + 1$. Therefore we absorb the normal magnetic moments into b_6^F in the rest of this thesis. We need to be careful that the values we show are different from the low energy constant b_6^F which appears in the ChPT.

Fitting the magnetic moments written in terms of b_6^D and b_6^F in Table 6.1, we find the fitted parameters [100]

$$b_6^D = 2.39, \quad b_6^F = 1.77, \tag{6.1.8}$$

and obtain the magnetic moments as shown in Table 6.1 (right column of $\mu_{\rm th}$). In spite of the use of only two parameters, they are in good agreement with data.

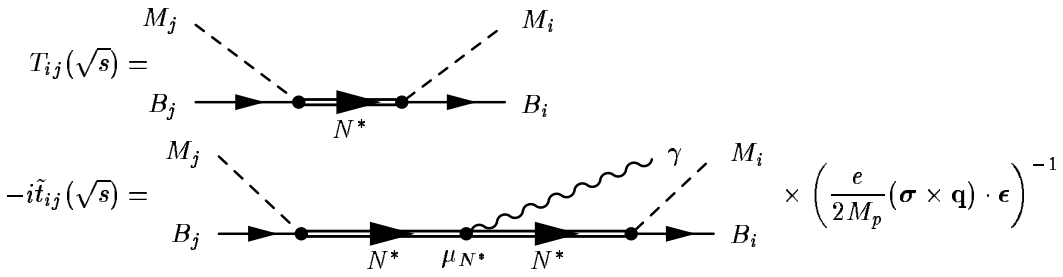

Figure 6.2: Feynman diagrams of $T_{ij}(\sqrt{s})$ and $-i\tilde{t}_{ij}(\sqrt{s})$. In calculating $-i\tilde{t}_{ij}(\sqrt{s})$, we consider the diagrams which contribute to the magnetic moments, and extract a factor in order to make the coupling of resonance to photon to be magnetic moment in units of the nuclear magneton.

Beyond the tree level with the lowest order ChPT, many calculations including the higher order contributions have been done [42, 101, 102]. In the one loop calculation, there appears the non-analytic corrections of the form $\sqrt{m_q}$ and $m_q \ln m_q$.

6.2 Formulation

In this section, we show a formulation to calculate the magnetic moments of resonances in the chiral unitary model [28]. There are two ways to calculate them, on the real axis and in the complex plane. Both two methods have advantages and disadvantages, which would be compensated each other.

As in the previous chapters, the chiral unitary model provides an amplitude

$$T_{ij}(\sqrt{s}) = \frac{g_i g_j}{\sqrt{s} - M_{N^*} + i\Gamma_{N^*}/2} + T_{ij}^{BG} \ , \tag{6.2.1}$$

From the terms of photon couplings (6.1.5), we have the vertex of $BB\gamma$ and $BBMM\gamma$. Using them, we calculate the photon coupling diagrams as

$$-i\tilde{t}_{ij}(\sqrt{s}) = \left(\frac{g_i}{\sqrt{s} - M_{N^*} + i\Gamma_{N^*}/2} + T^{BG}\right) \cdot \mu_{N^*} \cdot \left(\frac{g_j}{\sqrt{s} - M_{N^*} + i\Gamma_{N^*}/2} + T^{BG}\right) \ .$$

Feynman diagrams of $T_{ij}(\sqrt{s})$ and $-i\tilde{t}_{ij}(\sqrt{s})$ are shown in Fig. 6.2. In the following, we first calculate the $-i\tilde{t}_{ij}(\sqrt{s})$ diagrams in the chiral unitary model, and present two ways to extract μ using $T_{ij}(\sqrt{s})$.

6.2.1 Photon coupling diagrams

Here we compute the diagram $-i\tilde{t}_{ij}(\sqrt{s})$. Since we consider the baryon resonances as multi-scatterings of meson-baryon states, we have three kinds of diagrams of the photon couplings as shown in Fig. 6.3. Among them, the diagram (c) does not contribute to the present

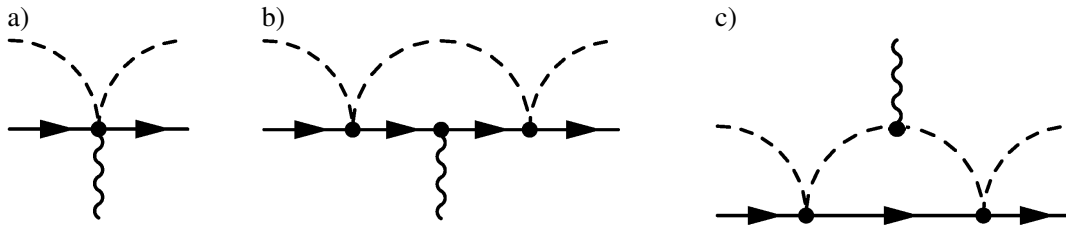

Figure 6.3: Photon coupling diagram in $-i\tilde{t}_{ij}(\sqrt{s})$. We consider that there are meson-baryon loops on the left and right sides of these vertices.

calculation, because we consider s wave scatterings. Therefore, we consider the diagrams (a) and (b), and we divide $-i\tilde{t}_{ij}(\sqrt{s})$ into two parts,

$$-i\tilde{t}_{ij}(\sqrt{s}) = \tilde{T}^{(a)}(\sqrt{s}) + \tilde{T}^{(b)}(\sqrt{s}) \ , \tag{6.2.2}$$

where $\tilde{T}^{(a)}(\sqrt{s})$ and $\tilde{T}^{(b)}(\sqrt{s})$ are the diagrams like $-i\tilde{t}_{ij}(\sqrt{s})$ with (a) and (b) photon couplings, respectively.

The five point vertex (a) is derived from the Lagrangian (6.1.5), by taking the terms of two mesons, as

$$\begin{aligned}\mathcal{L}^{BBMM\gamma} =& -e\frac{\boldsymbol{\sigma}\times\mathbf{q}}{2M_p}\cdot\boldsymbol{\epsilon}\frac{i}{4f^2}\mathrm{Tr}\Big(b_6^D\bar{B}\big\{(2\Phi Q\Phi-\Phi^2Q-Q\Phi^2),B\big\}\\ &+b_6^F\bar{B}\big[(2\Phi Q\Phi-\Phi^2Q-Q\Phi^2),B\big]\Big) \ .\end{aligned} \tag{6.2.3}$$

With this term, we calculate the amplitude of the tree vertex (a) as

$$\begin{aligned}V_{ij}^{BBMM\gamma} &= ie\frac{\boldsymbol{\sigma}\times\mathbf{q}}{2M_p}\cdot\boldsymbol{\epsilon}\frac{1}{2f^2}[X_{ij}b_6^D+Y_{ij}b_6^F]\bar{u}_i(p_i)u_j(p_j)\\ &= ie\frac{\boldsymbol{\sigma}\times\mathbf{q}}{2M_p}\cdot\boldsymbol{\epsilon}A_{ij} \ ,\end{aligned}$$

where we define

$$A_{ij} = \frac{1}{2f^2}[X_{ij}b_6^D+Y_{ij}b_6^F]\bar{u}_i(p_i)u_j(p_j) \ , \tag{6.2.4}$$

in order to extract a factor. Coefficients X_{ij} and Y_{ij} are shown in tables in Appendix C. Combining the T-matrix amplitude and A_{ij}, we obtain

$$\tilde{T}_{ij}^{(a)}(\sqrt{s}) = T_{il}(\sqrt{s})G_l(\sqrt{s})A_{lm}G_m(\sqrt{s})T_{mj}(\sqrt{s}) \ . \tag{6.2.5}$$

The diagram (b) is calculated by magnetic moments of the ground state baryons μ_i in Table 6.1, multiplying the propagator $\tilde{G}(\sqrt{s})$. In later calculations, we need to perform analytic continuation of $\sqrt{s}$, however, it is impossible to calculate the loop $\tilde{G}(\sqrt{s})$ in analytic form.

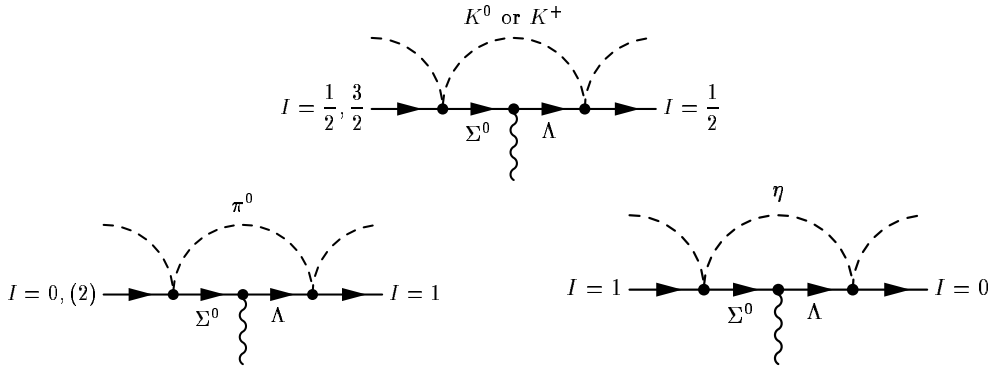

Figure 6.4: Diagrams of off-diagonal components in $\tilde{G}$ including $\Sigma^0\Lambda$ transition. Upper diagram corresponds to $S = 0$ channel and lower diagrams correspond to $S = -1$ channel.

Therefore, we neglect the small momentum of the photon in the second baryon propagator, and write

$$\tilde{G}_{ii}(\sqrt{s}) \sim i \int \frac{d^4q}{(2\pi)^4} \frac{2M_i}{(P-q)^2 - M_i^2 + i\epsilon} \frac{2M_i}{(P-q)^2 - M_i^2 + i\epsilon} \frac{1}{q^2 - m_i^2 + i\epsilon} \tag{6.2.6}$$

$$= -\frac{\partial}{\partial\sqrt{s}} G_i(\sqrt{s}) \ , \tag{6.2.7}$$

which can be calculated analytically. Then we obtain

$$\tilde{T}_{ij}^{(b)}(\sqrt{s}) = T_{il}(\sqrt{s}) \tilde{G}_{ll}(\sqrt{s}) \mu_l T_{lj}(\sqrt{s}) \ , \tag{6.2.8}$$

where μ_l are the magnetic moments of the ground state baryons.

However, since there is the $\Sigma^0\Lambda$ transition moment in the ground state, off-diagonal components exist in $\tilde{G}$. We need further approximation, because the masses in the first and second propagators in Eq. (6.2.6) are different. In Fig. 6.4, we show the diagrams where $\Sigma^0\Lambda$ transition occurs, in the $S = -1$ and $S = 0$ scatterings. These off-diagonal components are calculated by taking average of the Σ^0 and Λ propagators, namely,

$$\tilde{G}_{M\Sigma^0, M\Lambda}(\sqrt{s}) = \frac{1}{2} \left(\tilde{G}_{M\Sigma^0, M\Sigma^0}(\sqrt{s}) + \tilde{G}_{M\Lambda, M\Lambda}(\sqrt{s}) \right) \ , \tag{6.2.9}$$

where M denotes K^0, K^+, π^0 and η. Then Eq. (6.2.8) is modified as

$$\tilde{T}_{ij}^{(b)}(\sqrt{s}) = T_{il}(\sqrt{s}) \tilde{G}_{lm}(\sqrt{s}) \mu_{lm} T_{mj}(\sqrt{s}) \ , \tag{6.2.10}$$

where $\tilde{G}_{lm}(\sqrt{s})\mu_{lm}$ is diagonal plus components $\tilde{G}_{M\Sigma^0, M\Lambda}(\sqrt{s}) \times \mu_{\Sigma^0\Lambda}$. In this way, through Eqs. (6.2.2), (6.2.5) and (6.2.10), we calculate the diagram $-i\tilde{t}_{ij}(\sqrt{s})$.

6.2.2 Magnetic moments

Here we extract the magnetic moments of the resonances in two ways. When we differentiate $T_{ij}(\sqrt{s})$ in terms of $\sqrt{s}$, we have

$$\frac{\partial}{\partial\sqrt{s}}T_{ij}(\sqrt{s}) = -\frac{g_i g_j}{(\sqrt{s}-M_{N^*}+i\Gamma_{N^*}/2)^2} + \frac{\partial}{\partial\sqrt{s}}T_{ij}^{BG} \tag{6.2.11}$$

Therefore, if the derivative of the background term T_{ij}^{BG} is small, we can calculate the magnetic moments as

$$\begin{aligned}\frac{-i\tilde{t}_{ij}(\sqrt{s})}{-\frac{\partial}{\partial\sqrt{s}}T_{ij}(\sqrt{s})} &\sim \frac{\left(\frac{g_i}{\sqrt{s}-z_R}+T^{BG}\right)\cdot\mu_{N^*}(\sqrt{s})\cdot\left(\frac{g_j}{\sqrt{s}-z_R}+T^{BG}\right)}{\frac{g_i g_j}{(\sqrt{s}-z_R)^2}-\frac{\partial}{\partial\sqrt{s}}T^{BG}} \\ &\sim \mu_{N^*}(\sqrt{s}) + T^{BG}\frac{\sqrt{s}-z_R}{g_i} + T^{BG}\frac{\sqrt{s}-z_R}{g_j} + \left(T^{BG}\right)^2\frac{(\sqrt{s}-z_R)^2}{g_i g_j}\ ,\end{aligned} \tag{6.2.12}$$

where we neglect the derivative of the background term in the second line. Note that the second and third terms in Eq. (6.2.12) are not always regarded as small, because z_R has an imaginary part, so that $(\sqrt{s}-z_R)$ can not be zero. In order to make the background small, we take the value of μ_{N^*} around the position of the pole and for the channel whose coupling $|g_i|^2$ is large.

When we calculate on the complex plane, we can make the background effects negligible, because we can take the limit $z \to z_R$. We calculate

$$\begin{aligned}\lim_{z\to z_R}(z-z_R)\frac{-i\tilde{t}_{ij}(z)}{T_{ij}(z)} &\sim \lim_{z\to z_R}\frac{(z-z_R)\left[\left(\frac{g_i}{z-z_R}+T^{BG}\right)\cdot\mu_{N^*}(z)\cdot\left(\frac{g_j}{z-z_R}+T^{BG}\right)\right]}{\frac{g_i g_j}{z-z_R}+T^{BG}} \\ &= \lim_{z\to z_R}\left[\frac{\mu_{N^*}(z)}{1+(z-z_R)T^{BG}/(g_i g_j)}+\mathcal{O}(z-z_R)\right] \\ &= \mu_{N^*}(z_R)\ .\end{aligned} \tag{6.2.13}$$

In this way we obtain a value without background effects. However, this is the value at $z = z_R$, so that it has a complex phase.

Since the T-matrix amplitude contains a background term, the results on the real axis are unstable and channel dependent as we see in Eq. (6.2.12). Therefore, we need to choose the most relevant channel to calculate using the coupling strengths of the pole in Eq. (6.2.11). An advantage in this case is that the sign of the magnetic moments are fixed. On the other hand, the results in the complex plane, which are obtained at the position of the pole, have almost no background so that they are channel independent. However, in the complex plane,

	$\lvert g_{\pi N}\rvert^2$	$\lvert g_{\eta N}\rvert^2$	$\lvert g_{K\Lambda}\rvert^2$	$\lvert g_{K\Sigma}\rvert^2$
n^*	0.623	2.30	1.93	7.29
p^*	0.619	2.35	1.88	7.37

Table 6.2: Coupling strengths of the $N(1535)$ resonance to meson-baryon channels with physical meson decay constants. All channels are in $I = 1/2$.

we cannot fix the sign of the magnetic moments because of the complex phase. Hence, our strategy here is to determine the sign on the real axis and to fix the absolute value in the complex plane.

6.3 The $N(1535)$ resonance in the chiral unitary model

Since the $N(1535)$ resonance is an isospin doublet, there are two charge states of $Q = 1$(proton) and $Q = 0$(neutron), as the ground state nucleons. In the rest of this thesis, we denote them as p^* and n^*. We calculate magnetic moments for both cases, and compare the results. The corresponding meson-baryon channels are shown in Table B.1. Note that before including the photon couplings, the difference between $Q = 1$ and $Q = 0$ is only a small isospin violation due to the particle masses.

In order to calculate the magnetic moments of the $N(1535)$ resonance, we need to generate the corresponding pole at proper position. Therefore, we use the channel dependent subtraction constants in Table 4.1 and physical meson decay constants,

$$f_\pi = 93 \text{ [MeV]} , \quad f_K = 1.22 \times f_\pi , \quad f_\eta = 1.3 \times f_\pi . \tag{6.3.1}$$

Here we do not include the $SU(3)$ breaking effects. Using the same procedure in section 4.3, we calculate the scattering amplitudes and find poles, whose positions are

$$\begin{aligned} z_{n^*} &= 1536.01 - 37.06i \quad (Q = 0) , \\ z_{p^*} &= 1531.01 - 36.38i \quad (Q = 1) . \end{aligned} \tag{6.3.2}$$

The difference between p^* and n^* comes from the isospin violation of the physical masses of the particles. Their coupling strength to the meson-baryon channels are shown in Table 6.2. Qualitatively, they correspond to the results in section 4.3, where common meson decay constant $f = 1.15 \times 93$ MeV is used.

6.4 Estimation of the magnetic moments

Using the coupling strengths in Table 6.2, we present a simple estimation of the magnetic moments of the $N(1535)$ resonance. In Ref [27], considering $N(1535)$ as quasibound state of

$K\Sigma$, they decomposed the $K\Sigma$ state into physical states by Clebsh-Gordan coefficients,

$$\begin{aligned} |n^*\rangle &= -\sqrt{\frac{1}{3}}|K^0\Sigma^0\rangle + \sqrt{\frac{2}{3}}|K^+\Sigma^-\rangle \ , \\ |p^*\rangle &= \sqrt{\frac{1}{3}}|K^+\Sigma^0\rangle + \sqrt{\frac{2}{3}}|K^0\Sigma^+\rangle \ . \end{aligned} \tag{6.4.1}$$

Using the magnetic moments of the ground state baryons, they obtained

$$\begin{aligned} \mu_{n^*} &= \frac{1}{3}\mu_{\Sigma^0} + \frac{2}{3}\mu_{\Sigma^-} \sim -0.56\mu_N \ , \\ \mu_{p^*} &= \frac{1}{3}\mu_{\Sigma^0} + \frac{2}{3}\mu_{\Sigma^+} \sim 1.86\mu_N \ , \end{aligned} \tag{6.4.2}$$

where μ_N is the nuclear magneton.

In the present case, we know the coupling strengths between meson-baryon channels and $N(1535)$, therefore we sum up all the channels multiplying $|g_i|^2$ as weight. Using the Clebsh-Gordan coefficients, the magnetic moments of each channel is

$$\begin{aligned} &\mu_{\pi N}(Q=0) = \frac{1}{3}\mu_n + \frac{2}{3}\mu_p \sim 1.22\mu_N \ , && \mu_{\pi N}(Q=1) = \frac{2}{3}\mu_n + \frac{1}{3}\mu_p \sim -0.343\mu_N \ , \\ &\mu_{\eta N}(Q=0) = \mu_n \sim -1.91\mu_N \ , && \mu_{\eta N}(Q=1) = \mu_p \sim 2.79\mu_N \ , \\ &\mu_{K\Lambda}(Q=0) = \mu_\Lambda \sim -0.613\mu_N \ , && \mu_{K\Lambda}(Q=1) = \mu_\Lambda \sim -0.613\mu_N \ , \\ &\mu_{K\Sigma}(Q=0) = \frac{1}{3}\mu_{\Sigma^0} + \frac{2}{3}\mu_{\Sigma^-} \sim -0.557\mu_N \ , && \mu_{K\Sigma}(Q=1) = \frac{1}{3}\mu_{\Sigma^0} + \frac{2}{3}\mu_{\Sigma^+} \sim 1.86\mu_N \ , \end{aligned}$$

where we adopt $\mu_{\Sigma^0} = 0.649$, as predicted by the quark model. Multiplying the weight $|g_i|^2$, we obtain

$$\mu_{N^*} = \frac{|g_{\pi N}|^2}{\sum_j |g_j|^2}\mu_{\pi N} + \frac{|g_{\eta N}|^2}{\sum_j |g_j|^2}\mu_{\eta N} + \frac{|g_{K\Lambda}|^2}{\sum_j |g_j|^2}\mu_{K\Lambda} + \frac{|g_{K\Sigma}|^2}{\sum_j |g_j|^2}\mu_{K\Sigma} \ . \tag{6.4.3}$$

The results are

$$\begin{aligned} \mu_{n^*} &\sim -0.74\mu_N \ , \\ \mu_{p^*} &\sim 1.55\mu_N \ , \end{aligned} \tag{6.4.4}$$

which qualitatively agree with Eq. (6.4.2), because in Eq. (6.4.3) the $K\Sigma$ component ($|g_{K\Sigma}|^2$) dominates the $N(1535)$ resonance.

In the same way, we estimate the magnetic moments of the Λ resonances. In $S=-1$ and $I=0$, there are four channels

$$\begin{aligned} \mu_{\bar{K}N}(I=0) &= \frac{1}{2}\mu_n + \frac{1}{2}\mu_p \sim 0.44\mu_N \ , \\ \mu_{\pi\Sigma}(I=0) &= \frac{1}{3}\mu_{\Sigma^+} + \frac{1}{3}\mu_{\Sigma^0} + \frac{1}{3}\mu_{\Sigma^-} \sim 0.649\mu_N \ , \\ \mu_{\eta\Lambda}(I=0) &= \mu_\Lambda \sim -0.613\mu_N \ , \\ \mu_{K\Xi}(I=0) &= \frac{1}{2}\mu_{\Xi^0} + \frac{1}{2}\mu_{\Xi^-} \sim -0.95\mu_N \ , \end{aligned}$$

		$\lvert g_{\bar{K}N}\rvert^2$	$\lvert g_{\pi\Sigma}\rvert^2$	$\lvert g_{\eta\Lambda}\rvert^2$	$\lvert g_{K\Xi}\rvert^2$
$\Lambda(1405)$	z_1	7.4	2.3	2.0	0.12
	z_2	4.5	8.3	0.57	0.37
$\Lambda(1670)$		0.61	0.073	1.1	12

Table 6.3: Coupling strengths of the $\Lambda(1405)$ and $\Lambda(1670)$ resonances to meson-baryon channels, with the parameter sets in Ref. [19, 28], where $f = 1.123 \times 93$ MeV is used. All channels are in $I = 0$.

and the coupling strengths are shown in Table 6.3. Using them, we calculate Eq. (6.4.3), then obtain

$$\begin{aligned} \mu_{\Lambda(1405),z1} &\sim 0.287\mu_N \ , \\ \mu_{\Lambda(1405),z2} &\sim 0.485\mu_N \ , \\ \mu_{\Lambda(1670)} &\sim -0.853\mu_N \ , \end{aligned} \tag{6.4.5}$$

which qualitatively agree with the results of the chiral unitary model are [28]

$$\begin{aligned} \mu_{\Lambda(1405),z1} &\sim 0.41\mu_N \ , \\ \mu_{\Lambda(1405),z2} &\sim 0.30\mu_N \ , \\ \mu_{\Lambda(1670)} &\sim -0.29\mu_N \ . \end{aligned} \tag{6.4.6}$$

Although the absolute values of estimation (6.4.5) are different from the final results, we obtain the same signs. Since this estimation essentially corresponds to the amplitude $\tilde{T}^{(b)}$, the rest correction is considered to be given from the amplitude $\tilde{T}^{(a)}$.

6.5 Effects of the $\Sigma^0\Lambda$ transition

In the calculation of the diagrams $\tilde{T}^{(b)}_{ij}(\sqrt{s})$, there are couplings between the ground state octets and photon, and the $\Sigma^0\Lambda$ transition can take place. In the $S = 0$ channel, we show the corresponding diagram in the upper side of Fig. 6.4. In order to consider the $N(1535)$ resonance, which has $I = 1/2$, we take isospin combination at the end of calculations. Now $K\Sigma_0$ and $K\Lambda$ channels have the $I = 1/2$ components, so that this diagram can contribute to the $I = 1/2$ amplitudes after isospin combination. This is different from the $S = -1$ channel, where the corresponding diagrams are shown in the lower side of Fig. 6.4. The $\Lambda(1405)$ and $\Lambda(1670)$ resonances have $I = 0$, therefore, after isospin combination, these terms are dropped.

In Fig. 6.5 we plot the $N = -i\tilde{t}_{ij}(\sqrt{s}) = \tilde{T}^{(a)}_{ij}(\sqrt{s}) + \tilde{T}^{(b)}_{ij}(\sqrt{s})$ amplitudes of $\pi N \to \pi N(I = 1/2)$ in $S = 0$ and $\bar{K}N \to \bar{K}N(I = 0)$ in $S = -1$, with and without the $\Sigma^0\Lambda$ transition. We see that in $S = 0$, the $\Sigma^0\Lambda$ transition has moderate effects. The small difference in $S = -1$ channel is caused by the effect of isospin violation from particle masses.

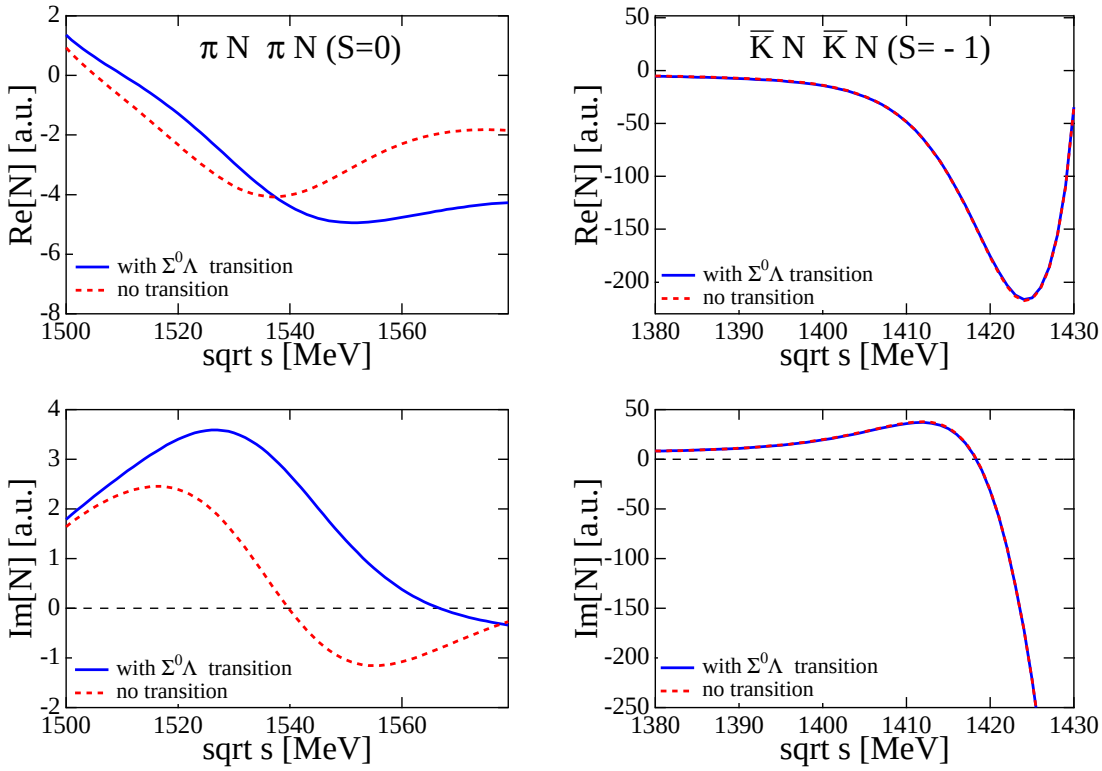

Figure 6.5: Effects of $\Sigma^0\Lambda$ transition. we plot the $N = -i\tilde{t}_{ij}(\sqrt{s})$ amplitudes of $\pi N \to \pi N(I = 1/2)$ in $S = 0$ and $\bar{K}N \to \bar{K}N(I = 0)$ in $S = -1$ with and without the $\Sigma^0\Lambda$ transition.

6.6 Results

Here we show the results. As we mentioned, there are two ways to calculate the magnetic moments. We first show the results on the real axis, then go to the complex plane. Finally we combine both the results and compare them with the estimation obtained in section 6.4.

In Fig. 6.6, we plot the T-matrix amplitudes $N = -i\tilde{t}_{ij}(\sqrt{s})$ and $D = -\frac{\partial}{\partial\sqrt{s}}t_{ij}(\sqrt{s})$, and the magnetic moments $\mu \sim N/D$. According to Table 6.2, the $N(1535)$ resonance strongly couples to the $K\Sigma$ channel. In order to make the background small, we plot the amplitudes of $K\Sigma \to K\Sigma(I = 1/2)$. It is important that in $Q = 0$, the sign of the amplitude N is opposite to the sign of D, while in $Q = 1$, the amplitudes D and N have same signs, because this determines the sign of the magnetic moments.

Next we consider to evaluate $\mu(\sqrt{s})$. If there is no background, for both N and D, extreme values of real parts and zeros of imaginary parts would take place at $\sqrt{s} = M_R$, where $\mu = N/D$ becomes pure real. However, in actual calculations these points differ slightly, especially in $Q = 0$, due to background contributions. Therefore, we evaluate the magnetic

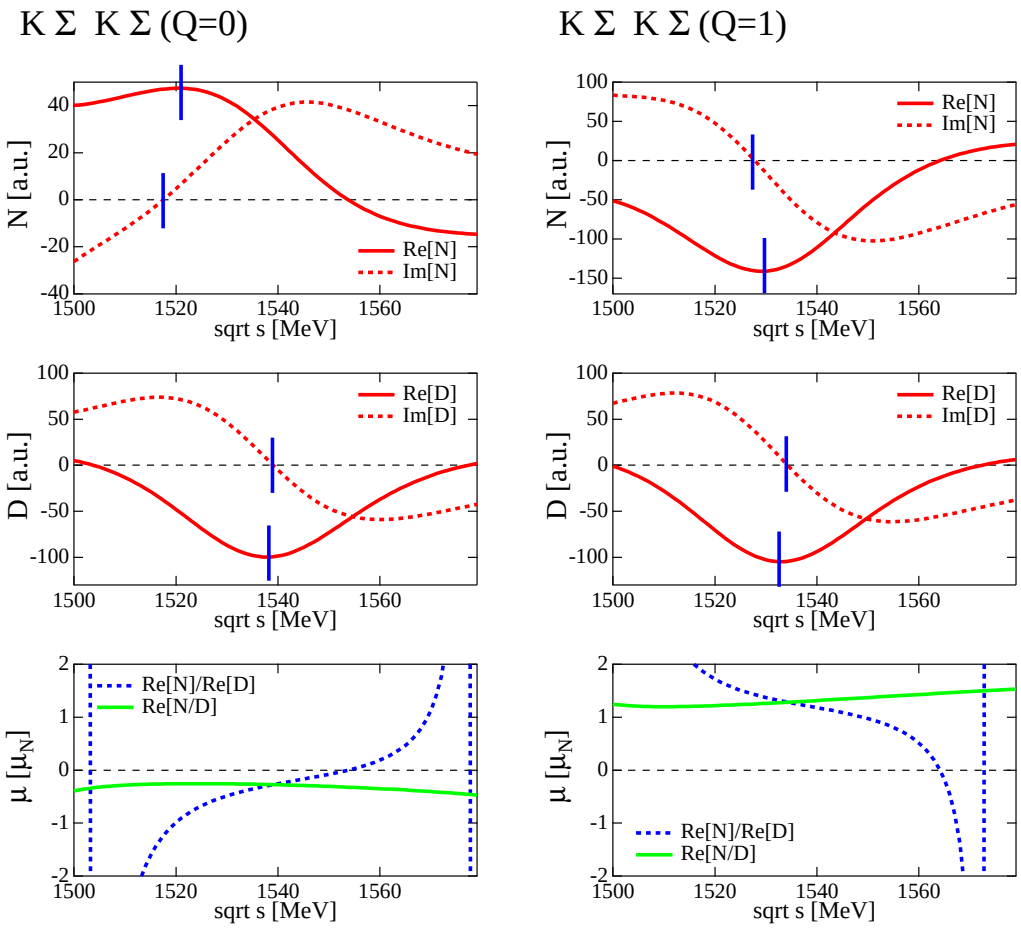

Figure 6.6: Magnetic moments on the real axis. We plot the T-matrix amplitudes $N = -i\tilde{t}_{ij}(\sqrt{s})$ and $D = -\frac{\partial}{\partial\sqrt{s}}t_{ij}(\sqrt{s})$, and the magnetic moments $\mu = [N/D]$ and $\mu = [N]/[D]$ in units of the nuclear magneton.

moments at all these points. Since $\mu = N/D$ has a small imaginary part, we calculate μ in the following two ways,

$$\mathrm{Re}[N/D] \equiv \mathrm{Re}\left[\frac{-i\tilde{t}_{ij}(\sqrt{s})}{-\frac{\partial}{\partial\sqrt{s}}t_{ij}(\sqrt{s})}\right] , \quad \mathrm{Re}[N]/\mathrm{Re}[D] \equiv \frac{\mathrm{Re}\left[-i\tilde{t}_{ij}(\sqrt{s})\right]}{\mathrm{Re}\left[-\frac{\partial}{\partial\sqrt{s}}t_{ij}(\sqrt{s})\right]} , \tag{6.6.1}$$

and we show the results in Table 6.4. The results of $\mathrm{Re}[N]/\mathrm{Re}[D]$ for n^* at $\mathrm{Re}[N]_{Ext.}$ and $\mathrm{Im}[N]_{Zero}$ are unstable as compared with those of $\mathrm{Re}[N/D]$. The reason for this is that those points are close to the zero of $\mathrm{Re}[D]$, which makes the ambiguity of $\mathrm{Re}[N]/\mathrm{Re}[D]$ large. Therefore, we take average value of $\mathrm{Re}[N/D]$ for the resonance the magnetic moments

$$\begin{aligned} \mu_{n^*} &= (-0.266 \pm 0.01)\mu_N , \\ \mu_{p^*} &= (1.26 \pm 0.02)\mu_N , \end{aligned} \tag{6.6.2}$$

with small uncertainties.

		at $\mathrm{Re}[N]_{Ext.}$	at $\mathrm{Im}[N]_{Zero}$	at $\mathrm{Re}[D]_{Ext.}$	at $\mathrm{Im}[D]_{Zero}$
n^*	$\mathrm{Re}[N/D]$	-0.256	-0.260	-0.272	-0.274
	$\mathrm{Re}[N]/\mathrm{Re}[D]$	-0.933	-1.30	-0.294	-0.275
p^*	$\mathrm{Re}[N/D]$	1.26	1.25	1.28	1.28
	$\mathrm{Re}[N]/\mathrm{Re}[D]$	1.40	1.42	1.31	1.29

Table 6.4: Magnetic moments on the real axis in units of the nuclear magneton. $\mathrm{Re}[N]_{Ext.}$ and $\mathrm{Im}[N]_{Zero}$ represent the extreme value of real part and zero of imaginary part, respectively.

In the complex plane, the magnetic moment of resonance is defined by Eq. (6.2.13). This is in general a complex value. So we take the absolute value. The results are

$$\begin{aligned} |\mu_{n^*}| &= 0.248\mu_N \\ |\mu_{p^*}| &= 1.13\mu_N \end{aligned} \tag{6.6.3}$$

which are almost channel independent.

Finally we summarize the results in Table 6.5. Compared with the estimation in section 6.4, we obtain the values with the same signs. The signs of the results also agree with the results in Ref. [27], where the constituent quark model is used. However, the magnitudes are different almost factor two for p^* and factor five for n^*. Since these two approaches have completely different picture for baryon resonances, the experimental results will give us insight of the baryon resonances.

Combining the present results with those of Ref. [28], we obtain the magnetic moments of the resonances in the chiral unitary model as

$$\mu_{p^*(1535)} \sim 1.1\mu_N \ , \quad \mu_{n^*(1535)} \sim -0.25\mu_N \ , \quad \mu_{\Lambda^*(1670)} \sim -0.29\mu_N \ . \tag{6.6.4}$$

These values imply that $1/2^-$ resonances form an $SU(3)$ octet. If the $SU(3)$ symmetry of is exact, and they are precisely the member of the octet, then their magnetic moments should satisfy the Coleman-Glashow relations (6.1.7), which tell us that

$$\mu_{n^*} = 2\mu_{\Lambda^*} \ . \tag{6.6.5}$$

This relation is satisfied up to the sign in the present calculation.

	n^*	p^*
μ (estimation)	-0.74	1.55
μ (real axis)	-0.266 ± 0.01	1.26 ± 0.02
$\lvert\mu\rvert$ (complex plane)	0.248	1.13
μ (quark model Ref. [27])	-1.28	1.89

Table 6.5: The magnetic moments of the $N(1535)$ resonance in units of the nuclear magneton.

Chapter 7

Summary

In this thesis, we have studied properties of baryon resonances in meson-baryon scatterings using the chiral unitary model. In the review part (chapters 2 and 3), we have formulated the chiral perturbation theory (ChPT), where, based on the nonlinear realization of chiral symmetry, the Lagrangians have been constructed. The method of unitarization has been presented and we have discussed the analytic structure of scattering amplitudes in detail. In the research part (chapters 4, 5 and 6), we have investigated the flavor $SU(3)$ breaking effects in the chiral unitary model, and computed the magnetic moments of the $N(1535)$ resonance. Here we discuss the results obtained in research part.

In chapter 4, we have tried to reproduce the observed cross sections and the resonance properties using a single common subtraction constant. In the $S = -1$ channel, $a \sim -2$ is fixed from the threshold branching ratios of the $K^- p$ scatterings. With this parameter, the total cross sections of the $K^- p$ scatterings are reproduced well, as well as the mass distribution for $\Lambda(1405)$ is. However, in this case the $\Lambda(1670)$ resonance cannot be reproduced. The subtraction constant $a \sim -2$ corresponds to $\Lambda_3 = 630$ MeV in the three-momentum cut-off reguralization of the meson-baryon loop integral [22]. This value is consistent with the one often used in single nucleon processes [103]. The elementary interaction of the $\bar{K}N$ system is sufficiently attractive, and a resummation of the coupled channel interactions provides the $\Lambda(1405)$ resonance at the correct position, by imposing the unitarity condition and by using the natural value for the cut-off parameter. Hence the wave function of $\Lambda(1405)$ is largely dominated by the $\bar{K}N$ component.

On the other hand, in the $S = 0$ channel, if one uses the natural value for the subtraction constant as in the $S = -1$ channel, the attraction of the meson-baryon interaction becomes so strong that an unexpected resonance is generated at around $\sqrt{s} \sim 1250$ MeV. Therefore, repulsive component is necessary to reproduce the observed πN scattering. The fitted subtraction constant using the low energy πN scattering amplitude is $a \sim 0.5$. With this value,

however, the $N(1535)$ resonance is not generated, while the agreement in the cross sections of $\pi^- p \to \eta n$ is rather good due to the threshold effects.

The unitarized amplitudes are very sensitive to the attractive component of the interaction. The interaction terms of the ChPT alone do not explain all scattering amplitudes simultaneously, but they must be complemented by the subtraction constants in the chiral unitary model. For small a, the interaction becomes more attractive, and for large a, less attractive. For $S = 0$, we need to choose $a \sim 0.5$ in order to suppress the attraction from the πN interaction in contrast to the natural value $a \sim -2$ in the $S = -1$ channel. Therefore, it is not possible to reproduce both the $\Lambda(1405)$ resonance properties and the low energy πN scattering with a common subtraction constant.

In chapter 5 we have introduced the flavor $SU(3)$ breaking Lagrangian, with the hope that the channel dependence in the subtraction constants would be absorbed into the coefficients in the chiral Lagrangian. The coefficients can be determined from other observables, and hence they are more controllable than the subtraction constants which have to be fitted by the experimental data. However, the channel dependence of the subtraction constants in each strangeness channel cannot be replaced by the $SU(3)$ breaking Lagrangian, although we have taken into account all possible breaking sources up to order $\mathcal{O}(m_q)$. Therefore, the suitable choice of the channel dependent subtraction constants is essential. Investigation of their microscopic origin is an important work in future.

From the results of the chapters 4 and 5, we conclude that the chiral unitary approach can reproduce cross sections and generate s wave resonances dynamically, once the subtraction constants are determined appropriately, using experimental data. This model is one of the powerful phenomenological methods, although it is not straightforward to apply the method to the channels where there are not sufficient experimental data, since they are required to determine the subtraction constants. As long as we concern with the $S = -1$ and $S = 0$ channels, the chiral unitary model gives satisfactory prediction.

In chapter 6, we have calculated the magnetic moments of the $N(1535)$ resonance in the chiral unitary model. We have estimated the magnetic moments based on the meson-baryon picture of the resonances, obtaining $\mu_{p^*(1535)} \sim +1.55\mu_N$ and $\mu_{n^*(1535)} \sim -0.74\mu_N$, where μ_N is the nuclear magneton. As the results of the chiral unitary model, we have obtained the magnetic moments of the resonances as $\mu_{p^*(1535)} \sim +1.1\mu_N$ and $\mu_{n^*(1535)} \sim -0.25\mu_N$. The sign of the present results agree with simple estimation and the results in Ref. [27], where the constituent quark model is used. However, the absolute values of these results are different at least factor two, so the experimental measurement will bring the information of the structure of the baryon resonances. Compared with the results of Λ resonances in Ref. [28], the Coleman-Glashow relations (6.1.7), which comes from the $SU(3)$ symmetry of

octet, are satisfied up to the sign among $\Lambda^*(1670)$ and $n^*(1535)$ in the chiral unitary model. This implies that $1/2^-$ resonances form an $SU(3)$ octet.

In closing this thesis, we briefly comment on the future plans. As we have studied in this thesis, there are two different directions of research in chiral unitary model. Although this model works in an excellent way, the origin of the channel dependent subtraction constants should be considered and clarified from microscopic point of view, such as quark degrees of freedom. Furthermore, approximations adopted in the present calculations, for instance the s-channel dominance, should be checked in more quantitative discussions. On the other hand, the success of the chiral unitary model enable us to apply it to the processes in the experiments, such as photoproduction of the $N(1535)$ resonance and the process $\gamma p \to \gamma \eta p$. They are linked to the current experiments and the prediction will give us an insight of the picture of the baryon resonances.

Appendix A

Kinematics and formulae

Here we summarize the kinematic variables used in this thesis and formulae with which we calculate several observables.

A.1 Kinematics

We consider scatterings of a meson with mass m and a baryon with mass M. The kinematics of the scattering is shown in Fig. A.1, and s is defined as $s = (k + p)^2$.

In the center of mass frame, the absolute value of three momenta of the meson and the baryon are same and given by

$$|\mathbf{p}_i| = |\mathbf{k}_i| = \frac{\sqrt{(s - (M_i - m_i)^2)(s - (M_i + m_i)^2)}}{2\sqrt{s}} \ . \tag{A.1.1}$$

The energy of the baryon E_i is

$$E_i = \frac{s - m_i^2 + M_i^2}{2\sqrt{s}} \ , \tag{A.1.2}$$

which is used in Eqs. (4.1.3) and (5.3.3).

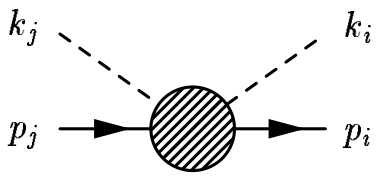

Figure A.1: Definition of the momentum variables. Dashed and solid lines represent mesons and baryons, respectively.

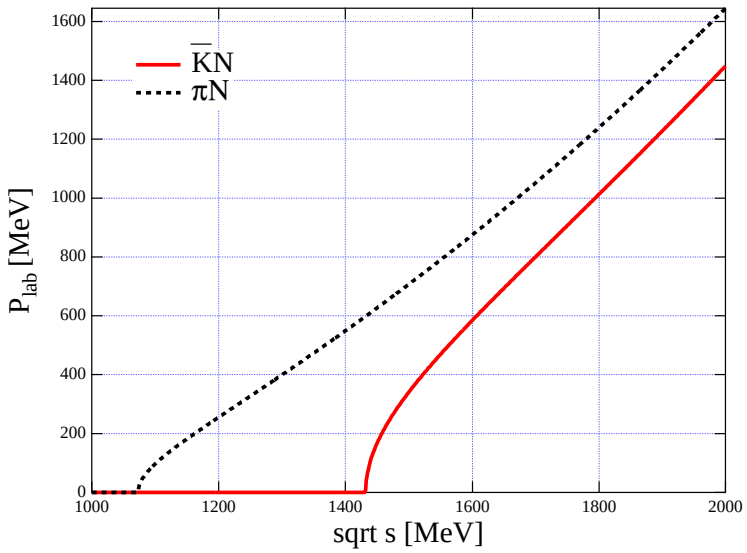

Figure A.2: Three momentum of the initial meson in the laboratory frame $P_{lab}(\sqrt{s})$. Here we show the $\bar{K}N$ and πN scatterings.

In the laboratory frame, the energy and momentum of initial meson are given by

$$E_{lab} = \frac{s - m^2 - M^2}{2M} \tag{A.1.3}$$

$$|P_{lab}| = \sqrt{E_{lab}^2 - m^2}\ , \tag{A.1.4}$$

which are used when we plot the total cross sections. In Fig. A.2 we plot $P_{lab}(\sqrt{s})$ in terms of $\sqrt{s}$.

A.2 Formulae of observables

Here we summarize the formulae used in the calculation in chapters 4 and 5. From T-matrix amplitude $|T_{ij}|$ given in Eqs. (4.1.6) and (5.3.4), the total cross sections plotted in Figs. 4.2, 4.4, 5.1 and 5.3 are given by

$$\begin{aligned}\sigma_{ij} &= \frac{1}{4\pi s}\frac{|\mathbf{k}_j|}{|\mathbf{k}_i|} M_i M_j |T_{ij}|^2 \quad [\text{MeV}]^{-2} \\ &= \frac{1}{4\pi s}\frac{|\mathbf{k}_j|}{|\mathbf{k}_i|} M_i M_j |T_{ij}|^2 \times 10 \times (\hbar c\ [\text{MeV}\cdot\ \text{fm}])^2 \quad [\text{mb}]\ .\end{aligned} \tag{A.2.1}$$

The mass distributions and T-matrix amplitudes plotted in Figs. 4.3, 4.5, 5.2 and 5.4 are given by

$$\frac{d\sigma}{dm_\alpha} = |\mathbf{k}_i||T|^2\ . \tag{A.2.2}$$

$$T_{ij}^{plot} = -\frac{1}{8\pi\sqrt{s}}\sqrt{\mathbf{k}_i}\sqrt{\mathbf{k}_j}\sqrt{2M_i}\sqrt{2M_j}T_{ij} \tag{A.2.3}$$

Threshold branching ratios are given explicitly by

$$\gamma = \frac{|T(K^- p \to \pi^+ \Sigma^-)|^2}{|T(K^- p \to \pi^- \Sigma^+)|^2}$$

$$R_c = \frac{|T(K^- p \to \pi^+ \Sigma^-)|^2 + |T(\to \pi^- \Sigma^+)|^2 + |T(\to K^- p)|^2}{|T(K^- p \to \pi^+ \Sigma^-)|^2 + |T(\to \pi^- \Sigma^+)|^2 + |T(\to \pi^0 \Sigma^0)|^2 + |T(\to \pi^0 \Lambda)|^2 + |T(\to K^- p)}|^2$$

$$R_n = \frac{|T(K^- p \to \pi^0 \Lambda)|^2}{|T(K^- p \to \pi^0 \Sigma^0)|^2 + |T(\to \pi^0 \Lambda)|^2}$$

Appendix B

Classification of meson-baryon channels

Here we classify the meson-baryon channels in terms of the conserved quantum numbers. There are 64 kinds of meson-baryon channels when we consider scatterings of octet mesons and octet baryons. They are coupled within groups which have the same quantum number.

B.1 Conservation of quantum numbers

Since we are considering the strong interaction, several quantum numbers should be conserved. The channels of the meson-baryon scatterings are specified by two quantum numbers, the hypercharge Y and the third component of isospin I_3, or equivalently the strangeness S and the electric charge Q, through the Gell-Mann-Nakano-Nishijima relation [104, 105]

$$\begin{aligned} Q &= T_3 + \frac{Y}{2} \ , \\ S &= Y - B \ , \end{aligned} \tag{B.1.1}$$

where the baryon number $B = 1$ for the meson-baryon scatterings. In Table B.1, all channels of octet mesons and octet baryons are classified in terms of quantum numbers. The channels with the same quantum numbers can couple each other.

In practical calculations, there is a small isospin violation effect when we use the physical masses for the particles. Because we have not broken the isospin symmetry in the interaction throughout this thesis (except for the photon couplings), isospin violation originates in the masses of the particles. This effect is proportional to the mass difference of the isospin multiplets, so that the effect is very small.

As an example, we consider the following process ($S = -1, T_3 = 0$).

$$\pi^0\Lambda(T = 1) \to \eta\Lambda(T = 0)$$

Table B.1: Channels of meson-baryon scatterings in particle basis. In this work we calculate the channels in $(S=-1,Q=0)$, $(S=0,Q=0)$ and $(S=0,Q=1)$.

Y	S	I_3	Q	channels
-2	-3	1	0	$\bar{K}^0\Xi^0$
		0	-1	$K^-\Xi^0,\ \bar{K}^0\Xi^-$
		-1	-2	$K^-\Xi^-$
-1	-2	$\frac{3}{2}$	1	$\pi^+\Xi^0,\ \bar{K}^0\Sigma^+$
		$\frac{1}{2}$	0	$\pi^0\Xi^0,\ \pi^+\Xi^-,\ \eta\Xi^0,\ \bar{K}^0\Lambda,\ \bar{K}^0\Sigma^0,\ K^-\Sigma^+$
		$-\frac{1}{2}$	-1	$\pi^0\Xi^-,\ \pi^-\Xi^0,\ \eta\Xi^-,\ K^-\Lambda,\ K^-\Sigma^0,\ \bar{K}^0\Sigma^-$
		$-\frac{3}{2}$	-2	$\pi^-\Xi^-,\ K^-\Sigma^-$
0	-1	2	2	$\pi^+\Sigma^+$
		1	1	$\bar{K}^0p,\ \pi^0\Sigma^+,\ \pi^+\Sigma^0,\ \pi^+\Lambda,\ \eta\Sigma^+,\ K^+\Xi^0$
		0	0	$K^-p,\ \bar{K}^0n,\ \pi^0\Lambda,\ \pi^0\Sigma^0,\ \eta\Lambda,\ \eta\Sigma^0,\ \pi^+\Sigma^-,\ \pi^-\Sigma^+,\ K^+\Xi^-,\ K^0\Xi^0$
		-1	-1	$K^-n,\ \pi^0\Sigma^-,\ \pi^-\Sigma^0,\ \pi^-\Lambda,\ \eta\Sigma^-,\ K^0\Xi^-$
		-2	-2	$\pi^-\Sigma^-$
1	0	$\frac{3}{2}$	2	$\pi^+p,\ K^+\Sigma^+$
		$\frac{1}{2}$	1	$\pi^0p,\ \pi^+n,\ \eta p,\ K^+\Lambda,\ K^+\Sigma^0,\ K^0\Sigma^+$
		$-\frac{1}{2}$	0	$\pi^0n,\ \pi^-p,\ \eta n,\ K^0\Lambda,\ K^0\Sigma^0,\ K^+\Sigma^-$
		$-\frac{3}{2}$	-1	$\pi^-n,\ K^0\Sigma^-$
2	1	1	2	K^+p
		0	1	$K^+n,\ K^0p$
		-1	0	K^0n

In the Weinberg-Tomozawa (WT) interaction (4.1.3) and the $SU(3)$ breaking interaction (5.3.3), direct coupling of these channels is zero, due to the isospin symmetry of Lagrangian. However, both $\pi^0\Lambda$ and $\eta\Lambda$ can couple to the K^-p state, which is a linear combination of $T=0$ and $T=1$

$$K^-p=\frac{1}{\sqrt{2}}\bar{K}N(T=0)-\frac{1}{\sqrt{2}}\bar{K}N(T=1)\ . \tag{B.1.2}$$

In the same way, $\bar{K}^0n$ and other channels which is a linear combination of $T=0$ and $T=1$ also couple to both $\pi^0\Lambda$ and $\eta\Lambda$. Therefore, through the $\bar{K}N$ channel, the amplitude of the process $\pi^0\Lambda\to\eta\Lambda$ is sum of the amplitudes

$$\begin{array}{l}\pi^0\Lambda\to K^-p\to\eta\Lambda\\ \pi^0\Lambda\to\bar{K}^0n\to\eta\Lambda\end{array}\ . \tag{B.1.3}$$

When we adopt the Isospin averaged mass for the $\bar{K}N$ channels, these two amplitudes cancel each other. If we adopt the physical masses for K^-p and $\bar{K}^0n$, the sum does not vanish any longer. The breaking effect is proportional to the mass difference of K^-p and $\bar{K}^0n$, which is very small.

B.2 Particle basis and isospin basis

In Table B.1, we show the meson-baryon channels in particle basis. It is also useful to express them in isospin basis using the $SU(2)$ Clebsch-Gordan coefficients. We define particle basis (P) as

$$(P) \equiv \begin{pmatrix} \text{channel 1 in particle basis} \\ \text{channel 2 in particle basis} \\ . \\ . \\ . \\ . \\ . \end{pmatrix} .$$

Here we choose the channels which can couple each other. Since these channels are specified by Y and I_3, there are several isospin multiplets among them, such as (K^-p, $\bar{K}^0 n$) and ($\pi^+\Sigma^-$, $\pi^0\Sigma^0$, $\pi^-\Sigma^+$). Using the Clebsch-Gordan coefficients, we perform isospin combination and the resulting channels are written in isospin basis (I)

$$(I) \equiv \begin{pmatrix} \text{channel 1 with } I_1 \text{ in isospin basis} \\ \text{channel 2 with } I_1 \text{ in isospin basis} \\ . \\ \text{channel 1 with } I_2 \text{ in isospin basis} \\ \text{channel 2 with } I_2 \text{ in isospin basis} \\ . \\ . \end{pmatrix} ,$$

where I_i means each values of total isospin I. The numbers of the channels in (P) and (I) are the same. In Table B.2 the channels in isospin basis are shown.

Now we define the transformation matrix (Ω) between particle basis and isospin basis as

$$(I) \equiv (\Omega) \cdot (P) , \quad (P) = (\Omega)^{-1} \cdot (I) .$$

The components of Ω is determined by the Clebsch-Gordan coefficients and suitable phase conventions of the fields. Mathematically this is a transformation between bases of finite dimension complex vector space, therefore, it is expressed by a unitary matrix in order to conserve the norm of basis.

$$\Omega^{-1} = \Omega^\dagger$$

In practice, all elements of Ω are real numbers, so that it becomes orthogonal matrix $\Omega^{-1} = \Omega^t$, where ^{t} denotes transpose of matrices.

Table B.2: Channels of meson-baryon scatterings in isospin basis. The number in the bracket denotes the total isospin I.

Y	S	I_3	Q	channels
-2	-3	1	0	$\bar{K}\Xi(1)$
		0	-1	$\bar{K}\Xi(0)$, $\bar{K}\Xi(1)$
		-1	-2	$\bar{K}\Xi(1)$
-1	-2	$\frac{3}{2}$	1	$\pi\Xi(3/2)$, $\bar{K}\Sigma(3/2)$
		$\frac{1}{2}$	0	$\pi\Xi(1/2)$, $\eta\Xi(1/2)$, $\bar{K}\Lambda(1/2)$, $\bar{K}\Sigma(1/2)$, $\pi\Xi(3/2)$, $\bar{K}\Sigma(3/2)$
		$-\frac{1}{2}$	-1	$\pi\Xi(1/2)$, $\eta\Xi(1/2)$, $\bar{K}\Lambda(1/2)$, $\bar{K}\Sigma(1/2)$, $\pi\Xi(3/2)$, $\bar{K}\Sigma(3/2)$
		$-\frac{3}{2}$	-2	$\pi\Xi(3/2)$, $\bar{K}\Sigma(3/2)$
0	-1	2	2	$\pi\Sigma(2)$
		1	1	$\bar{K}N(1)$, $\pi\Sigma(1)$, $\pi\Lambda(1)$, $\eta\Sigma(1)$, $K\Xi(1)$, $\pi\Sigma(2)$
		0	0	$\bar{K}N(0)$, $\pi\Sigma(0)$, $\eta\Lambda(0)$, $K\Xi(0)$, $\bar{K}N(1)$, $\pi\Sigma(1)$, $\pi\Lambda(1)$, $\eta\Sigma(1)$, $K\Xi(1)$, $\pi\Sigma(2)$
		-1	-1	$\bar{K}N(1)$, $\pi\Sigma(1)$, $\pi\Lambda(1)$, $\eta\Sigma(1)$, $K\Xi(1)$, $\pi\Sigma(2)$
		-2	-2	$\pi\Sigma(2)$
1	0	$\frac{3}{2}$	2	$\pi N(3/2)$, $K\Sigma(3/2)$
		$\frac{1}{2}$	1	$\pi N(1/2)$, $\eta N(1/2)$, $K\Lambda(1/2)$, $K\Sigma(1/2)$, $\pi N(3/2)$, $K\Sigma(3/2)$
		$-\frac{1}{2}$	0	$\pi N(1/2)$, $\eta N(1/2)$, $K\Lambda(1/2)$, $K\Sigma(1/2)$, $\pi N(3/2)$, $K\Sigma(3/2)$
		$-\frac{3}{2}$	-1	$\pi N(3/2)$, $K\Sigma(3/2)$
2	1	1	2	$KN(1)$
		0	1	$KN(0)$, $KN(1)$
		-1	0	$KN(1)$

Relation between a matrix M (for example, C_{ij} coefficients or the T-matrix) in (P) basis and (I) basis is

$$\begin{aligned}(\bar{I})\cdot M^I\cdot(I) &= (\bar{P})\cdot M^P\cdot(P)\\ &= (\bar{I})\cdot(\Omega)\cdot M^P\cdot(\Omega)^{-1}\cdot(I)\end{aligned}$$

So we have relations

$$\begin{aligned}M^I &= (\Omega)\cdot M^P\cdot(\Omega)^{-1}\\ M^P &= (\Omega)^{-1}\cdot M^I\cdot(\Omega)\end{aligned}$$

In this way we can change basis for any matrices. The form of these basis and Ω are given explicitly as follows.

$S = -1, T_3 = 0$

$$(P) \equiv \begin{pmatrix} K^- p \\ \bar{K}^0 n \\ \pi^0 \Lambda \\ \pi^0 \Sigma^0 \\ \eta \Lambda \\ \eta \Sigma^0 \\ \pi^+ \Sigma^- \\ \pi^- \Sigma^+ \\ K^+ \Xi^- \\ K^0 \Xi^0 \end{pmatrix} \qquad (I) \equiv \begin{pmatrix} \bar{K}N(0) \\ \pi\Sigma(0) \\ \eta\Lambda(0) \\ K\Xi(0) \\ \bar{K}N(1) \\ \pi\Sigma(1) \\ \pi\Lambda(1) \\ \eta\Sigma(1) \\ K\Xi(1) \\ \pi\Sigma(2) \end{pmatrix}$$

$$(\Omega) = \begin{pmatrix} \sqrt{\frac{1}{2}} & \sqrt{\frac{1}{2}} & 0 & 0 & 0 & 0 & 0 & 0 & 0 & 0 \\ 0 & 0 & 0 & -\sqrt{\frac{1}{3}} & 0 & 0 & -\sqrt{\frac{1}{3}} & -\sqrt{\frac{1}{3}} & 0 & 0 \\ 0 & 0 & 0 & 0 & 1 & 0 & 0 & 0 & 0 & 0 \\ 0 & 0 & 0 & 0 & 0 & 0 & 0 & 0 & -\sqrt{\frac{1}{2}} & -\sqrt{\frac{1}{2}} \\ -\sqrt{\frac{1}{2}} & \sqrt{\frac{1}{2}} & 0 & 0 & 0 & 0 & 0 & 0 & 0 & 0 \\ 0 & 0 & 0 & 0 & 0 & 0 & -\sqrt{\frac{1}{2}} & \sqrt{\frac{1}{2}} & 0 & 0 \\ 0 & 0 & 1 & 0 & 0 & 0 & 0 & 0 & 0 & 0 \\ 0 & 0 & 0 & 0 & 0 & 1 & 0 & 0 & 0 & 0 \\ 0 & 0 & 0 & 0 & 0 & 0 & 0 & 0 & -\sqrt{\frac{1}{2}} & \sqrt{\frac{1}{2}} \\ 0 & 0 & 0 & \frac{2}{\sqrt{6}} & 0 & 0 & -\sqrt{\frac{1}{6}} & -\sqrt{\frac{1}{6}} & 0 & 0 \end{pmatrix}$$

$S = 0, T_3 = -1/2$

$$(P) \equiv \begin{pmatrix} \pi^0 n \\ \pi^- p \\ \eta n \\ K^0 \Lambda \\ K^0 \Sigma^0 \\ K^+ \Sigma^- \end{pmatrix} \qquad (I) \equiv \begin{pmatrix} \pi N(1/2) \\ \eta N(1/2) \\ K\Lambda(1/2) \\ K\Sigma(1/2) \\ \pi N(3/2) \\ K\Sigma(3/2) \end{pmatrix}$$

$$(\Omega) = \begin{pmatrix} \sqrt{\frac{1}{3}} & -\sqrt{\frac{2}{3}} & 0 & 0 & 0 & 0 \\ 0 & 0 & 1 & 0 & 0 & 0 \\ 0 & 0 & 0 & 1 & 0 & 0 \\ 0 & 0 & 0 & 0 & \sqrt{\frac{1}{3}} & -\sqrt{\frac{2}{3}} \\ \sqrt{\frac{3}{2}} & \sqrt{\frac{1}{3}} & 0 & 0 & 0 & 0 \\ 0 & 0 & 0 & 0 & \sqrt{\frac{3}{2}} & \sqrt{\frac{1}{3}} \end{pmatrix}$$

Appendix C

Coefficients of the interactions

We summarize the coefficients of meson-baryon vertex obtained from the Lagrangian of the chiral perturbation theory. Here we show the coefficients of the Weinberg-Tomozawa (WT) terms, flavor $SU(3)$ breaking terms and the photon coupling terms in the meson-baryon interactions. Tables of specific channels which we have used in this thesis are presented.

C.1 Lagrangian and coefficients

We use the following terms in the Lagrangian of the chiral perturbation theory

$$\begin{aligned}
\mathcal{L}_1^{(B)} =& \mathrm{Tr}\Big(\bar{B}(i\not{\mathcal{D}} - M_0)B - D(\bar{B}\gamma^\mu\gamma_5\{A_\mu, B\}) - F(\bar{B}\gamma^\mu\gamma_5[A_\mu, B])\Big) \ , \\
\mathcal{L}_{SB} =& -\frac{Z_0}{2}\mathrm{Tr}\Big(d_m\bar{B}\{\xi\mathbf{m}\xi + \xi^\dagger\mathbf{m}\xi^\dagger, B\} + f_m\bar{B}[\xi\mathbf{m}\xi + \xi^\dagger\mathbf{m}\xi^\dagger, B]\Big) \\
& -\frac{Z_1}{2}\mathrm{Tr}(\bar{B}B)\mathrm{Tr}(\mathbf{m}U + U^\dagger\mathbf{m}) \ , \\
\mathcal{L}_{(\gamma)}^{MB} =& e\frac{\boldsymbol{\sigma}\times\mathbf{q}}{2M_p}\cdot\boldsymbol{\epsilon}\left(-\frac{i}{2}b_6^D\mathrm{Tr}\left(\bar{B}\left\{(\xi^\dagger Q\xi + \xi Q\xi^\dagger), B\right\}\right) - \frac{i}{2}b_6^F\mathrm{Tr}\left(\bar{B}\left[(\xi^\dagger Q\xi + \xi Q\xi^\dagger), B\right]\right)\right) \ .
\end{aligned}$$

The terms corresponding to the meson-baryon scattering are given by

$$\begin{aligned}
\mathcal{L}_{WT} =& \frac{1}{4f^2}\mathrm{Tr}\Big(\bar{B}i\gamma^\mu\left[(\Phi\partial_\mu\Phi - \partial_\mu\Phi\Phi), B\right]\Big) \ , \\
\mathcal{L}_{SB}^{(2)} =& \frac{Z_0}{4f^2}\mathrm{Tr}\Big(d_m\bar{B}\big\{(2\Phi\mathbf{m}\Phi + \Phi^2\mathbf{m} + \mathbf{m}\Phi^2), B\big\} + f_m\bar{B}\big[(2\Phi\mathbf{m}\Phi + \Phi^2\mathbf{m} + \mathbf{m}\Phi^2), B\big]\Big) \\
& + \frac{Z_1}{f^2}\mathrm{Tr}(\bar{B}B)\mathrm{Tr}(\mathbf{m}\Phi^2) \ , \\
\mathcal{L}^{MMBB\gamma} =& -e\frac{\boldsymbol{\sigma}\times\mathbf{q}}{2M_p}\cdot\boldsymbol{\epsilon}\frac{i}{4f^2}\mathrm{Tr}\Big(b_6^D\bar{B}\big\{(2\Phi Q\Phi - \Phi^2 Q - Q\Phi^2), B\big\} \\
& + b_6^F\bar{B}\big[(2\Phi Q\Phi - \Phi^2 Q - Q\Phi^2), B\big]\Big) \ .
\end{aligned}$$

Table C.1: $D_i^{Z_1}$.

meson	π	$K, \bar{K}$	η
$D_i^{Z_1}$	$2\hat{m}$	$\hat{m}+m_s$	$\frac{2}{3}(\hat{m}+2m_s)$

From these terms, the basic interaction at the tree level is given by

$$V_{ij}^{(WT)} = -\frac{C_{ij}}{4f^2}\bar{u}_i(p_i)(\not{k}_i+\not{k}_j)u_j(p_j)\ , \tag{C.1.1}$$

$$V_{ij}^{(SB)} = -\frac{1}{f^2}\Big[Z_0\Big((A_{ij}^d d_m + A_{ij}^f f_m)\hat{m} + (B_{ij}^d d_m + B_{ij}^f f_m)m_s\Big) + Z_1\delta_{ij}D_i^{Z_1}\Big]\bar{u}_i(p_i)u_j(p_j)\ , \tag{C.1.2}$$

$$V_{ij}^{MMBB\gamma} = ie\frac{\boldsymbol{\sigma}\times\mathbf{q}}{2M_p}\cdot\boldsymbol{\epsilon}\frac{1}{2f^2}[X_{ij}b_6^D + Y_{ij}b_6^F]\bar{u}_i(p_i)u_j(p_j)\ . \tag{C.1.3}$$

where the coefficients C, A, B, D, X and Y are the numbers in matrix form and the indices (i,j) denote the channels of the meson-baryon scatterings as shown in Table B.1.

The coefficient $D_i^{Z_1}$ is specified only by the meson in channel i independently of baryons, because $\mathrm{Tr}(\bar{B}B)$ in the last term of Eq. (C.1.2) gives a common contribution to all baryons. Also, there is no off-diagonal component when the isospin symmetry is assumed. The explicit form of $D_i^{Z_1}$ is shown in Table C.1.

The values of the coefficients C (WT interactions) are shown in the following tables;

- Table C.3 ($S=0$ Isospin basis)
- Table C.4 ($S=0, Q=0$)
- Table C.5 ($S=0, Q=1$)
- Table C.6 ($S=-1$ Isospin basis)
- Table C.7 ($S=0, Q=0$).

The values of the coefficients A and B (Flavor $SU(3)$ breaking interactions) are shown in the following tables;

- Tables C.8 and C.9 ($S=0, Q=0$)
- Tables C.10,C.11, C.12 and C.13 ($S=-1, Q=0$).

The values of the coefficients X and Y (photon coupling interactions) are shown in the following tables;

- Table C.14 ($S=0, Q=0$)

Table C.2: Quantum numbers of channels i, j, i' and j'

channel	hypercharge			third component of isospin		
	meson	baryon	total	meson	baryon	total
i	y_i	$Y - y_i$	Y	i_{3i}	$I_3 - i_{3i}$	I_3
j	y_j	$Y - y_j$	Y	i_{3j}	$I_3 - i_{3j}$	I_3
i'	$-y_i$	$-Y + y_i$	$-Y$	$-i_{3i}$	$-I_3 + i_{3i}$	$-I_3$
j'	$-y_j$	$-Y + y_j$	$-Y$	$-i_{3j}$	$-I_3 + i_{3j}$	$-I_3$

- Table C.15 ($S = 0, Q = 1$)
- Tables C.16 and C.17 ($S = -1, Q = 0$).

C.2 Relations among coefficients

There are two symmetry relations among coefficients. Using these relations, we can derive the coefficients which are not shown in the tables.

First, the channels, which have the same strangeness S and different charge Q, are related through the $SU(2)$ Clebsch-Gordan coefficients due to the isospin symmetry. This relation is valid for the WT interactions and the $SU(3)$ breaking interactions because they do not break the isospin symmetry. This is the relation among the channels in the block separated by the horizontal lines in Table B.1.

Second, the coefficients of the sector (Y, I_3) are related with those of $(-Y, -I_3)$. Let us consider the channels (i, j) and (i', j') in the sectors (Y, I_3) and $(-Y, -I_3)$, respectively, as shown in Table C.2. Then the coefficients of the sector $(-Y, -I_3)$ are given by

$$\begin{aligned}
&C_{i'j'}(-Y,-I_3) = C_{ij}(Y,I_3)\ , \\
&A^d_{i'j'}(-Y,-I_3) = A^d_{ij}(Y,I_3)\ , \quad A^f_{i'j'}(-Y,-I_3) = -A^f_{ij}(Y,I_3)\ , \\
&B^d_{i'j'}(-Y,-I_3) = B^d_{ij}(Y,I_3)\ , \quad B^f_{i'j'}(-Y,-I_3) = -B^f_{ij}(Y,I_3)\ , \\
&X_{i'j'}(-Y,-I_3) = X_{ij}(Y,I_3)\ , \quad Y_{i'j'}(-Y,-I_3) = -Y_{ij}(Y,I_3)\ .
\end{aligned} \tag{C.2.1}$$

Also, using the relation (C.2.1), the coefficients of the sector $(S = -2, Q = 0)$ are obtained from the tables of the sector $(S = 0, Q = 0)$. For example, if we specify (i, j) to be $(\pi^0 n, K^0\Lambda)$, the corresponding (i', j') is $(\pi^0\Xi^0, \bar{K}^0\Lambda)$. The coefficients for (i', j') are obtained by $A^d_{i'j'} = \sqrt{3}/8$, $A^f_{i'j'} = -3\sqrt{3}/8$, $B^d_{i'j'} = 1/(8\sqrt{3})$ and $B^f_{i'j'} = -\sqrt{3}/8$.

$S=0$		$I=\frac{1}{2}$				$I=\frac{3}{2}$	
		πN	ηN	$K\Lambda$	$K\Sigma$	πN	$K\Sigma$
$I=\frac{1}{2}$	πN	2	0	$\frac{3}{2}$	$\frac{1}{2}$		
	ηN		0	$-\frac{3}{2}$	$\frac{3}{2}$		
	$K\Lambda$			0	0		
	$K\Sigma$				2		
$I=\frac{3}{2}$	πN					-1	-1
	$K\Sigma$						-1

Table C.3: $C_{ij}(S=0)$ Isospin basis

$I_3=-1/2$	$\pi^0 n$	$\pi^- p$	ηn	$K^0\Lambda$	$K^0\Sigma^0$	$K^+\Sigma^-$
$\pi^0 n$	0	$-\sqrt{2}$	0	$\frac{\sqrt{3}}{2}$	$-\frac{1}{2}$	$-\frac{1}{\sqrt{2}}$
$\pi^- p$		1	0	$-\sqrt{\frac{3}{2}}$	$-\frac{1}{\sqrt{2}}$	0
ηn			0	$-\frac{3}{2}$	$\frac{\sqrt{3}}{2}$	$-\sqrt{\frac{3}{2}}$
$K^0\Lambda$				0	0	0
$K^0\Sigma^0$					0	$-\sqrt{2}$
$K^+\Sigma^-$						1

Table C.4: $C_{ij}(S=0,Q=0)$ Particle basis

$I_3=1/2$	$\pi^0 p$	$\pi^+ n$	ηp	$K^+\Lambda$	$K^+\Sigma^0$	$K^0\Sigma^+$
$\pi^0 p$	0	$\sqrt{2}$	0	$-\frac{\sqrt{3}}{2}$	$-\frac{1}{2}$	$\frac{1}{\sqrt{2}}$
$\pi^+ n$		1	0	$-\sqrt{\frac{3}{2}}$	$\frac{1}{\sqrt{2}}$	0
ηp			0	$-\frac{3}{2}$	$-\frac{\sqrt{3}}{2}$	$-\sqrt{\frac{3}{2}}$
$K^+\Lambda$				0	0	0
$K^+\Sigma^0$					0	$\sqrt{2}$
$K^0\Sigma^+$						1

Table C.5: $C_{ij}(S=0,Q=1)$ Particle basis

$S=-1$		$I=0$				$I=1$					$I=2$
		$\bar{K}N$	$\pi\Sigma$	$\eta\Lambda$	$K\Xi$	$\bar{K}N$	$\pi\Sigma$	$\pi\Lambda$	$\eta\Sigma$	$K\Xi$	$\pi\Sigma$
$I=0$	$\bar{K}N$	3	$-\sqrt{\frac{3}{2}}$	$\frac{3}{\sqrt{2}}$	0						
	$\pi\Sigma$		4	0	$\sqrt{\frac{3}{2}}$						
	$\eta\Lambda$			0	$-\frac{3}{\sqrt{2}}$						
	$K\Xi$				3						
$I=1$	$\bar{K}N$					1	-1	$-\sqrt{\frac{3}{2}}$	$-\sqrt{\frac{3}{2}}$	0	
	$\pi\Sigma$						2	0	0	1	
	$\pi\Lambda$							0	0	$-\sqrt{\frac{3}{2}}$	
	$\eta\Sigma$								0	$-\sqrt{\frac{3}{2}}$	
	$K\Xi$									1	
$I=2$	$\pi\Sigma$										-2

Table C.6: $C_{ij}(S=-1)$ Isospin basis

$I_3=0$	K^-p	$\bar{K}^0n$	$\pi^0\Lambda$	$\pi^0\Sigma^0$	$\eta\Lambda$	$\eta\Sigma^0$	$\pi^+\Sigma^-$	$\pi^-\Sigma^+$	$K^+\Xi^-$	$K^0\Xi^0$
K^-p	2	1	$\frac{\sqrt{3}}{2}$	$\frac{1}{2}$	$\frac{3}{2}$	$\frac{\sqrt{3}}{2}$	0	1	0	0
$\bar{K}^0n$		2	$-\frac{\sqrt{3}}{2}$	$\frac{1}{2}$	$\frac{3}{2}$	$-\frac{\sqrt{3}}{2}$	1	0	0	0
$\pi^0\Lambda$			0	0	0	0	0	0	$\frac{\sqrt{3}}{2}$	$-\frac{\sqrt{3}}{2}$
$\pi^0\Sigma^0$				0	0	0	2	2	$\frac{1}{2}$	$\frac{1}{2}$
$\eta\Lambda$					0	0	0	0	$\frac{3}{2}$	$\frac{3}{2}$
$\eta\Sigma^0$						0	0	0	$\frac{\sqrt{3}}{2}$	$-\frac{\sqrt{3}}{2}$
$\pi^+\Sigma^-$							2	0	1	0
$\pi^-\Sigma^+$								2	0	1
$K^+\Xi^-$									2	1
$K^0\Xi^0$										2

Table C.7: $C_{ij}(S=-1,Q=0)$ Particle basis

	A^d_{ij}						A^f_{ij}					
$I_3=-1/2$	$\pi^0 n$	$\pi^- p$	ηn	$K^0\Lambda$	$K^0\Sigma^0$	$K^+\Sigma^-$	$\pi^0 n$	$\pi^- p$	ηn	$K^0\Lambda$	$K^0\Sigma^0$	$K^+\Sigma^-$
$\pi^0 n$	1	0	$-\frac{1}{\sqrt{3}}$	$\frac{\sqrt{3}}{8}$	$\frac{3}{8}$	$\frac{3}{4\sqrt{2}}$	1	0	$-\frac{1}{\sqrt{3}}$	$\frac{3\sqrt{3}}{8}$	$-\frac{3}{8}$	$-\frac{3}{4\sqrt{2}}$
$\pi^- p$		1	$\sqrt{\frac{2}{3}}$	$-\frac{\sqrt{6}}{8}$	$\frac{3}{4\sqrt{2}}$	0		1	$\sqrt{\frac{2}{3}}$	$-\frac{3\sqrt{6}}{8}$	$-\frac{3}{4\sqrt{2}}$	0
ηn			$\frac{1}{3}$	$-\frac{1}{24}$	$-\frac{1}{8\sqrt{3}}$	$\frac{1}{4\sqrt{6}}$			$\frac{1}{3}$	$-\frac{1}{8}$	$\frac{1}{8\sqrt{3}}$	$-\frac{1}{4\sqrt{6}}$
$K^0\Lambda$				$\frac{5}{6}$	$-\frac{1}{2\sqrt{3}}$	$\frac{1}{\sqrt{6}}$				0	0	0
$K^0\Sigma^0$					$\frac{1}{2}$	0					0	$\frac{1}{\sqrt{2}}$
$K^+\Sigma^-$						$\frac{1}{2}$						$-\frac{1}{2}$

Table C.8: A^d_{ij} and $A^f_{ij}(S=0,Q=0)$

	B^d_{ij}						B^f_{ij}					
$I_3=-1/2$	$\pi^0 n$	$\pi^- p$	ηn	$K^0\Lambda$	$K^0\Sigma^0$	$K^+\Sigma^-$	$\pi^0 n$	$\pi^- p$	ηn	$K^0\Lambda$	$K^0\Sigma^0$	$K^+\Sigma^-$
$\pi^0 n$	0	0	0	$\frac{1}{8\sqrt{3}}$	$\frac{1}{8}$	$\frac{1}{4\sqrt{2}}$	0	0	0	$\frac{\sqrt{3}}{8}$	$-\frac{1}{8}$	$-\frac{1}{4\sqrt{2}}$
$\pi^- p$		0	0	$-\frac{1}{4\sqrt{6}}$	$\frac{1}{4\sqrt{2}}$	0		0	0	$-\frac{\sqrt{6}}{8}$	$-\frac{1}{4\sqrt{2}}$	0
ηn			$\frac{4}{3}$	$\frac{5}{24}$	$\frac{5}{8\sqrt{3}}$	$-\frac{5}{4\sqrt{6}}$			$-\frac{4}{3}$	$\frac{5}{8}$	$-\frac{5}{8\sqrt{3}}$	$\frac{5}{4\sqrt{6}}$
$K^0\Lambda$				$\frac{5}{6}$	$-\frac{1}{2\sqrt{3}}$	$\frac{1}{\sqrt{6}}$				0	0	0
$K^0\Sigma^0$					$\frac{1}{2}$	0					0	$\frac{1}{\sqrt{2}}$
$K^+\Sigma^-$						$\frac{1}{2}$						$-\frac{1}{2}$

Table C.9: B^d_{ij} and $B^f_{ij}(S=0,Q=0)$

$I_3=0$	$K^- p$	$\bar{K}^0 n$	$\pi^0\Lambda$	$\pi^0\Sigma^0$	$\eta\Lambda$	$\eta\Sigma^0$	$\pi^+\Sigma^-$	$\pi^-\Sigma^+$	$K^+\Xi^-$	$K^0\Xi^0$
$K^- p$	1	$\frac{1}{2}$	$-\frac{\sqrt{3}}{8}$	$\frac{3}{8}$	$-\frac{1}{24}$	$\frac{1}{8\sqrt{3}}$	0	$\frac{3}{4}$	0	0
$\bar{K}^0 n$		1	$\frac{\sqrt{3}}{8}$	$\frac{3}{8}$	$-\frac{1}{24}$	$-\frac{1}{8\sqrt{3}}$	$\frac{3}{4}$	0	0	0
$\pi^0\Lambda$			$\frac{2}{3}$	0	0	$\frac{2}{3}$	0	0	$-\frac{\sqrt{3}}{8}$	$\frac{\sqrt{3}}{8}$
$\pi^0\Sigma^0$				2	$\frac{2}{3}$	0	0	0	$\frac{3}{8}$	$\frac{3}{8}$
$\eta\Lambda$					$\frac{2}{9}$	0	$\frac{2}{3}$	$\frac{2}{3}$	$-\frac{1}{24}$	$-\frac{1}{24}$
$\eta\Sigma^0$						$\frac{2}{3}$	0	0	$\frac{1}{8\sqrt{3}}$	$-\frac{1}{8\sqrt{3}}$
$\pi^+\Sigma^-$							2	0	$\frac{3}{4}$	0
$\pi^-\Sigma^+$								2	0	$\frac{3}{4}$
$K^+\Xi^-$									1	$\frac{1}{2}$
$K^0\Xi^0$										1

Table C.10: $A^d_{ij}(S=-1,Q=0)$

$I_3=0$	K^-p	$\bar{K}^0n$	$\pi^0\Lambda$	$\pi^0\Sigma^0$	$\eta\Lambda$	$\eta\Sigma^0$	$\pi^+\Sigma^-$	$\pi^-\Sigma^+$	$K^+\Xi^-$	$K^0\Xi^0$
K^-p	0	$\frac{1}{2}$	$-\frac{3\sqrt{3}}{8}$	$-\frac{3}{8}$	$-\frac{1}{8}$	$-\frac{1}{8\sqrt{3}}$	0	$-\frac{3}{4}$	0	0
$\bar{K}^0n$		0	$\frac{3\sqrt{3}}{8}$	$-\frac{3}{8}$	$-\frac{1}{8}$	$\frac{1}{8\sqrt{3}}$	$-\frac{3}{4}$	0	0	0
$\pi^0\Lambda$			0	0	0	0	0	0	$\frac{3\sqrt{3}}{8}$	$-\frac{3\sqrt{3}}{8}$
$\pi^0\Sigma^0$				0	0	0	0	0	$\frac{3}{8}$	$\frac{3}{8}$
$\eta\Lambda$					0	0	0	0	$\frac{1}{8}$	$\frac{1}{8}$
$\eta\Sigma^0$						0	$\frac{2}{\sqrt{3}}$	$-\frac{2}{\sqrt{3}}$	$\frac{1}{8\sqrt{3}}$	$-\frac{1}{8\sqrt{3}}$
$\pi^+\Sigma^-$							0	0	$\frac{3}{4}$	0
$\pi^-\Sigma^+$								0	0	$\frac{3}{4}$
$K^+\Xi^-$									0	$-\frac{1}{2}$
$K^0\Xi^0$										0

Table C.11: $A^f_{ij}(S=-1,Q=0)$

$I_3=0$	K^-p	$\bar{K}^0n$	$\pi^0\Lambda$	$\pi^0\Sigma^0$	$\eta\Lambda$	$\eta\Sigma^0$	$\pi^+\Sigma^-$	$\pi^-\Sigma^+$	$K^+\Xi^-$	$K^0\Xi^0$
K^-p	1	$\frac{1}{2}$	$-\frac{1}{8\sqrt{3}}$	$\frac{1}{8}$	$\frac{5}{24}$	$-\frac{5}{8\sqrt{3}}$	0	$\frac{1}{4}$	0	0
$\bar{K}^0n$		1	$\frac{1}{8\sqrt{3}}$	$\frac{1}{8}$	$\frac{5}{24}$	$\frac{5}{8\sqrt{3}}$	$\frac{1}{4}$	0	0	0
$\pi^0\Lambda$			0	0	0	0	0	0	$-\frac{1}{8\sqrt{3}}$	$\frac{1}{8\sqrt{3}}$
$\pi^0\Sigma^0$				0	0	0	0	0	$\frac{1}{8}$	$\frac{1}{8}$
$\eta\Lambda$					$\frac{16}{9}$	0	0	0	$\frac{5}{24}$	$\frac{5}{24}$
$\eta\Sigma^0$						0	0	0	$-\frac{5}{8\sqrt{3}}$	$\frac{5}{8\sqrt{3}}$
$\pi^+\Sigma^-$							0	0	$\frac{1}{4}$	0
$\pi^-\Sigma^+$								0	0	$\frac{1}{4}$
$K^+\Xi^-$									1	$\frac{1}{2}$
$K^0\Xi^0$										1

Table C.12: $B^d_{ij}(S=-1,Q=0)$

$I_3=0$	K^-p	$\bar{K}^0n$	$\pi^0\Lambda$	$\pi^0\Sigma^0$	$\eta\Lambda$	$\eta\Sigma^0$	$\pi^+\Sigma^-$	$\pi^-\Sigma^+$	$K^+\Xi^-$	$K^0\Xi^0$
K^-p	0	$\frac{1}{2}$	$-\frac{\sqrt{3}}{8}$	$-\frac{1}{8}$	$\frac{5}{8}$	$\frac{5}{8\sqrt{3}}$	0	$-\frac{1}{4}$	0	0
$\bar{K}^0n$		0	$\frac{\sqrt{3}}{8}$	$-\frac{1}{8}$	$\frac{5}{8}$	$-\frac{5}{8\sqrt{3}}$	$-\frac{1}{4}$	0	0	0
$\pi^0\Lambda$			0	0	0	0	0	0	$\frac{\sqrt{3}}{8}$	$-\frac{\sqrt{3}}{8}$
$\pi^0\Sigma^0$				0	0	0	0	0	$\frac{1}{8}$	$\frac{1}{8}$
$\eta\Lambda$					0	0	0	0	$-\frac{5}{8}$	$-\frac{5}{8}$
$\eta\Sigma^0$						0	0	0	$-\frac{5}{8\sqrt{3}}$	$\frac{5}{8\sqrt{3}}$
$\pi^+\Sigma^-$							0	0	$\frac{1}{4}$	0
$\pi^-\Sigma^+$								0	0	$\frac{1}{4}$
$K^+\Xi^-$									0	$-\frac{1}{2}$
$K^0\Xi^0$										0

Table C.13: $B^f_{ij}(S=-1,Q=0)$

	X_{ij}						Y_{ij}					
$I_3 = -1/2$	$\pi^0 n$	$\pi^- p$	ηn	$K^0\Lambda$	$K^0\Sigma^0$	$K^+\Sigma^-$	$\pi^0 n$	$\pi^- p$	ηn	$K^0\Lambda$	$K^0\Sigma^0$	$K^+\Sigma^-$
$\pi^0 n$	0	$\frac{1}{\sqrt{2}}$	0	0	0	$\frac{1}{2\sqrt{2}}$	0	$\frac{1}{\sqrt{2}}$	0	0	0	$-\frac{1}{2\sqrt{2}}$
$\pi^- p$		-1	0	$\frac{1}{2\sqrt{6}}$	$-\frac{1}{2\sqrt{2}}$	0		-1	0	$\frac{\sqrt{6}}{4}$	$\frac{1}{2\sqrt{2}}$	0
ηn			0	0	0	$\frac{\sqrt{6}}{4}$			0	0	0	$-\frac{\sqrt{6}}{4}$
$K^0\Lambda$				0	0	$-\frac{1}{\sqrt{6}}$				0	0	0
$K^0\Sigma^0$					0	0					0	$-\frac{1}{\sqrt{2}}$
$K^+\Sigma^-$						-1						1

Table C.14: $X_{ij}, Y_{ij}(S = 0, Q = 0)$

	X_{ij}						Y_{ij}					
$I_3 = 1/2$	$\pi^0 p$	$\pi^+ n$	ηp	$K^+\Lambda$	$K^+\Sigma^0$	$K^0\Sigma^+$	$\pi^0 p$	$\pi^+ n$	ηp	$K^+\Lambda$	$K^+\Sigma^0$	$K^0\Sigma^+$
$\pi^0 p$	0	$\frac{1}{\sqrt{2}}$	0	$-\frac{1}{4\sqrt{3}}$	$\frac{1}{4}$	0	0	$\frac{1}{\sqrt{2}}$	0	$-\frac{\sqrt{3}}{4}$	$-\frac{1}{4}$	0
$\pi^+ n$		1	0	$-\frac{1}{\sqrt{6}}$	$-\frac{1}{\sqrt{2}}$	0		1	0	$-\sqrt{\frac{3}{2}}$	$\frac{1}{\sqrt{2}}$	0
ηp			0	$-\frac{1}{4}$	$\frac{\sqrt{3}}{4}$	0			0	$-\frac{3}{4}$	$-\frac{\sqrt{3}}{4}$	0
$K^+\Lambda$				1	$-\frac{1}{\sqrt{3}}$	$-\frac{1}{\sqrt{6}}$				0	0	0
$K^+\Sigma^0$					-1	0					0	$\frac{1}{\sqrt{2}}$
$K^0\Sigma^+$						0						0

Table C.15: $X_{ij}, Y_{ij}(S = 0, Q = 1)$

$I_3 = 0$	K^-p	$\bar{K}^0n$	$\pi^0\Lambda$	$\pi^0\Sigma^0$	$\eta\Lambda$	$\eta\Sigma^0$	$\pi^+\Sigma^-$	$\pi^-\Sigma^+$	$K^+\Xi^-$	$K^0\Xi^0$
K^-p	0	$-\frac{1}{2}$	$-\frac{1}{4\sqrt{3}}$	$\frac{1}{4}$	$-\frac{1}{4}$	$\frac{3}{4\sqrt{3}}$	0	1	0	0
$\bar{K}^0n$		0	0	0	0	0	$-\frac{1}{2}$	0	0	0
$\pi^0\Lambda$			0	0	0	0	$\frac{1}{\sqrt{3}}$	$\frac{1}{\sqrt{3}}$	$-\frac{1}{4\sqrt{3}}$	0
$\pi^0\Sigma^0$				0	0	0	0	0	$\frac{1}{4}$	0
$\eta\Lambda$					0	0	0	0	$-\frac{1}{4}$	0
$\eta\Sigma^0$						0	0	0	$\frac{3}{4\sqrt{3}}$	0
$\pi^+\Sigma^-$							0	0	1	0
$\pi^-\Sigma^+$								0	0	$-\frac{1}{2}$
$K^+\Xi^-$									0	$-\frac{1}{2}$
$K^0\Xi^0$										0

Table C.16: $X_{ij}(S = -1, Q = 0)$

$I_3 = 0$	K^-p	$\bar{K}^0n$	$\pi^0\Lambda$	$\pi^0\Sigma^0$	$\eta\Lambda$	$\eta\Sigma^0$	$\pi^+\Sigma^-$	$\pi^-\Sigma^+$	$K^+\Xi^-$	$K^0\Xi^0$
K^-p	-2	$-\frac{1}{2}$	$-\frac{3}{4\sqrt{3}}$	$-\frac{1}{4}$	$-\frac{3}{4}$	$-\frac{3}{4\sqrt{3}}$	0	-1	0	0
$\bar{K}^0n$		0	0	0	0	0	$\frac{1}{2}$	0	0	0
$\pi^0\Lambda$			0	0	0	0	0	0	$\frac{3}{4\sqrt{3}}$	0
$\pi^0\Sigma^0$				0	0	0	1	-1	$\frac{1}{4}$	0
$\eta\Lambda$					0	0	0	0	$\frac{3}{4}$	0
$\eta\Sigma^0$						0	0	0	$\frac{3}{4\sqrt{3}}$	0
$\pi^+\Sigma^-$							2	0	1	0
$\pi^-\Sigma^+$								-2	0	$-\frac{1}{2}$
$K^+\Xi^-$									2	$\frac{1}{2}$
$K^0\Xi^0$										0

Table C.17: $Y_{ij}(S = -1, Q = 0)$

Bibliography

[1] A. Hosaka and H. Toki, *Quarks, baryons and chiral symmetry* (World Scientific, Singapore, 2001).

[2] S. Weinberg, *The Quantum theory of fields* volume 2: Modern applications (Cambridge University Press, London, 1996).

[3] M. L. Goldberger and S. B. Treiman, Phys. Rev. **111**, 354 (1958).

[4] S. Weinberg, Physica **A96**, 327 (1979).

[5] J. Gasser and H. Leutwyler, Nucl. Phys. **B250**, 465 (1985).

[6] J. Gasser and H. Leutwyler, Nucl. Phys. **B250**, 517 (1985).

[7] J. Gasser and H. Leutwyler, Nucl. Phys. **B250**, 539 (1985).

[8] S. Weinberg, Nucl. Phys. **B363**, 3 (1991).

[9] N. Kaiser, P. B. Siegel, and W. Weise, Nucl. Phys. **A594**, 325 (1995).

[10] N. Kaiser, P. B. Siegel, and W. Weise, Phys. Lett. **B362**, 23 (1995).

[11] N. Kaiser, T. Waas, and W. Weise, Nucl. Phys. **A612**, 297 (1997).

[12] B. Krippa, Phys. Rev. **C58**, 1333 (1998).

[13] E. Oset and A. Ramos, Nucl. Phys. **A635**, 99 (1998).

[14] M. F. M. Lutz and E. E. Kolomeitsev, Nucl. Phys. **A700**, 193 (2002).

[15] C.-H. Lee, D.-P. Min, and M. Rho, Nucl. Phys. **A602**, 334 (1996).

[16] B. Krippa and J. T. Londergan, Phys. Rev. **C58**, 1634 (1998).

[17] N. Isgur and G. Karl, Phys. Rev. **D18**, 4187 (1978).

[18] N. Isgur and G. Karl, Phys. Rev. **D20**, 1191 (1979).

[19] E. Oset, A. Ramos, and C. Bennhold, Phys. Lett. **B527**, 99 (2002).

[20] T. Inoue, E. Oset, and M. J. Vicente Vacas, Phys. Rev. **C65**, 035204 (2002).

[21] A. Ramos, E. Oset, and C. Bennhold, Phys. Rev. Lett. **89**, 252001 (2002).

[22] J. A. Oller and U. G. Meissner, Phys. Lett. **B500**, 263 (2001).

[23] D. Jido, E. Oset, and A. Ramos, Phys. Rev. **C66**, 055203 (2002).

[24] B. M. K. Nefkens *et al.*, Phys. Rev. **D18**, 3911 (1978).

[25] A. Bosshard *et al.*, Phys. Rev. **D44**, 1962 (1991).

[26] M. Kotulla *et al.*, Phys. Rev. Lett. **89**, 272001 (2002).

[27] W.-T. Chiang, S. N. Yang, M. Vanderhaeghen, and D. Drechsel, nucl-th/0211061.

[28] D. Jido, A. Hosaka, J. C. Nacher, E. Oset, and A. Ramos, Phys. Rev. **C66**, 025203 (2002).

[29] T. Hyodo, S. I. Nam, D. Jido, and A. Hosaka, nucl-th/0212026.

[30] A. Pich, Rept. Prog. Phys. **58**, 563 (1995).

[31] G. Ecker, Prog. Part. Nucl. Phys. **35**, 1 (1995).

[32] V. Bernard, N. Kaiser, and U.-G. Meissner, Int. J. Mod. Phys. **E4**, 193 (1995).

[33] U. G. Meissner, Rept. Prog. Phys. **56**, 903 (1993).

[34] B. W. Lee, *Chiral dynamics* (Gordon and Breach science publishers, New York, 1972).

[35] J. Goldstone, A. Salam, and S. Weinberg, Phys. Rev. **127**, 965 (1962).

[36] H. Leutwyler, Ann. Phys. **235**, 165 (1994).

[37] S. R. Coleman, J. Wess, and B. Zumino, Phys. Rev. **177**, 2239 (1969).

[38] C. G. Callan, S. R. Coleman, J. Wess, and B. Zumino, Phys. Rev. **177**, 2247 (1969).

[39] S. Weinberg, Phys. Rev. **166**, 1568 (1968).

[40] R. Haag, Phys. Rev. **112**, 669 (1958).

[41] M. Gell-Mann, R. J. Oakes, and B. Renner, Phys. Rev. **175**, 2195 (1968).

[42] A. Krause, Helv. Phys. Acta **63**, 3 (1990).

[43] J. F. Donoghue, E. Golowich, and B. R. Holstein, *Dynamics of the standard model* (Cambridge University Press, London, 1992).

[44] E. Jenkins and A. V. Manohar, Phys. Lett. **B255**, 558 (1991).

[45] E. Jenkins and A. V. Manohar, Phys. Lett. **B259**, 353 (1991).

[46] N. Isgur and M. B. Wise, Phys. Lett. **B232**, 113 (1989).

[47] N. Isgur and M. B. Wise, Phys. Lett. **B237**, 527 (1990).

[48] H. Georgi, Phys. Lett. **B240**, 447 (1990).

[49] G. F. Chew and S. Mandelstam, Phys. Rev. **119**, 467 (1960).

[50] A. Gomez Nicola, J. Nieves, J. R. Pelaez, and E. Ruiz Arriola, Phys. Lett. **B486**, 77 (2000).

[51] U.-G. Meissner and J. A. Oller, Nucl. Phys. **A673**, 311 (2000).

[52] G. Arfken, *Mathematical methods for physicists*, second ed. (Academic press international edition, New York, 1970).

[53] M. E. Peskin and D. V. Schroeder, *An Introduction to quantum field theory* (Addison-Wesley, 1995).

[54] J. D. Bjorken and S. D. Drell, *Relativistic quantum fields* (McGraw-Hill, New York, 1965).

[55] P. Buttiker and U.-G. Meissner, Nucl. Phys. **A668**, 97 (2000).

[56] L. Castillejo, R. H. Dalitz, and F. J. Dyson, Phys. Rev. **101**, 453 (1956).

[57] S. Mandelstam, Phys. Rev. **112**, 1344 (1958).

[58] R. J. Nowak *et al.*, Nucl. Phys. **B139**, 61 (1978).

[59] D. N. Tovee *et al.*, Nucl. Phys. **B33**, 493 (1971).

[60] T. S. Mast *et al.*, Phys. Rev. **D14**, 13 (1976).

[61] J. Ciborowski *et al.*, J. Phys. **G8**, 13 (1982).

[62] R. O. Bangerter *et al.*, Phys. Rev. **D23**, 1484 (1981).

[63] T. S. Mast *et al.*, Phys. Rev. **D11**, 3078 (1975).

[64] M. Sakitt *et al.*, Phys. Rev. **139**, B719 (1965).

[65] M. B. Watson, M. Ferro-Luzzi, and R. D. Tripp, Phys. Rev. **131**, 2248 (1963).

[66] J. K. Kim, Phys. Rev. Lett. **14**, 29 (1965); Columbia University Report, Nevis 149 (1966).

[67] M. Ferro-Luzzi, R. D. Tripp, and M. B. Watson, Phys. Rev. Lett. **8**, 28 (1962).

[68] M. Csejthey-Barth *et al.*, Phys. Lett. **16**, 89 (1965).

[69] J. Paul Nordin, Phys. Rev. **123**, 2168 (1961).

[70] W. Kittel, G. Ptter, and I. Wacek, Phys. Lett. **21**, 349 (1966).

[71] H. Going, Nuovo Cim. **16**, 848 (1960).

[72] Rutherford-London, G. P. Gopal *et al.*, Nucl. Phys. **B119**, 362 (1977).

[73] R. J. Hemingway, Nucl. Phys. **B253**, 742 (1985).

[74] M. Batinic, I. Slaus, A. Svarc, and B. M. K. Nefkens, Phys. Rev. **C51**, 2310 (1995).

[75] J. C. Hart *et al.*, Nucl. Phys. **B166**, 73 (1980).

[76] D. H. Saxon *et al.*, Nucl. Phys. **B162**, 522 (1980).

[77] R. D. Baker *et al.*, Nucl. Phys. **B145**, 402 (1978).

[78] R. D. Baker *et al.*, Nucl. Phys. **B141**, 29 (1978).

[79] B. Nelson *et al.*, Phys. Rev. Lett. **31**, 901 (1973).

[80] D. W. Thomas, A. Engler, H. E. Fisk, and R. W. Kraemer, Nucl. Phys. **B56**, 15 (1973).

[81] J. J. Jones *et al.*, Phys. Rev. Lett. **26**, 860 (1971).

[82] T. O. Binford *et al.*, Phys. Rev. **183**, 1134 (1969).

[83] O. Van Dyck *et al.*, Phys. Rev. Lett. **23**, 50 (1969).

[84] T. M. Knasel *et al.*, Phys. Rev. **D11**, 1 (1975).

[85] R. L. Crolius *et al.*, Phys. Rev. **155**, 1455 (1967).

[86] J. Keren, Phys. Rev. **133**, B457 (1963).

[87] L. L. Yoder, C. T. Coffin, D. I. Meyer, and K. M. Terwilliger, Phys. Rev. **132**, 1778 (1963).

[88] L. B. Leipuner and R. K. Adair, Phys. Rev. **109**, 1358 (1958).

[89] L. Bertanza *et al.*, Phys. Rev. Lett. **8**, 332 (1962).

[90] F. S. Crawford *et al.*, Phys. Rev. Lett. **3**, 394 (1959).

[91] R. T. V. de Walle, C. L. A. Pols, D. J. Schotanus, H. J. G. M. Tiecke, and D. Z. Toet, Nuovo Cim. **A53**, 745 (1968).

[92] O. Goussu *et al.*, Nuovo Cim. **42A**, 606 (1966).

[93] F. Eisler *et al.*, Nuovo Cim. **10**, 468 (1958).

[94] Center of Nuclear Study, http://gwdac.phys.gwu.edu .

[95] C. Garcia-Recio, J. Nieves, E. Ruiz Arriola, and M. J. Vicente Vacas, Phys. Rev. D **67**, 076009 (2003).

[96] M. Gell-Mann, Phys. Rev. **125**, 1067 (1962).

[97] S. Okubo, Prog. Theor. Phys. **27**, 949 (1962).

[98] S. R. Coleman and S. L. Glashow, Phys. Rev. Lett. **6**, 423 (1961).

[99] Particle Data Group, K. Hagiwara *et al.*, Phys. Rev. **D66**, 010001 (2002).

[100] U.-G. Meissner and S. Steininger, Nucl. Phys. **B499**, 349 (1997).

[101] D. G. Caldi and H. Pagels, Phys. Rev. **D10**, 3739 (1974).

[102] J. Gasser, M. E. Sainio, and A. Svarc, Nucl. Phys. **B307**, 779 (1988).

[103] C. Bennhold and H. Tanabe, Nucl. Phys. **A530**, 625 (1991).

[104] M. Gell-Mann, Phys. Rev. **92**, 833 (1954).

[105] T. Nakano and K. Nishijima, Prog. Theor. Phys. **10**, 581 (1954).